



UNITED NATIONS EDUCATIONAL, SCIENTIFIC AND CULTURAL ORGANIZATION  
INTERNATIONAL ATOMIC ENERGY AGENCY  
INTERNATIONAL CENTRE FOR THEORETICAL PHYSICS



SMR/917 - 7

**SECOND WORKSHOP ON  
SCIENCE AND TECHNOLOGY OF THIN FILMS**

**( 11 - 29 March 1996 )**

---

Reading material about:  
" Atomic layer epitaxy "

presented by:

**T. SUNTOLA**  
Microchemistry Ltd.  
P.O. Box 45  
FIN-02151 Espoo  
Finland

---

These are preliminary lecture notes, intended only for distribution to participants.



REPRINTED FROM

# HANDBOOK OF CRYSTAL GROWTH 3

## THIN FILMS AND EPITAXY

### Part B: Growth Mechanisms and Dynamics

Edited by

D.T.J. Hurle

H.H. Wills Physics Laboratory

University of Bristol

Bristol, UK BS8 1TL

## CHAPTER 14

# Atomic Layer Epitaxy

TUOMO SUNTOLA

*Microchemistry Ltd., P.O. Box 45, FIN-02151, Finland*

<i>Contents</i>	
1. Introduction, definitions	605
1.1. The atomic layer epitaxy process	605
1.2. Chemisorption, surface reactions, precursor states, activation energies	608
1.3. Description of additive reactions using elemental precursors	611
1.4. Saturation of the surface in an additive surface reaction	612
1.5. Exchange reactions using compound reactants	613
1.6. ALE processing window	615
2. ALE processing, reactors	615
2.1. ALE processing requirements	616
2.2. The ALE reactor	617
2.3. ALE cycles, dosing of the reactants	622
2.4. Transport of the reactants	624
2.5. Valving with inert gas flow	626
2.6. Purge time	627
3. ALE processes for different materials	627
3.1. II-VI compounds	627
3.1.1. Cadmium sulphide (CdS)	627
3.1.1.1. CdS/Cd + S	627
3.1.1.2. CdS/CdCl <sub>2</sub> + H <sub>2</sub> S	628
3.1.2. Cadmium selenide (CdSe)	628
3.1.3. Cadmium telluride (CdTe)	628
3.1.3.1. CdTe/Cd + Te	629
3.1.4. Zinc sulphide (ZnS)	629
3.1.4.1. ZnS/Zn + S	629
3.1.4.2. ZnS/ZnCl <sub>2</sub> + H <sub>2</sub> S	632
3.1.4.3. ZnS/Zn(CH <sub>3</sub> COO) <sub>2</sub> (zinc acetate) + H <sub>2</sub> S	632
3.1.4.4. ZnS/DMZn (dimethylzinc) + H <sub>2</sub> S	632

HANDBOOK OF CRYSTAL GROWTH, VOL. 3

edited by D.T.J. Hurle

© 1994 Elsevier Science B.V. All rights reserved



1994

ELSEVIER

Amsterdam - Lausanne - New York - Oxford - Shannon - Tokyo

3.1.5. Zinc selenide (ZnSe)	633
3.1.5.1. ZnSe/Zn + Se, DESe (diethylselenium)	633
3.1.5.2. ZnSe/DMZn (dimethylzinc) + H <sub>2</sub> Se	634
3.1.5.3. ZnSe/DEZn (diethylzinc) + H <sub>2</sub> Se	635
3.1.5.4. ZnSe/ZnCl <sub>2</sub> + H <sub>2</sub> Se	635
3.1.6. Zinc telluride (ZnTe)	636
3.1.6.1. ZnTe/Zn + Te	636
3.1.7. Other sulphides	637
3.1.7.1. CaS, SrS, BaS/M(thd) <sub>2</sub> + H <sub>2</sub> S	637
3.1.8. I/III-VI chalcopyrites	637
3.1.9. II-VI superlattices	637
3.2. III-V materials	638
3.2.1. Aluminium arsenide (AlAs)	638
3.2.1.1. AlAs/TMAI, MMAI (tri/monomethylaluminium) + AsH <sub>3</sub>	638
3.2.1.2. AlAs/AlCl <sub>3</sub> + AsH <sub>3</sub>	639
3.2.2. Gallium arsenide (GaAs)	639
3.2.2.1. GaAs/Ga + As <sub>4</sub>	639
3.2.2.2. GaAs/TMGa (trimethylgallium) + AsH <sub>3</sub> (arsine)	639
3.2.2.3. GaAs/TEGa (triethylgallium) + AsH <sub>3</sub> (arsine)	646
3.2.2.4. GaAs/TMGa (trimethylgallium) + TBAs (tertiarybutylarsine)	647
3.2.2.5. GaAs/GaCl + AsH <sub>3</sub>	648
3.2.2.6. GaAs/DEGaCl (diethylgalliumchloride) + AsH <sub>3</sub>	648
3.2.2.7. GaAs/GaCl <sub>3</sub> + AsH <sub>3</sub>	649
3.2.3. Indium arsenide (InAs)	649
3.2.3.1. InAs/TMIn (trimethylindium) + AsH <sub>3</sub>	649
3.2.4. Indium phosphide (InP)	650
3.2.4.1. InP/TMIn (trimethylindium) + PH <sub>3</sub> (phosphine)	650
3.2.5. III-V superalloys and superlattices	651
3.2.6. GaAs/Si interface	652
3.3. Oxides, nitrides	653
3.3.1. Aluminium oxide (Al <sub>2</sub> O <sub>3</sub> )	653
3.3.1.1. Al <sub>2</sub> O <sub>3</sub> /AlCl <sub>3</sub> + H <sub>2</sub> O	653
3.3.1.2. Al <sub>2</sub> O <sub>3</sub> /TMAI (trimethylaluminium) + H <sub>2</sub> O	653
3.3.1.3. Al <sub>2</sub> O <sub>3</sub> /AlCl <sub>3</sub> + O <sub>2</sub>	653
3.3.1.4. Al <sub>2</sub> O <sub>3</sub> /TMAI (trimethylaluminium) + H <sub>2</sub> O <sub>2</sub>	654
3.3.1.5. Al <sub>2</sub> O <sub>3</sub> /AlCl <sub>3</sub> , Al(OR) <sub>3</sub> (aliphatic alcohols) + H <sub>2</sub> O, O <sub>2</sub>	654
3.3.2. Tantalum pentoxide (Ta <sub>2</sub> O <sub>5</sub> )	654
3.3.2.1. Ta <sub>2</sub> O <sub>5</sub> /TaCl <sub>5</sub> + H <sub>2</sub> O	654
3.3.3. Titanium dioxide (TiO <sub>2</sub> )	654
3.3.3.1. TiO <sub>2</sub> /TiCl <sub>4</sub> + H <sub>2</sub> O	654
3.3.4. Nitrides	657
3.3.4.1. Indium nitride (InN)	657
3.3.4.2. Gallium nitride (GaN)/TMGa, TEGa + NH <sub>3</sub>	657
3.3.4.3. Aluminium nitride (AlN)	658
3.3.4.4. Niobium nitride (NbN)	658

3.4. Group-IV semiconductors	658
3.4.1. Germanium (Ge)	658
3.4.1.1. Ge/GeH <sub>4</sub> (germane) + thermal cycling	658
3.4.1.2. Ge/DEGeH <sub>2</sub> (diethylgermane) + thermal cycling	659
3.4.2. Silicon (Si)	659
3.4.2.1. Si/Si <sub>2</sub> H <sub>6</sub> (or Si <sub>3</sub> H <sub>8</sub> ) (di- or trisilane) + thermal cycling	659
3.4.2.2. Si/DESiH <sub>2</sub> + thermal cycling	659
3.4.2.3. Si/SiH <sub>2</sub> Cl <sub>2</sub> (chlorosilane) + thermal cycling	659
3.4.3. Silicon carbide (SiC)	660
4. Summary	660
Acknowledgements	660
References	661

## 1. Introduction, definitions

### 1. The atomic layer epitaxy process

Atomic layer epitaxy (ALE) is a surface controlled process for thin-film manufacturing and for epitaxial growth of single crystals. It is primarily developed for compound materials such as II-VI and III-V semiconductors, oxides and nitrides but it can also be extended to covalent materials [1]. The term epitaxy comes from the Greek and means "arranged-on". Traditionally it has been used to describe the growth of single crystal layers onto a host crystal surface which controls the structure of the growing layer. In ALE, an "on arrangement" is obtained by sequentially controlled surface conditions which not only control the structure of the growing material layer but also the rate of the growth, to one atomic layer or "monolayer" in one reaction sequence. The inherent structural control of the material and the "digital" rate control of the growth process makes ALE attractive for the growth of crystalline compound layers, complex layered structures, superlattices and layered alloys. Originally ALE was developed for the growth of polycrystalline and amorphous thin films of ZnS and dielectric oxides for electroluminescent display devices [2, 3]. In large-area thin films ALE can be used to produce high-quality material with excellent uniformity and reproducibility. The inherent control feature of ALE is also the key in cost efficiency of the process.

The sequential control of the growth in ALE is based on saturating surface reactions between the substrate and each of the reactants needed for the compound to be grown. Each surface reaction adds one monoatomic layer of the material on the surface. A monolayer obtained in a reaction sequence may be a "full monolayer" corresponding to the density of atoms in the corresponding crystal plane of a bulk crystal or it may be a "partial monolayer" due to preferred surface reconstructions or steric-hindrance effects related to the reactant used.

If the reactants used are elements of the material to be grown, the surface reactions are additive reactions and the necessary condition for saturation is that condensation of the reactant does not occur (fig. 1A). In the case of compound reactants there are several mechanisms of saturation, depending on the nature of the surface reactions in question (fig. 1B). Saturation of each surface reaction is the characteristic feature of atomic layer epitaxy, sequencing alone does not result in the surface control. Saturation makes the growth rate proportional to the number of reaction cycles instead of to the intensity of the reactant flux. Instead of monitoring thickness during the growth process, in ALE the thickness can be determined by counting the number of reaction steps.

For ALE of covalent (elemental) materials a compound reactant or a pair of compound reactants is needed. Two approaches to saturated reactions can be used. The first approach comprises a reaction adding a monolayer of the covalent material to be grown and a separate reduction sequence activated with extra energy which re-establishes the surface for a new monolayer (fig. 2). The reduction sequence may also be a chemical reaction resulting in release of the surface ligands (fig. 3). In the best case the release of the surface ligand is performed with a reactant also adding a monolayer of

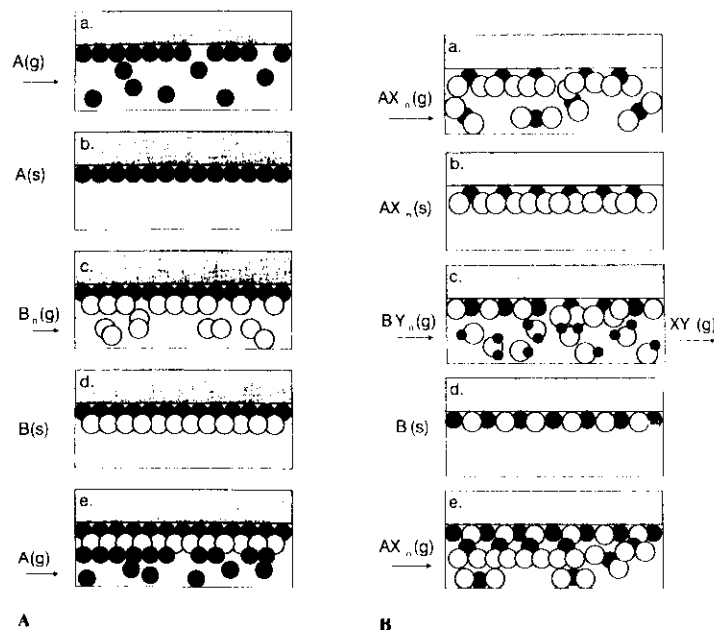


Fig. 1. Basic sequences of ALE for compound AB. "A" denotes a group-I, II, III element, "B" denotes a group-V, VI, VII element. "X<sub>n</sub>" and "Y<sub>n</sub>" denote ligands of the reactants AX<sub>n</sub> and BY<sub>n</sub>, respectively. In (B) it is required that the ligands are able to form volatile compounds in a surface exchange reaction (see also fig. 6). (A) Sequences for elemental reactants, A(g) and B<sub>n</sub>(g): (a) introduction of A(g) onto the substrate surface, (b) formation of an A(s) monolayer surface, (c) introduction of B<sub>n</sub>(g) onto A(s) surface, (d) formation of B(s) monolayer surface, (e) repetition of the cycle from (a). (B) Sequences for compound reactants, AX<sub>n</sub>(g) and BY<sub>n</sub>(g): (a) introduction of AX<sub>n</sub>(g) onto the substrate surface, (b) formation of an AX<sub>n</sub>(s) monolayer surface, (c) introduction of BY<sub>n</sub>(g) onto AX<sub>n</sub>(s) surface, (d) formation of B(s) monolayer surface, release of XY(g), (e) repetition of the cycle from (a). The release of ligands X<sub>n</sub> and Y<sub>n</sub> may also take place partially in each reaction sequence (see section 1.5).

the material grown (fig. 4). A pair comprised of a halide and a hydride of a group-IV material could satisfy such a requirement. The saturation mechanisms in this approach are basically similar to the saturation mechanisms of ALE of compound materials using compound reactants.

Advantages obtainable with ALE are dependent on the material to be processed and the type of application in question. In single crystal epitaxy ALE may be a way of obtaining a lower epitaxial crystal growth temperature. It is also a method for making precise interface and material layers needed in superlattice structures and superalloys. In thin-film applications ALE makes it possible to obtain excellent thickness uniformity over large areas. The surface control of ALE results in reproducible physical characteristics with good homogeneity and thickness uniformity. It also results in an effective step coverage and in a very low pinhole density in thin films.

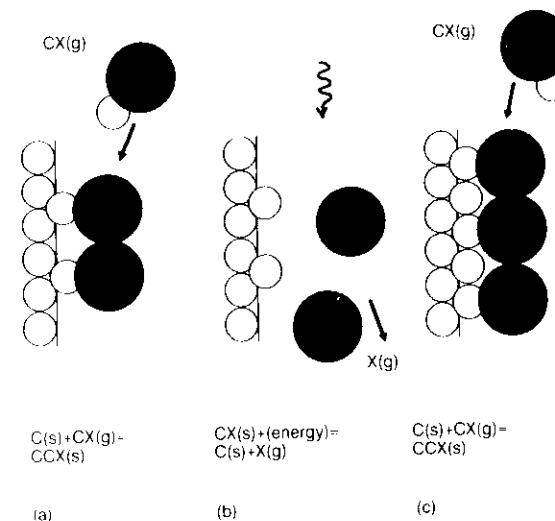


Fig. 2. ALE of covalent material "C" (group-IV element) comprising (a) a sequence for formation of a monolayer using reactant CX<sub>n</sub> and (b) a sequence for re-activating the surface for the next monolayer by extra energy, heat, or photons, (c) sequence for next monolayer.

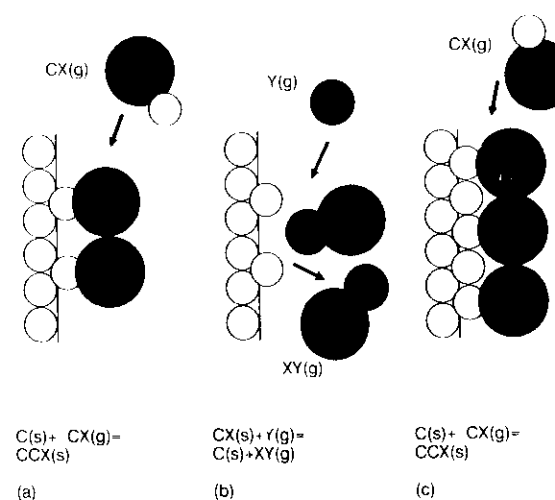


Fig. 3. ALE of covalent material "C" (group-IV element) comprising (a) a sequence for a monolayer formation using reactant CX<sub>n</sub> and (b) a sequence for releasing the surface ligands by a reaction with Y<sub>n</sub> (g) gas, (c) sequence for next monolayer.

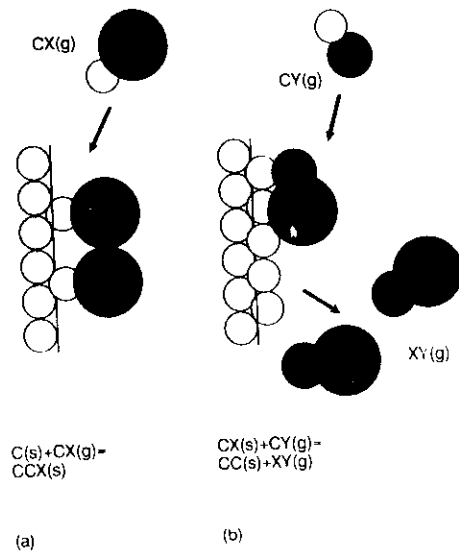


Fig. 4. ALE of elemental materials by a pair of reactants  $CX_n$  and  $CY_n$ , each adding a monolayer of the material. (a) The reactant  $CX_n(g)$  adds a monolayer  $CX_n(s)$  onto the  $C(s)$  surface. (b) the reactant  $CY_n(g)$  adds a  $C(s)$  layer while releasing the  $X_n(s)$  surface ligand as  $nXY(g)$  vapour. The ligand exchange may also be divided between the  $CX_n(g)$  and  $CY_n(g)$  reactions. Then the surface can be expressed as  $CX_n(s)$  and  $CY_n(s)$ , respectively.

The ALE process can be performed either in a vacuum system like MBE or in an inert gas system like CVD. ALE can be considered as a special mode of an MBE or a CVD process. When running a process in ALE mode, the reactants are supplied to the growing surface sequentially, one at a time, under conditions which result in a saturated surface reaction for each of the reactants used. Basic requirements for saturation conditions can be derived from the vapour pressure data of the reactants and the reaction kinetics of the surface reactions. Surface reconstructions can strongly influence the saturation characteristics.

The use of an MBE-type system makes it possible to use a variety of in situ surface analysis methods in the study of the growth mechanism and the surface structures formed. The advantages of a CVD-type system are mainly a more productive processing and greater freedom in choosing the reaction dynamics. In comparison with conventional CVD processing, a major advantage of ALE is the elimination of gas phase reactions, which is a consequence of the sequencing in ALE.

### 1.2. Chemisorption, surface reactions, precursor states, activation energies

In its simplest mode of operation ALE is performed using the elements of the compound to be grown as the reactants. In this mode the compound grows one full or

partial monolayer in each reaction step as a result of an additive chemisorption in each cycle. For monoatomic elemental reactants additive surface reaction may occur directly, without a precursor state or an activation energy. For such a reaction one must also assume that there are bonding sites directly available on the surface (fig. 5a). If a modification of the surface structure such as breaking of a surface reconstruction is needed to create a bonding site, an activation energy of the surface reaction must be assumed. The activation energy can be described with a precursor state connected to the final bonding site (fig. 5b). A precursor state and an activation energy can also be used to describe the surface reaction condition when modification of the reactant molecule, such as dissociation or structural modification, is needed before chemisorption. Further, the surface model of fig. 5b is applicable to surface exchange reactions where the chemisorption of the reactant molecule is accompanied by the production of a byproduct which desorbs from the surface.

In order to express the surface reactions in ALE sequences in a descriptive way the formalism defined in fig. 6 will be used. In ALE the reactions occur between a gas and a solid surface. The symbols in fig. 6 indicate not only the chemical form of a surface compound but also give an indication of the surface structure, especially the topmost atom of a surface formed.

The characteristic feature of ALE in all modes of operation is the saturation of each surface reaction, which causes the growth to proceed incrementally, one reaction step at a time. Accordingly, the surface reactions control the growth of the material. The structure and the density of a monolayer formed in an ALE reaction sequence is

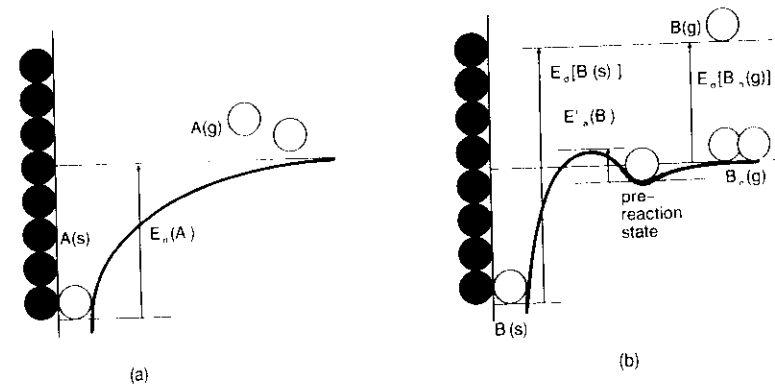


Fig. 5. Langmuir model of surface energies. (a) Chemisorption of atom  $A$  on a  $B(s)$  surface without a precursor state or an activation energy.  $E_n[A(s)]$  is the desorption energy (bonding energy) of an  $A(s)$  surface atom. (b) Chemisorption of reactant molecule  $B_n(g)$  on an  $A(s)$  surface via a precursor state  $B'(s)$ . An activation energy  $E'_n(B)$  results from a change in the surface structure necessary to create a bonding site and/or from a change in the state of reactant molecule  $B_n$ , such as dissociation or structural modification.  $E_n[B_n(g)]$  denotes the dissociation energy of  $B_n(g)$  gas.  $E_n[B(s)]$  denotes the desorption energy of a  $B(s)$  surface atom as  $B(g)$  monoatomic gas.

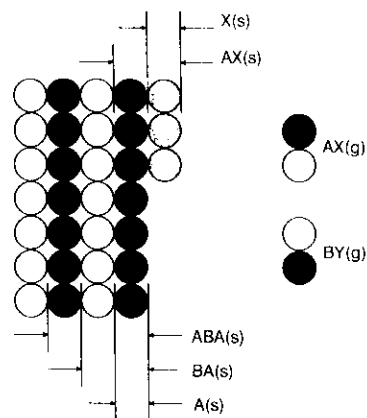


Fig. 6. Formalism of chemical symbols used for the surface structures formed in an ALE sequence. The symbol expresses the depth of the surface counted as well as the order of atomic layers in the surface structure. A, symbol for elements ionizing typically as cations (such as groups I, II, III). A(s), A as surface atoms of material A in the solid phase, A(g), element A in gas phase (when vapourization is monoatomic), B, symbol for elements ionizing typically as anions (such as group V, VI, VII), B(s), B atoms as surface atoms of solid AB material, B<sub>n</sub>(g), element B in gas phase (when vapourization occurs as *n*-atom molecules), B(s), atom of a dissociated B<sub>n</sub>(g) molecule in a precursor state, C, symbol for group-IVA elements, AB, compound of elements A and B, AB(s), surface of compound AB with B as the surface atom, ABA(s), surface of compound AB with Y ligand surface bonded on B-atoms, BA(s), surface of compound AB with A as the surface atom, AX(s), surface of compound AB with X ligand surface bonded on A-atoms.

strongly dependent on the characteristic surface reconstruction of the material and the crystalline face in question. For some III–V materials the saturation density has been observed to correspond to the density of atoms in a crystalline face of the bulk material. This case is often referred to as “a full monolayer per cycle” growth. In most cases the saturation density has been observed to be less than a “full monolayer”, which refers to the important role of surface reconstructions in ALE growth steps. Use of large reactant molecules may also reduce the saturation density of a monolayer.

In contrast to the requirements for reactants in CVD processes, optimal reactants in ALE should react aggressively with each other, i.e. the activation energy of the surface reaction should be low. In CVD a reaction threshold is needed for uniformity of thickness. A reaction threshold is also needed to avoid gas phase reactions. In ALE, gas phase reactions between reactants are automatically eliminated by the sequencing of the reactants. Thickness uniformity results from the saturation mechanism. High reactivity assures efficient saturation and a high material utilization factor. For a uniform saturation it is also important that the reactants used are stable at the processing temperature. Undesirable decomposition or partially completed exchange reactions may be reasons for non-complete saturation or sources of impurities in the resulting material. Unstable ligands formed in the surface reactions may make the process sensitive to the gas flow dynamics of the system.

### 1.3. Description of additive reactions using elemental precursors

Additive ALE growth is based on the use of the elements A and B of the compound AB as the reactants. This mode of ALE growth is possible when the vapour pressures of the elements A and B have suitable values for the necessary vapour transport at the growth temperature. Examples of successful additive ALE processes are the growth of several II–VI compounds, such as ZnS, ZnSe, ZnTe, CdS, CdSe and CdTe.

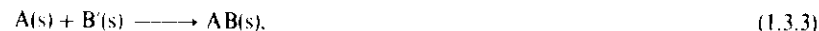
In the ALE process the reaction between the elements A and B has to be divided into subreactions between a solid surface of one of the elements and the second element in the vapour phase. To create a monolayer of A on a B(s) surface the B(s) surface is exposed to an A(g) flux:



The reaction stops when the B(s) surface is fully converted into BA(s), which means the build-up of an A(s) surface. Necessary requirements for A(s) monolayer formation are that the dose is sufficient and that the condensation of extra A(g) vapour on the A(s) surface is prevented, which is done by choosing the reaction temperature high enough. It is further required that the A(s) surface formed is stable enough to stay until the reaction with B(g) vapour occurs, which is described as dissociation of the B<sub>n</sub>(g) vapour in a precursor state B'(s).



followed by the surface reaction



which establishes the original B(s) surface necessary for the next cycle of reaction sequences.

### 1.4. Saturation of the surface in an additive surface reaction

A basic requirement for monolayer saturation is selective desorption, i.e. the desorption rate of atoms A from an A(s) surface formed should be higher than that of atoms A from a B(s) surface.

For selective desorption the bond energy between atoms A and a B(s) surface must be higher than the bond energy between atoms A and an A(s) surface. For the utilization of this condition, the processing temperature and the sequence time should be set to values which result in an effective desorption of atoms A from A(s) and a negligible desorption of atoms A from B(s).

For real surfaces the bond energy of atoms A on a B(s) surface may be a function of the filling density or the surface reconstruction of the BA(s) surface. Accordingly, the saturation of the surface reaction, eq. (1.3.1), does not necessarily result in full monolayer coverage but in a partial monolayer, determined by the energetically most favourable surface reconstruction at the temperature used. In the case of different surface reconstructions at different temperatures, saturation density versus process temperature may show threshold behaviour in the case of some single crystal surfaces.



such as CdTe in fig. 16 below, or a continuous temperature dependence as observed in the case of some polycrystalline or amorphous surfaces. In the latter case it might be more correct to refer to the change in saturation density as a consequence of the distribution of surface bond energies available on disordered surfaces. Ligands from compound reactants may essentially influence both the surface bond energies and the preferred surface reconstructions when compound reactants instead of elemental reactants are used.

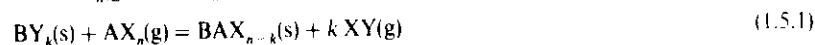
Additive ALE reactions based on the direct use of elements as the reactants are limited to compounds for which the elemental components have the necessary vapour pressure for practical processing. The II–VI compounds of Zn, Cd and S, Se, Te, can be processed by ALE using the elements as the reactants.

### 1.5. Exchange reactions using compound reactants

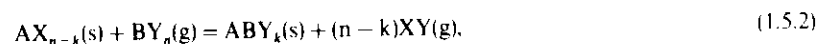
The use of compounds as the reactants extends the use of the ALE process to materials where the vapour pressures of the elemental components are too low to give rise to the additive mode of the ALE process. A basic requirement of a reactant is a reasonable vapour pressure at the processing temperature. Low vapour pressure of a reactant leads to slow processing, especially with large-area substrates. Other requirements of the reactant are a good reactivity with the surface it is reacting with and also that the surface formed after the reaction is reactive with the second reactant used.

Full advantage of the saturation of the surface reactions in ALE is obtained when the process is performed in thermal equilibrium. This also means that the reactant should be chemically stable at the processing temperature. In the case of additive ALE processes it was stated that the saturation densities of the monolayers are mainly determined by the surface reconstructions formed in each reaction sequence. In the case of compound reactants, the saturation densities are also subject to the effects of surface reconstructions, but they may also be determined by the physical sizes of the ligands of the reactant molecules. Ligands may suppress the formation of surface reconstructions. This may help in obtaining a "full monolayer per cycle" growth condition. The ligands have an important role in the surface reactions; accordingly, the choice of the compound reactants has a major effect on the ALE process.

In its simplest form the ALE reaction forming compound AB from compound reactants  $AX_n(g)$  and  $BY_n(g)$  can be described by the equations



and



where the reaction pathway is determined by the index  $k$ , which may have any value between 0 and  $n$ . The reaction pathway is complicated if thermal desorption of the ligands occurs on the surface. Any decomposition of the surface species results in a dependence of the reaction pathway on the dynamics of the process. Fast sequencing may utilize full ligand interaction and selective exchange reactions in the process, while slow sequencing causes the process to proceed through reconstructed A(s) or B(s)

surfaces and thermal desorption of the ligands in each sequence. The loss of ligands most probably reduces the selectivity of the surface. *This is probably a basic reason for the different results obtained in ALE of GaAs/TMGa + AsH<sub>3</sub> in different experimental setups* (section 3.1). Under dynamic process conditions the role of a non-inert carrier gas might also become important by enhancing the release of the surface ligands or by re-establishing the ligands. For example, H<sub>2</sub> as carrier gas may enhance the release of methyl groups and, on the other hand, it may re-establish O–H or As–H structures.

For a chemically balanced reaction cycle the release of ligands of each reactant has to be balanced. If one of the ligands is desorbed thermally, there is no exchange available for the ligands of the second reactant. This is an important difference between the sequential ALE reactions and the conventional homogeneous reactions. If the dynamics of the thermal release of the ligands is unbalanced, some additional interaction such as a chemically active transport gas, extra energy (photons, etc.) or an extra reaction step is needed.

Full or partial thermal release of the ligands in an ALE sequence results both in a temperature-dependent and in a sequence-time-dependent process. Surface ligands also have an important role in terminating open bonds on the surface and thereby in preventing the formation of surface reconstructions.

The doses of  $AX_n(g)$  and  $BY_n(g)$  must fulfil the requirements of saturation in the same way as discussed for elemental reactants. Highly reactive reactants are advantageous in an ALE process, i.e. the activation energy of each surface reaction should be low. On an atomic scale a low activation energy means a high probability of reaction at a hit of a gas molecule to a surface site. Macroscopically, a low activation energy can be seen as a high reaction speed and a high utilization factor of the reactant.

Saturation mechanisms of the exchange reactions are related to the reaction pathway. If the reactants used and the surface ligands formed in the surface reactions are stable in the timeframe of the cycle time used, the exchange reactions have a major role in the surface saturation. This type of reaction leads to a wide temperature window of saturation. When thermal dissociation of the reactants or thermal release of the surface ligands occurs, the saturation becomes more temperature sensitive as well as sensitive to other process parameters such as dosing, timing and type of inert gas.

The saturation density of an  $AX_{n-k}(s)$  surface is dependent on the reaction pathway, the surface reconstruction and the physical size of the ligands staying on the surface after the reaction. While the ligands may have an essential role in controlling the saturation mechanism, they may also have a very important role in blocking the formation of surface reconstructions while terminating dangling bonds on the surface.

In practical processing a purge sequence between each reaction sequence is needed. When compound reactants are used not only the surplus of the reactant vapour but also the gaseous reaction products or decomposition products are removed during the purge sequences.

### 1.6. ALE processing window

The most important parameter available to control the saturation mechanism of an ALE process is the processing temperature. A certain temperature is needed to keep the

reactants in the vapour phase, to supply the activation energies necessary for the reactions and to desorb extra surface species after monolayer formation. As a summary of the factors to be considered in choosing the reactants and the reaction temperature of an ALE process, fig. 7 defines the ALE processing-temperature window for monolayer saturation. For further characterization of an ALE process one can define ALE processing windows related to other process parameters such as the dose of each reactant and the timing of the reaction as well as the purge sequences. For any material to be processed by ALE, the choice of reactants is a major factor in determining the processing windows available.

Observation of the growth rate as a function of temperature gives a first indication of the limiting mechanisms of an ALE process. One should, however, note that the limiting mechanisms of saturation are individual to each reaction sequence and the growth rate characteristics reflect the total effect of the different sequences. With reference to the symbols in fig. 7:

- L1: An increasing growth per cycle at the low end of the processing window may indicate condensation of a reactant or the result of an exchange reaction.
- L2: A decreasing growth per cycle indicates an activation energy limited process (poor reactivity of a reactant).
- W1: A 1 ML per cycle growth indicates full monolayer saturation in each reaction cycle. It also indicates that the formation of surface reconstructions has been inhibited.
- W2: A less than 1 ML per cycle growth may indicate surface reconstruction in at least one of the monolayers formed. It may also indicate steric hindrance in a monolayer, probably due to large surface ligands. A decreasing growth per cycle with an increasing temperature may indicate surface sites with distributed bond energies. This is characteristic of disordered surfaces such as surfaces of polycrystalline and amorphous materials.
- H1: An increasing growth per cycle at the high end of the processing window may indicate formation of non-volatile cracking products from a reactant or a surface ligand.

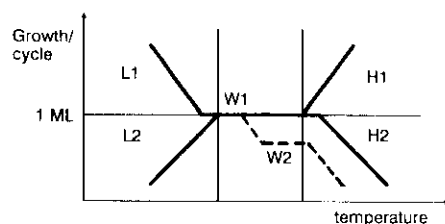


Fig. 7. Temperature windows of ALE processing. W1 denotes the part of the processing window where the saturation density is 1 ML/cycle. W2 denotes the part of the processing window where the saturation density is less than a monolayer/cycle. The meaning of L1, L2, H1 and H2 is explained in the text.

- H2: A decreasing growth per cycle at the high end of the processing window may indicate desorption of a monolayer formed or desorption or dissociation of a surface ligand essential to activate the surface for the next reactant.

## 2. ALE processing, reactors

### 2.1. ALE processing requirements

Table 1 summarizes some of the unique features of the ALE process and the related challenges in practical processing. For an efficient ALF reactor as many of the listed challenges as possible should be met.

Two types of conventional approaches to gas phase material processing are molecular beam epitaxy (MBE) and related vacuum processing methods and chemical vapour deposition (CVD) in its different forms (low pressure, metalorganic, plasma assisted, etc.). All these processes can be classified as flux-controlled or source-controlled methods of material growth. This means that the rate of growth is mainly controlled by the intensity of the reactant flux onto the substrate surface. By contrast, ALE can be classified as a surface-controlled process, which means that the rate of growth is controlled by the substrate surface rather than the incoming flux of the reactant. One consequence of this difference is that, for a uniform material thickness the flux of reactants to each section of the substrate area must be equal in MBE, CVD and related techniques while in ALE it is enough to provide a sufficient dose of reactants to each section of the substrate area. This gives extra freedom in the geometrical design of ALE equipment compared to MBE and CVD equipment. On the

Table 1  
Features of the ALE process and related challenges for practical processing

ALE process features	Challenges of ALE equipment and processing
Inherent control of growth rate (and uniformity)	Highly automated processing Large-area capability Large batch capability Freedom in reactant supply geometry
Atomic layer level control of material composition	Capability to produce multilayer structures of different materials or superlattices
Inherent stoichiometry control	Capability to produce complex compounds
Conformal coating characteristics	Capability to grow on non-planar surfaces and to provide coatings on porous materials
Separated supply of reactants, gas phase reactions eliminated	Favours highly reactive reactants, high material utilization possible High partial pressures of reactants possible

other hand, a special requirement of ALE equipment is fast sequencing of the reactants, supplemented by an effective purging between the sequences of reactant supply.

Any MBE or CVD system can be used in ALE mode provided that there are means for switching the fluxes of the reactants. The switching of the reactants alone does not make the process an ALE process. The characteristic feature of ALE is that each reaction sequence is fed to a saturated surface condition on the substrate, which means that the substrate temperature and the vapour pressures of the reactants as well as the reaction products must fulfil the requirements discussed in section 1.6.

## 2.2. The ALE reactor

The main building blocks of an ALE reactor are presented in fig. 8.

Atomic layer epitaxy processes can be carried out in vacuum or in an inert gas atmosphere. Any molecular beam epitaxy reactor can be operated in ALE mode by choosing a substrate temperature that fulfils the surface saturating conditions for each reactant and by sequencing the supply of reactants onto the substrates with necessary purge time between the sequences. Solid sources in an MBE system are most often Knudsen cells. For Knudsen cells the necessary sequencing can be obtained with standard shutters. If volatile reactants are used (often referred to as chemical (vapour molecular) beam epitaxy, CBE), sequencing can be performed with valves in the gas supply lines. Combination of Knudsen-cell sources and volatile gas sources in one process may result in poisoning of hot Knudsen cells in the vacuum chamber.

Chemical vapour deposition (CVD) reactors can be operated in ALE mode provided that there are means for independent valving of the sources. Most CVD reactors, especially metal-organic chemical vapour deposition (MOCVD) reactors, are designed for reactants which are volatile at room temperature. Most CVD reactors have a

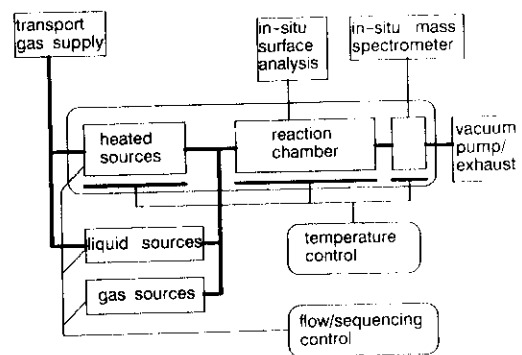


Fig. 8. Block diagram of an ALE reactor. The reaction zone may be in a vacuum system or an inert gas system at low pressure or at atmospheric pressure.

cold-wall design with inductive heating of the substrates. This minimizes the hot surface area and reduces undesirable growth on the reactor walls. In order to minimize gas phase reactions in a CVD process reactants which are too aggressive are avoided.

In MBE and MOCVD it is essential that, for uniform thickness, the reactant flux onto the substrate surface is uniform over the whole substrate area. In ALF, the rate of growth is controlled by the surface saturation mechanism. A uniform thickness in a material layer is achieved provided that the supply of each reactant is high enough for the saturation of every part of the substrate surface. This gives extra freedom and different boundary conditions for the design of ALE reactors. In a travelling-wave ALE reactor the reactants are fed through a cassette of substrates by an inert gas flow. A travelling-wave reactor utilizes multiple hits of reactant molecules on the substrate, which results in a high material utilization efficiency. The saturation mechanism of ALE ensures uniform thickness over the whole length of the substrate. Figure 9 summarizes some reactor constructions used for atomic layer epitaxy.

A travelling-wave reactor is typically a hot-wall reactor, which means that growth also occurs on the surfaces of the reaction chamber. In the F-120 (Microchemistry Ltd) travelling-wave reactor the reaction chamber is formed by the 1 mm spacing between two  $50 \times 50 \text{ mm}^2$  substrate faces, which minimizes extra surfaces subject to undesirable material growth (fig. 9e). Material growth on the walls of the reactant supply tubes can be avoided by supplying the different reactants through different tubes as close to the reaction chamber as possible. A great advantage of the travelling-wave reactor is that it is easily scalable to large substrates and to very large batches. At laboratory scale the travelling-wave reactor is an effective tool for studying the reaction kinetics of the ALE process. Figure 10 summarizes different types of thickness profiles which can be observed in a travelling-wave reactor. The profile type can be used to characterize the ALE process.

For in situ observation of the reactions, a mass-spectrometer can be used to monitor the exhaust of a travelling-wave reactor. In order to detect low vapour pressure exhausts the mass gauge as well as the gas sample line must be heated [5].

Sequencing, which is a characteristic feature of an ALE process, can be performed either by valving the fluxes of the reactants or by using a moving substrate holder which exposes the substrates sequentially to fluxes of different reactants. Examples of ALE reactor constructions using rotating substrate holders for sequencing are presented in [2] and [6], see also figs. 9b and 9c. Advantages of a rotating substrate holder are a high sequencing speed, reliable operation and easy application to different types of reactants, including reactants which need high-temperature sources. A disadvantage of systems based on rotating substrate holders is a smaller flexibility to achieve the complex sequences needed in superlattices or multilayer structures. Also scaling up of systems with moving substrates is more difficult than for systems with static substrates.

## 2.3. ALE cycles, dosing of the reactants

In an ALE process the rate of growth is proportional to the speed of sequencing of the reactants and to the saturation density of the reactants. A full ALE cycle consists of

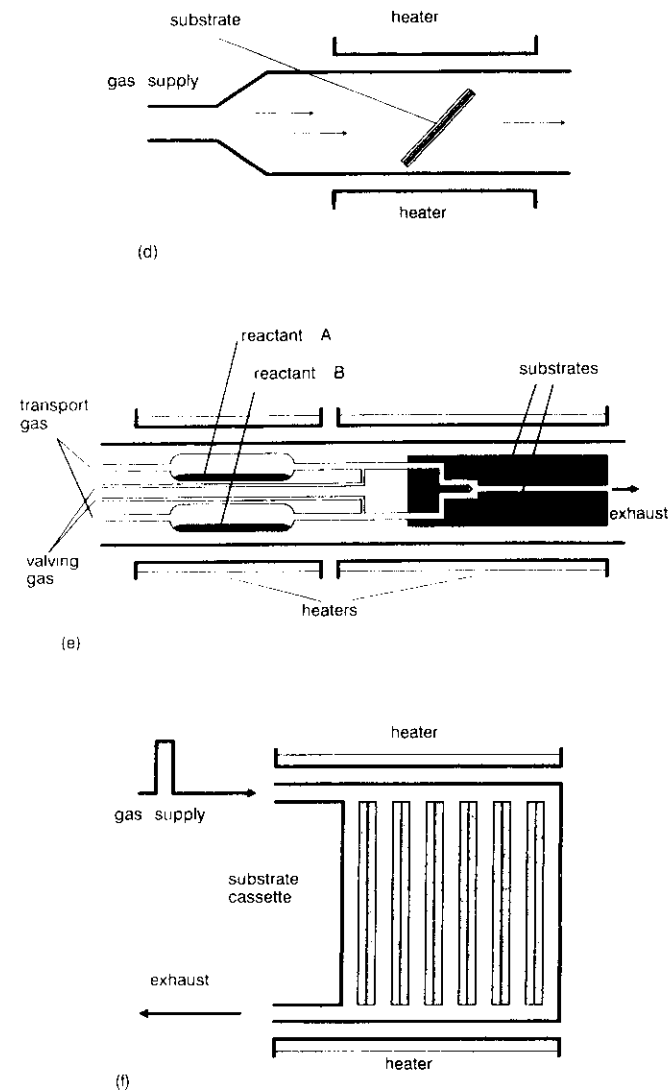
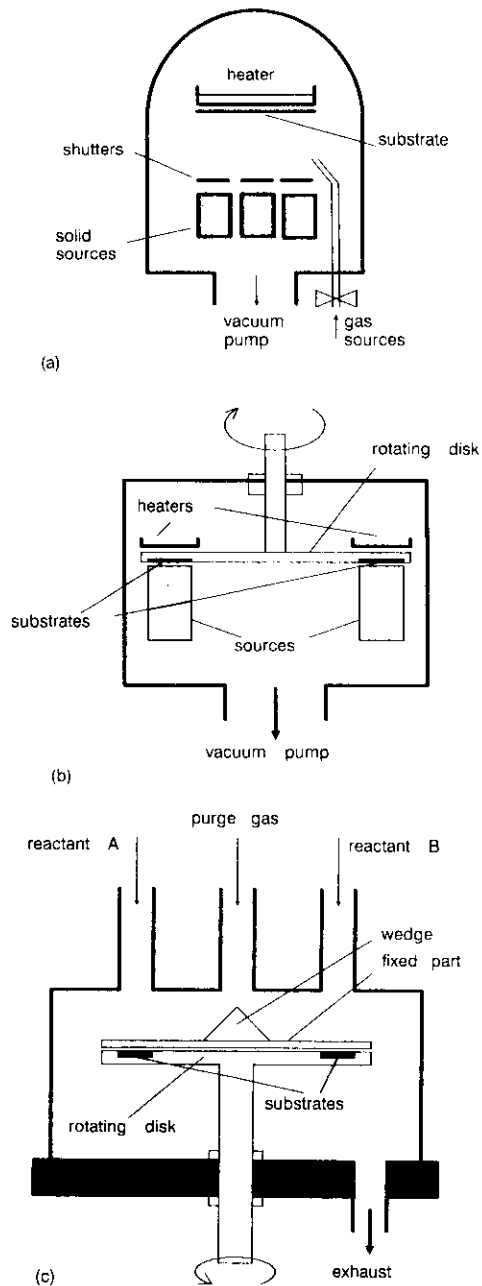


Fig. 9. ALE reactors. (a) High-vacuum (MBE-type) system with Knudsen-cell solid sources and gas inlet for volatile reactants. Sequencing of solid sources is carried out by mechanical shutters. (b) High-vacuum reactor with a rotating substrate holder [2]. (c) CVD-type reactor utilizing rotating disk for sequencing. Purging and separation of the different reactants is enhanced by a purge gas supplied to the center of the rotating disk (by Colter et al. [6]). (d) Flow-tube-type reactor often used in atmospheric-pressure CVD. For cold-wall operation inductive heating of the substrate is used. (e) A "travelling-wave" ALE reactor comprising hot-wall design, fast flow-dynamics and inert-gas-valved hot sources (by Microchemistry Ltd). (f) A cassette design of a travelling-wave reactor for production quantity processing (by Microchemistry Ltd).

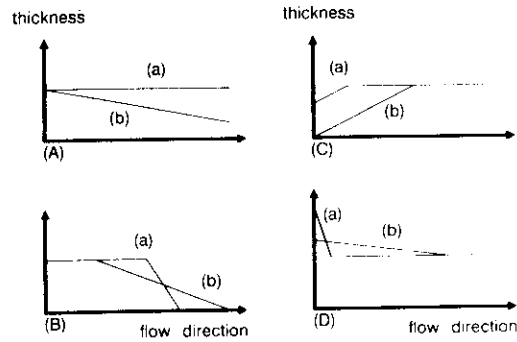


Fig. 10. Characterization of ALE processes by observing the thickness profile of the film grown on a substrate (in the direction of transport gas flow). (A) A good ALE process: sufficient dosing and purging, good saturation. (B) Study of reactivity by using insufficient dosing of a reactant: (a) good reactivity is observed as a steep ending profile, (b) poor reactivity is observed as a shallow ending profile. (Must be studied separately for each reaction sequence.) (C) (a) Slight, (b) strong desorption of formed monolayer occurs (too high temperature, too long purging). (D) (a) Slight, (b) strong effect of insufficient purging (a CVD-type growth component observed at the feeding end of the substrate).

reactant supply sequences and a purge sequence after each reactant sequence (fig. 11).

The dose of reactant needed in a sequence is determined by the total surface area of the substrates, the saturation density, the reaction probability per hit and the hitting efficiency. In vacuum systems and in cold-wall CVD systems the hitting efficiency is generally less than one, i.e. only a fraction of the reactant flux hits the substrate surface. In a travelling-wave reactor the hitting efficiency may be orders of magnitude greater than one, i.e. reactant molecules which hit the surface but do not react make another hit or several further hits onto the substrate before leaving the reaction chamber. In the following we study the dosing requirements for monolayer saturation; we will use  $d_r$  to denote the dose of the reactant (reactant molecules per substrate surface unit area supplied from the source to the reaction chamber in one sequence ( $\text{cm}^{-2}$ )).  $t_r$  is the length of the reactant supply sequence(s),  $\text{eff}_h$  is the hitting efficiency (apparatus parameter, it represents the number of hits on the substrate per number of reactant molecules in the dose),  $h = d_r \text{eff}_h / t_r$  is the hitting density of the reactant on the substrate ( $\text{cm}^{-2} \text{s}^{-1}$ ) and  $\text{eff}_r$  is the reaction efficiency (process parameter, it represents the reaction probability per hit).

When assuming an immediate desorption of  $A(g)$  atoms hitting the  $A(s)$  surface formed and no surface mobility or precursor states of  $A$  atoms on  $B(s)$  or  $A(s)$  surfaces, the build-up of an  $A(s)$  surface proceeds as

$$d[A(s)]/dt = h \text{eff}_r [1 - A(s)/A_s] - A(s)R[A, B(s)], \quad (2.3.1)$$

where  $A_s$  is the saturation density of  $BA(s)$  surface and  $R[A, B(s)]$  the desorption rate of the  $A(s)$  surface formed.

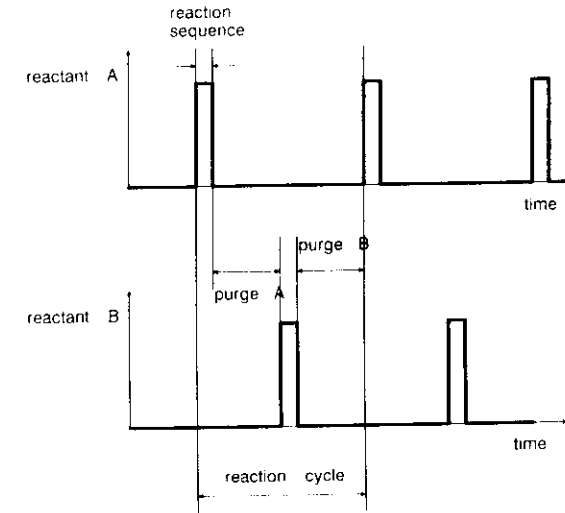


Fig. 11. Definition of reaction and purge sequences.

If the desorption of the formed  $A(s)$  surface is neglected, a simple asymptotic approach to saturation occurs, see fig. 12,

$$A(s) = A_s \{1 - \exp[-t/t_s]\}, \quad (2.3.2)$$

where  $t_s$  is the saturation time-constant and equals  $A_s/(h \text{eff}_r)$ .

With the pre-assumptions above, an effective dose per unit area  $d_r$  needed for a reasonable saturation of an  $A(s)$  surface must be well in excess of the saturation density  $A_s$  of the  $A(s)$  surface. In practice, the perfection of the saturation and the dose needed are highly dependent on the specific surface conditions, such as the reaction probability upon a hit (often referred to as the reaction speed), possible precursor states, surface mobilities on filled and non-filled surface areas, surface reconstructions, preferred nucleation mode and desorption rate.

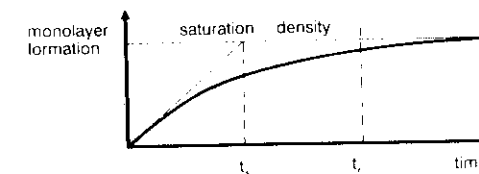


Fig. 12. Build-up of an  $A(s)$  surface.

The filling density obtained in a reaction sequence time  $t_r$  can now be expressed as

$$a(s) = a_s \{1 - \exp[-t_r/t_s]\} = a_s \{1 - \exp[-d_r \text{eff}_h \text{eff}_r/a_s]\}. \quad (2.3.3)$$

In a "single-shot" reactor remarkable overdosing is necessary for a satisfactory saturation,

$$d_r \text{eff}_h \text{eff}_r \gg a_s. \quad (2.3.4)$$

If one assumes a residence time and a certain surface migration of the reactant on the filled surface sites, the filling of the surface approaches a linear filling mode, i.e. molecules hitting the substrate surface migrate into empty sites until saturation is obtained. In such a case the material utilization efficiency is limited by the flux efficiency only and the effective dose approaches the number of surface sites:

$$d_r \text{eff}_h = a_s. \quad (2.3.5)$$

Surface migration is a part of the reaction kinetics which is characteristic of the reactants, the reacting surface and the processing conditions used.

Material utilization efficiency in an ALE process can be improved with hot-wall reactor designs, such as the travelling-wave reactor described in fig. 9e. In such a reactor the primary hitting efficiency is close to unity and an "effective hitting density" is obtained as the sum of the primary hits plus secondary hits created by reactant molecules desorbed after the first hit, i.e.  $\text{eff}_h \gg 1$ .

In a travelling-wave reactor the number of hits by a reactant molecule on the substrate is proportional to the ratio of the thermal speed of the molecules to the drift speed of the travelling wave. Typically the thermal speed of the reactant molecules is 100 to 1000 times higher than the drift speed of the travelling-wave, which results in an effective multiple hit condition in the reaction chamber. The number of hits is also dependent on the reactor geometry and the diffusion constant of the reactant in the transport gas. A high diffusion constant is advantageous for high hitting efficiency, which can be obtained at a low transport gas pressure. While the reactant carrying capability of the transport gas is directly proportional to the pressure, the optimal pressure of the transport gas is a compromise between the diffusion and the reactant transport efficiency.

In a travelling-wave reactor the density of reactant molecules is gradually decreased while passing the substrate surfaces as a consequence of surface reaction, i.e. the effective hitting rate decreases in the direction of the flow. Due to the multi-hitting condition the material efficiency may still be high, provided that the number of hits per unit surface area stays higher than the product of reaction efficiency and saturation density of the monolayer for the whole length of the substrate.

#### 2.4. Transport of the reactants

In high-vacuum systems the dosing and the transport of the reactants do not generally need any special arrangements. The reactant fluxes are simply directed to the substrates from Knudsen-cell-type evaporation sources or through valves from separate gas

sources. Pulsing is carried out either by mechanical shutters in the vacuum vessel or by fast valves for externally fed reactants.

In CVD-type equipment inert gas can be used for reactant transport both from internally heated sources and from external gas sources. In the case of gas sources the use of a transport gas is necessary if the system pressure is higher than the vapour pressure of the reactant in the gas source.

The dose of reactant needed to give a monolayer coverage on substrates with a total surface area  $A$  ( $\text{m}^2$ ) can be expressed as

$$D_r = a_s A / \text{eff}_R \quad (\text{molecules}), \quad (2.4.1)$$

where  $\text{eff}_R$  is the reactant utilization efficiency. The reactant molecule density  $n_r$  in a gas can be expressed as

$$n_r = p_r / kT \quad (\text{m}^{-3}), \quad (2.4.2)$$

where  $p_r$  is the partial pressure of the reactant in the source (Pa),  $k$  Boltzmann's constant ( $\text{J/K}$ ) and  $T$  the temperature (K).

In order to express the necessary transport flow for a reactant with a source vapour pressure  $p_r$ , we still need the following definitions:  $p_s$  is the partial pressure of the transport gas (Pa),  $p_c$  the source pressure ( $p_c = p_r + p_s$ ) (Pa),  $r = p_r/p_c$  is the reactant pressure ratio,  $t_r$  is the time of the reactant dosing sequence (s),  $T_0$  is room temperature, where the gas flow is measured (300 K),  $T_c$  is the temperature of the reactant source (where the partial pressure  $p_r$  was generated) (K),  $T_r$  is the temperature of the reaction chamber (K),  $F_c$  is the transport gas flow at room temperature ( $\text{Pa m}^3/\text{s}$ ),  $F_s$  is the gas output from a source ( $F_s = (1-r)^{-1} F_c T_c T_0^{-1}$ ) ( $\text{Pa m}^3/\text{s}$ ),  $F_r$  is the gas flow in the reaction chamber from non-activated sources to the reaction chamber ( $\text{Pa m}^3/\text{s}$ ) and  $F_t$  is the total gas flow in the reaction chamber ( $F_t = F_r + F_s T_r/T_c$ ) ( $\text{Pa m}^3$ ).

A dose of reactant supplied from a source, see fig. 13, can now be expressed as

$$D_r = t_r F_s (p_r n_r) = t_r F_s r / kT_c \quad (\text{molecules}). \quad (2.4.3)$$

By combining eqs. (2.4.1) and (2.4.3) we can express the source output flow as

$$F_s = A a_s k T_c (r \text{eff}_R t_r) \quad (\text{Pa m}^3/\text{s}). \quad (2.4.4)$$

The necessary transportation-gas input flow supplied at room temperature will be

$$F_c = (T_0/T_c)(1-r)F_s = [A a_s k T_0 (1-r) / r] / \text{eff}_R t_r \quad (\text{Pa m}^3/\text{s}), \quad (2.4.5)$$

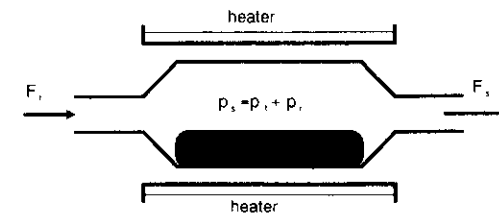


Fig. 13. Supply of reactants by transport gas.

or the necessary length of a reactant transport sequence is

$$t_r = [Aa_s/\text{eff}_R kT_0(1-r)/r]/(\text{eff}_R F_i) \quad (2.4.6)$$

For volatile reactants dosed without a transport gas the necessary dose in the reaction chamber can be expressed using eq. (2.4.4) simply by setting  $r = 1$ . The necessary flow from a source is then

$$F_s = Aa_s kT_s/(\text{eff}_R t_r) \quad (2.4.7)$$

*Example:* ALE growth of CdS from the elements, Cd and S<sub>8</sub>, on two 50 × 50 mm<sup>2</sup> substrates at 380°C temperature in a travelling-wave reactor (fig. 9e). Then  $A = 50 \text{ cm}^2 = 5 \times 10^{-3} \text{ m}^2$ ,  $a_s(\text{Cd}) = 1.5 \times 10^{19}/3 = 5 \times 10^{18}$  atoms/m<sup>2</sup> (saturation density  $\frac{1}{3}$ ),  $\text{eff}_R = 0.8$ ,  $k = 1.38 \times 10^{-23} \text{ J/K}$ ,  $t_s = 0.2 \text{ s}$  and  $r = 0.01$ . If sulphur vapour is assumed to be S<sub>2</sub> S<sub>8</sub> the number of molecules needed to give the  $\frac{1}{3}$  saturation density is  $a_s(\text{S}) < 0.25 \times 10^{14}$  molecules/cm<sup>2</sup> or  $< 2.5 \times 10^{17}$  molecules/m<sup>2</sup>. By applying eq. (2.4.5) the transport flow for Cd can now be expressed as

$$\begin{aligned} F_i(\text{Cd}) &= 5 \times 10^{-3} \times 5 \times 10^{18} \times 300 \times 1.38 \times 10^{-23} \times 99/(0.2 \times 0.8) \\ &= 6.4 \times 10^{-3} \text{ (Pa m}^3/\text{s)} = 640 \text{ (mbar cm}^3/\text{s)}. \end{aligned}$$

Due to the S<sub>2</sub> - S<sub>8</sub> molecule, the transfer flow for sulphur is less than one half of the flow needed for cadmium. Accordingly,

$$F_i(\text{S}_2) > 320 \text{ (mbar cm}^3/\text{s)}$$

for a 0.2 s reactant supply sequence.

If the total pressure of the sources is 10 mbar, we need a partial vapour pressure of 0.1 mbar for each reactant to obtain  $r = 0.01$ . The source temperatures needed for the 0.1 mbar partial pressures of Cd and S<sub>2</sub> are about 340 and 150 C, respectively. In a hot-source reactor, it is important that there is no decrease of temperature between the source and the reaction chamber in order to avoid condensation of the source materials. Accordingly, a reaction temperature equal to or in excess of 340 C is required.

The choice of the total flow and the total pressure of the system is a compromise between inert gas valving, transportation of reactants, speed, inert gas consumption, material utilization efficiency, system cost, etc. In small reactors, as in the example above, a useful pressure range is 5–20 mbar. In bigger reactors for large substrates a pressure range 1–5 mbar is more nearly optimal.

### 2.5. Valving with inert gas flow

Valving of the reactants is a characteristic feature of the ALE process. For gas sources at room temperature valving can be performed simply using fast solenoid valves in the reactant supply lines directly. Valving of low vapour pressure reactants from heated sources is technically much more difficult. Valving must be performed at a high temperature and the reactants are typically aggressive chemicals. The speed and reliability requirements of the valving are very high because there might be thousands

of valvings in one ALE process. An effective way of performing the valving of high-temperature sources is the use of inert gas flows to block and open the gas flow from the sources to the reaction chamber [7, 8] (fig. 14).

The basis of inert gas valving is a blocking of transport flow and diffusion of the reactant with a laminar flow of inert gas. In a one-dimensional case, which can be applied to tubes, we can get the speed of a diffusion front by solving the diffusion equation

$$dp_i/dt = D d^2 p_i/dx^2 \quad (2.5.1)$$

If the source is opened to a tube at  $t = 0$ , the partial pressure of the reactant  $p_r(x, t)$  in the tube (without inert gas flow) starts to develop as

$$p_r(x, t)/p_{r0} = \text{erfc}(x/2\sqrt{Dt}), \quad (2.5.2)$$

where  $p_{r0}$  is the partial vapor pressure of the reactant in the source and  $x$  the distance from the source (in the tube). For a fixed  $p_r(x, t)/p_{r0} = c$  ratio we get

$$x/2\sqrt{Dt} = \text{erfc}^{-1}(c) \quad (2.5.3)$$

or

$$x/2\sqrt{Dt} = C_c, \quad (2.5.4)$$

where the  $\text{erfc}^{-1}(c)$  function has been replaced by the content ratio factor  $C_c$ , which has a fixed value for any  $p_r/p_{r0}$  ratio. If a limited diffusion source is assumed, the solution of the diffusion equation (2.5.1) is a Gaussian function instead of the erfc function and eq. (2.5.4) applies by counting the content ratio factor  $C_c$  as a Gaussian function.

	$\text{erfc}^{-1}(c)$
$p_r/p_{r0} = 10^{-1}$	$C_c(-1) = 1.2$
$p_r/p_{r0} = 10^{-2}$	$C_c(-2) = 1.8$
$p_r/p_{r0} = 10^{-3}$	$C_c(-3) = 2.3$
$p_r/p_{r0} = 10^{-4}$	$C_c(-4) = 2.8$
$p_r/p_{r0} = 10^{-5}$	$C_c(-5) = 3.2$
$p_r/p_{r0} = 10^{-6}$	$C_c(-6) = 3.6$

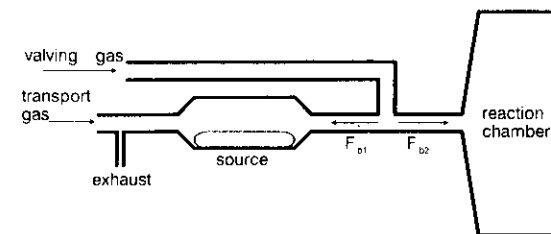


Fig. 14. Two-way blocking flows  $F_{b1}$  and  $F_{b2}$  between a source and the reaction chamber.

The speed of a front for a given  $C_c(p_i/p_{i0})$  value can be obtained by solving  $dx/dt$  from eq. (2.5.4):

$$dx/dt = 2C_c(p_i/p_{i0})2D/x \quad (2.5.5)$$

Equation (2.5.5) gives the speed of a  $(p_i/p_{i0})$ -front as a function of  $x$ . By setting a blocking speed  $v_b$  of an inert gas in the opposite direction we can express the blocking distance  $X_b$  as a function of the ppm-level blocking speed  $v_b$  as

$$X_b = 2C_c(-6)^2 D/v_b. \quad (2.5.6)$$

The diffusion constant  $D$  in the gas can be expressed as

$$D = (2/3d^2)(kT_0)^{3/2} \langle m \rangle^{-1/2} / p \quad (\text{m}^2/\text{s}), \quad (2.5.7)$$

where  $d$  is the diameter of a gas molecule (m),  $m$  the mass of a gas molecule (kg) and  $p$  the pressure (Pa). Most often the diffusion constants are based on experimental values. Useful information in eq. (2.5.7) is the temperature and pressure dependence of the diffusion constant:

$$D = D_0(T/T_0)^{3/2}(p_0/p) \quad (\text{m}^2/\text{s}), \quad (2.5.8)$$

where  $D_0$  is the diffusion constant at  $T_0, p_0$ . By combining eqs. (2.5.6) and (2.5.8) and by expressing the blocking flow as

$$F_b = F_{b0}T/T_0 = pv_bA \quad (\text{Pa m}^3/\text{s}), \quad (2.5.9)$$

where  $F_{b0}$  is the blocking gas flow measured at  $T_0$  and  $A$  the cross section of the blocking channel, we can derive an expression for the ppm-blocking length of a flow channel with a cross section  $A$  as

$$X_p = (2C_c(-6)^2 D_0 p_0 (T/T_0)^{0.5} A) / F_{b0}. \quad (2.5.10)$$

Expression (2.5.10) states that the blocking length is independent of the pressure when the gas flow is used as a parameter. At high pressure both the diffusion constant and the speed of the blocking flow are low; at low pressure both of them are high.

*Example:* To block a sulphur source at ppm level in a 10 cm long feeding tube of 0.3 cm in diameter at a temperature of 140 °C, we need a blocking flow of

$$F_{b0} = \{2 \times 13 \times 180 [(140 + 293)/293]^{0.5} \times 0.3^2/4\} / 10 = 39.3 \text{ (mbar cm}^3/\text{s)},$$

since  $D_0 p_0 = 180 \text{ cm}^2/\text{s mbar}$  and  $T_0 = 20^\circ\text{C} = 293 \text{ K}$ .

## 2.6. Purge time

The widening of "a travelling wave of a reactant" can be estimated from the diffusion equation by assuming a limited source instead of a constant diffusion source and by applying the analysis derived for static blocking to blocking of the "moving source" presented by the travelling-wave of the reactant.

In practice, the gas volume in the reaction chamber is changed very quickly. In an F-120 reactor the typical flow speed in the reaction zone is of the order of 10 m/s, which

means that the gas volume in the reaction chamber is changed in about 5 ms. This is faster than the valving times and the purge time will be determined mainly by the geometry and the chemistry of the surfaces.

For a fast travelling-wave reactor it is important that the valving takes place close to the reaction chamber. Also, to optimize the necessary gas flow, it is advantageous to minimize the flow cross section in the reaction chamber. This supports the use of cassette-type substrate holders in travelling-wave reactors of industrial size. A limit on the packaging density of the substrates is set by the gas conductivity of the flow channels between the substrates.

With a good gas flow design, sequence times of the order of a second can be achieved also with large-area substrates and big cassettes of substrates. This results in a high throughput and a high production efficiency of the ALE reactor.

## 3. ALE processes for different materials

### 3.1. II-VI compounds

#### 3.1.1. Cadmium sulphide (CdS)

*3.1.1.1. CdS/Cd + S.* Cadmium sulphide can be produced by ALE using an additional reaction of the elements [9]. On an amorphous  $\text{Al}_2\text{O}_3$  substrate a growth rate of about  $\frac{1}{3}$  of a monolayer per cycle can be observed at growth temperatures between 350 and 420 °C (fig. 15). CdS grown from the elements shows  $\beta$ -cubic crystalline structure primarily oriented in the (111) direction.

*3.1.1.2. CdS/CdCl<sub>2</sub> + H<sub>2</sub>S.* CdS grown from  $\text{CdCl}_2$  and  $\text{H}_2\text{S}$  shows a growth rate of 1 ML/cycle [8]. Due to the low vapour pressure of  $\text{CdCl}_2$  a minimum growth

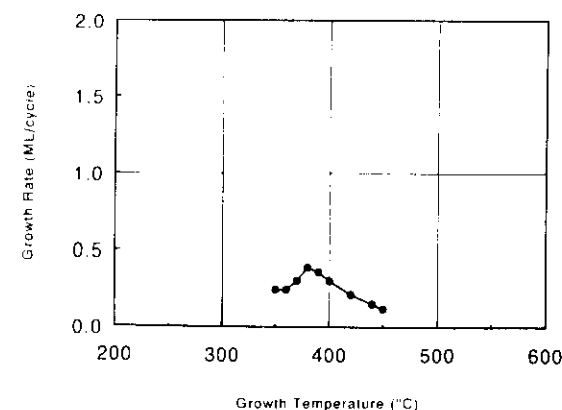


Fig. 15. Growth characteristics of  $\text{CdS} = \text{Cd} + (1/m)\text{S}_n$  [8].



temperature of 470°C was needed. The crystalline structure of the CdS was observed to be sensitive to the starting surface. On an amorphous  $\text{Al}_2\text{O}_3$  surface the CdS showed a mixture of cubic and hexagonal structures. When a few atomic layers thick indium oxide interface layer was grown on the alumina, the CdS layer showed pure hexagonal crystalline structure.

### 3.1.2. Cadmium selenide (CdSe)

There are no published works on ALE of CdSe. According to the author's experience CdSe can be grown from the elements at temperatures between 350 and 450 °C.

### 3.1.3. Cadmium telluride (CdTe)

**3.1.3.1. CdTe/Cd + Te.** As with most of the II-VI compounds, CdTe can be most conveniently grown using elemental reactants. The growth rate is temperature dependent and controlled by surface reconstructions. Faschinger and Sitter [10] have grown monocrystalline (10%) CdTe on (100) GaAs. At substrate temperatures between 260 and 290 °C the growth rate is one monolayer per cycle. At higher temperatures the rate decreases to 0.5 ML/cycle and stays at this value until it decreases exponentially at temperatures near 400 °C (fig. 16). RHEED patterns of the Cd and Te saturated surfaces show basically similar surface reconstructions at the different temperature ranges where growth rates of 1 and 0.5 ML/cycle were observed. For Cd stabilized surfaces the typical reconstruction was a mixture of  $(2 \times 1)$ - $(2 \times 2)$  and for Te stabilized surfaces  $(2 \times 1)$  [11].

CdTe on *p*-type CdTe (100) and (111)A substrates has been grown at temperatures of 120–270 °C. The best crystal structure was obtained in the temperature range 220–270 °C [12–14].

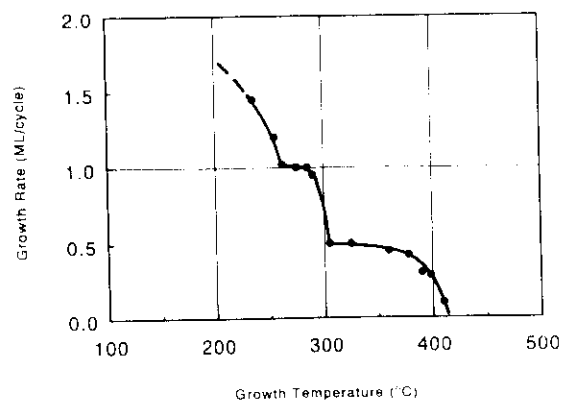


Fig. 16. ALE processing characteristics of CdTe: Cd + Te. Several saturation densities can be observed [10].

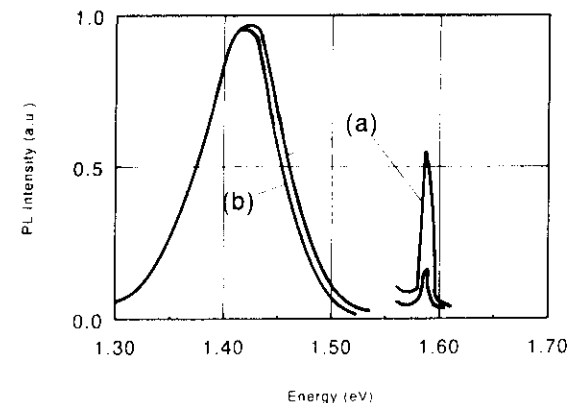


Fig. 17. PL spectra of polycrystalline CdTe [16]. Thickness of sample (a) is 2060 nm and of sample (b) 1060 nm. For sample (b) the intensity of the peak at 1.45 eV is monitored using  $\times 10$  amplification compared to other peaks.

ALE-grown CdTe on amorphous substrates shows good crystallinity. Figure 17 shows the PL spectra measured from two samples having different CdTe layer thicknesses. The growth of the samples has been carried out at 430 °C [15]. The bound-exciton peak is relatively higher by a factor of three for sample (a), of thickness 2060 nm, than for sample (b), of thickness 1060 nm, in fig. 17. The crystalline quality of the thicker sample is somewhat better than that of the thin one. It should be noted that the luminescence radiation originates mostly from the surface layer of the sample, so it would be more correct to say that the crystalline quality of the surface layer improves with increasing layer thickness [16].

### 3.1.4. Zinc sulphide (ZnS)

**3.1.4.1. ZnS<sub>2</sub>/Zn + S.** ALE was demonstrated for the first time by growing ZnS using elemental zinc and sulphur as the reactants [2]. On a glass substrate the growth rate was typically about  $\frac{1}{3}$  of a monolayer per cycle. The growth can be carried out in a temperature range of 250 to 450 °C. The rate of the growth decreases with increasing temperature. The growth rate can be enhanced within certain limits by fast sequencing and by high dosing of the reactants.

**3.1.4.2. ZnS/ZnCl<sub>2</sub> + H<sub>2</sub>S.** The ZnCl<sub>2</sub> + H<sub>2</sub>S (zinc chloride + hydrogen sulphide) ALE process for ZnS was developed in the 1970s to meet the requirements of electroluminescent display devices [3]. In spite of the practical goal of the development, some quantum chemical studies of the mechanism of the process were carried out [17, 18].

Results from quantum chemical calculations of the initial (low-coverage) chemisorption of ZnCl<sub>2</sub> and H<sub>2</sub>S were extrapolated to saturated surface configurations with

molecular modelling techniques [17, 18]. The chemisorption of  $\text{ZnCl}_2$  on the polar sulphur-ending (002) crystal face of hexagonal ZnS was taken as the starting point for the investigation. The first step of the ALE reaction is critically important since different adsorption modes and thus surface coverages of  $\text{ZnCl}_2$  lead to different growth mechanisms.

The single  $\text{ZnCl}_2$  adsorbate, binding from the zinc atom to the surface sulphur atom, forms a stable surface complex. Linear in the gas phase, the adsorbate will bend at the surface. This associative adsorption of  $\text{ZnCl}_2$  is energetically favourable compared to the dissociative adsorption at two sulphur atoms (fig. 18).

When the interactions between different  $\text{ZnCl}_2$  adsorbates on the ZnS surface were taken into account, two extreme modes of adsorption were obtained.  $\text{ZnCl}_2$  adsorbates at adjacent sulphur centres were shown to associate, forming a bridged structure. For adsorbates at next-nearest-neighbour sites, however, the bridging is no longer possible, and the optimum adsorbate orientations are determined by the chlorine-chlorine repulsion. For the independently chemisorbed  $\text{ZnCl}_2$ , the maximum surface coverage was  $\frac{1}{3}$  of the sulphur sites, whereas for the linear bridged  $\text{ZnCl}_2$  chains it was  $\frac{1}{2}$ . Two different growth mechanisms were developed on the basis of these different adsorption modes.

The  $\text{ZnCl}_2$  overlayers on ZnS expose zinc and chlorine atoms to the  $\text{H}_2\text{S}$  adsorbates. The strongest interaction can be expected between the zinc and sulphur atoms. A clear difference was found for the  $\text{H}_2\text{S}$  interaction between the chained  $\text{ZnCl}_2$  overlayer and the independently chemisorbed  $\text{ZnCl}_2$  surface. In the  $\text{ZnCl}_2$ -chain case the reduction of the chlorides by the hydrogens of the  $\text{H}_2\text{S}$  leads to the formation of ZnS chains with energetically favoured proper six-membered ring structure. HCl is released in the exchange reaction. When the independently chemisorbed  $\text{ZnCl}_2$  initiates the reaction, the critical step is the release of HCl. In this case an additive reaction of  $\text{H}_2\text{S}$  to the adsorbed  $\text{ZnCl}_2$  molecules is preferred.

The chain mechanism, see fig. 19, was shown to give a new ZnS surface layer in two  $\text{ZnCl}_2$  -  $\text{H}_2\text{S}$  cycles, whereas the mechanism initiated by independently chemisorbed  $\text{ZnCl}_2$  needed three cycles. In the first case HCl was released only after the exposure to

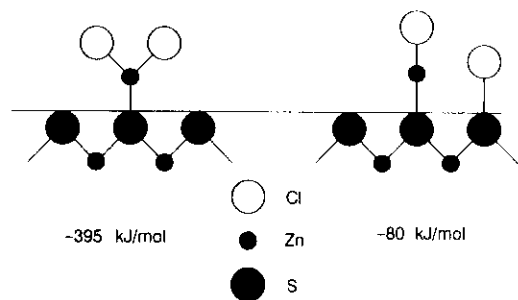


Fig. 18.  $\text{ZnCl}_2$  adsorbate on an S-surface.

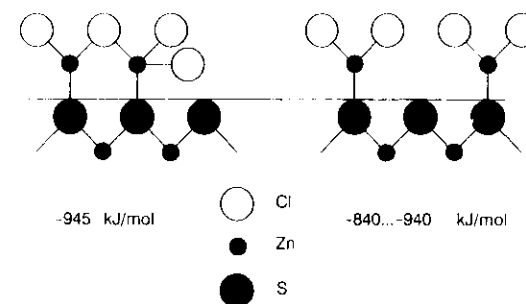


Fig. 19. Build-up of Zn-S bonds.

$\text{H}_2\text{S}$ . In the second case HCl was, on average, released both after the exposure to  $\text{ZnCl}_2$  and to  $\text{H}_2\text{S}$ .

A mass-spectroscopic study of the ALE of ZnS using  $\text{ZnCl}_2$  and  $\text{H}_2\text{S}$  as the reactants showed HCl production after the  $\text{H}_2\text{S}$  sequence but not after the  $\text{ZnCl}_2$  sequence [5]. This suggests the reactions:

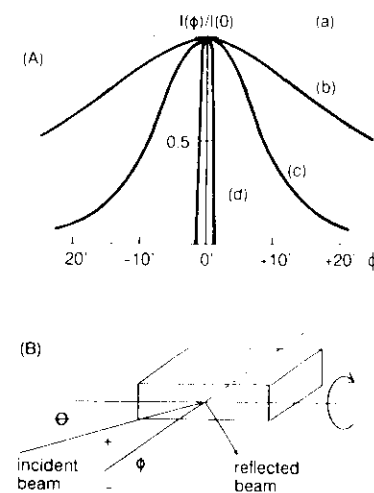
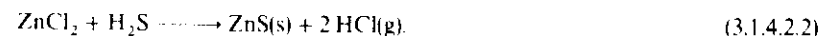


Fig. 20. (A) X-ray diffraction results for ZnS [19]. (a) Polycrystalline ZnS powder. (b) ZnS film grown at 350 C. (c) ZnS film grown at 500 C. (d) Si single crystal (as a reference of the width of a single crystal peak). (B) Test setup for (A).

ZnS grown from  $\text{ZnCl}_2$  and  $\text{H}_2\text{S}$  on  $\text{Al}_2\text{O}_3$  thin films made by ALE on soda-glass substrates shows hexagonal or cubic crystalline structure depending on the temperature of the growth. The thin films grown at or below  $350^\circ\text{C}$  were found to be polycrystalline, mainly cubic structures. In thin films grown at  $500^\circ\text{C}$  purely hexagonal X-ray diffraction peaks can be observed [19-21].

The ZnS films, having thicknesses in the range 10–500 nm, were strongly oriented with the (001) hexagonal or (111) cubic direction perpendicular to the substrate. Figure 20 shows the degree of orientation of samples grown at  $350$ – $500^\circ\text{C}$  measured by the reflection method.

Zero phonon lines of ZnS thin films grown on  $\text{Al}_2\text{O}_3$  thin films confirm the high crystalline perfection of the material [22].

**3.1.4.3. ZnS/ $\text{Zn}(\text{CH}_3\text{COO})_2$  (zinc acetate) +  $\text{H}_2\text{S}$ .** successful growth of ZnS using zinc acetate and hydrogen sulphide as the reactants has been reported [16] at  $290$ – $360^\circ\text{C}$ .

Ellipsometric study of the optical properties of ZnS grown by  $\text{Zn}(\text{CH}_3\text{COO})_2$  on a soda-glass substrate showed high-density film with good crystallinity [23]. From the refractive index results, the volume fraction of ZnS was 0.95–0.97, except in a 200 nm thick interface region against the amorphous substrate. The ZnS films studied had a columnar structure with large crystallites.

**3.1.4.4. ZnS/ $\text{DMZn}$  (dimethylzinc) +  $\text{H}_2\text{S}$ .** The growth has been carried out at atmospheric pressure in the temperature range  $25$ – $500^\circ\text{C}$ . Close to 1 ML/cycle growth was observed over the whole temperature range. The grain size of the resulting polycrystalline film obtained on single crystal silicon wafers on Corning 7095 glass increases with increasing temperature. The reaction cycle time used was typically 3 s [24].

ZnS has been grown using dimethyl zinc and  $\text{H}_2\text{S}$  cracked at temperatures of  $950$  and  $1080^\circ\text{C}$ , respectively [25]. The process was carried out in a vacuum system. The substrate was a (001) oriented GaAs surface. With the cracking conditions used 90% of the DMZn and 65% of the  $\text{H}_2\text{S}$  were estimated to be decomposed. A full monolayer per cycle growth was observed at  $250$ – $310^\circ\text{C}$ , see fig. 21, curve (a). The growth speed of ZnS when elemental Zn and S are used as the reactants is typically about  $\frac{1}{3}$  monolayer [2]. One has to assume that the non-cracked compound reactants have a role in the surface reactions. This was also supported by ZnS grown on a borosilicate-glass substrate from DMZn and  $\text{H}_2\text{S}$  without crackers by Yamaga and Yoshikawa [26]. A wide 1 ML/cycle temperature window was observed in a low-pressure MOCVD system with  $\text{H}_2$  as the carrier gas, see fig. 21, curve (b) [26].

The process showed sensitivity to  $\text{H}_2$  purge and also to the dosage of DMZn. It was found that the growth rate decreased when the hydrogen flow rate exceeded a certain value, either as the purge gas or as the transport gas of DMZn. It can be considered as a physical "blow-off effect", but also as a chemical-reaction interaction of the  $\text{H}_2$  gas removing the  $\text{CH}_3$  groups from the Zn surface.  $\text{H}_2\text{S}$  does not react on an elemental Zn surface (author's experience). Accordingly, the reaction can be described by the equations

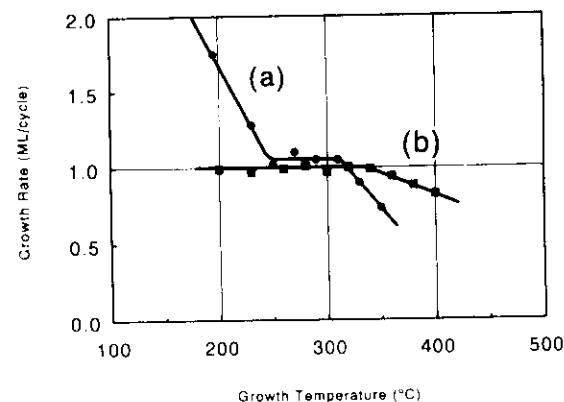
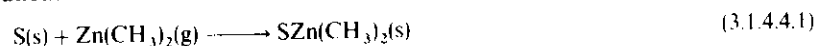
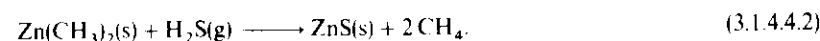
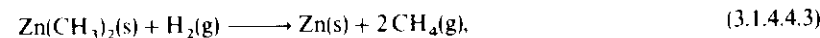


Fig. 21. ALE processing characteristics of ZnS:DMZn +  $\text{H}_2\text{S}$ . (a) Pre-cracking of the reactants was used [25]. (b) No pre-cracking of the reactants [26].

and



The growth is probably inhibited by the reaction



resulting in a Zn surface which is inactive to  $\text{H}_2\text{S}$  interaction.

### 3.1.5. Zinc selenide ( $\text{ZnSe}$ )

**3.1.5.1. ZnSe/ $\text{Zn} + \text{Se}$ ,  $\text{DESe}$  (diethylselenium).** Yao et al. [27] studied II–VI growth from elemental reactants by using in situ RHEED analysis. For ZnSe they observed that the surface reconstruction patterns changed from  $(2 \times 1)$  to  $c(2 \times 2)$  and vice versa when the Se-covered surface is turned into the Zn-covered surface. The substrate used was GaAs (001).

Growth of 1 monolayer/cycle of ZnSe on a GaAs (001) substrate has been observed at  $280^\circ\text{C}$  [28] and between  $250$  and  $350^\circ\text{C}$  [29], see fig. 22.

RHEED analysis has been used in studying the growth mechanism of ZnSe and a four step model was suggested [30, 31]:

- (1) Adsorption of atoms in mobile precursor states.
- (2) Desorption of atoms from the states, characterized by a desorption energy.
- (3) Chemisorption of atoms into the states on the surface.
- (4) Sublimation of atoms from the surface to the precursor stage, characterized by a sublimation energy.

By observing the changes in the RHEED pattern intensities Yao et al. [27] have determined the desorption coefficient for the reactants as well as the desorption rate constant of the adsorbed surface species from different sites.

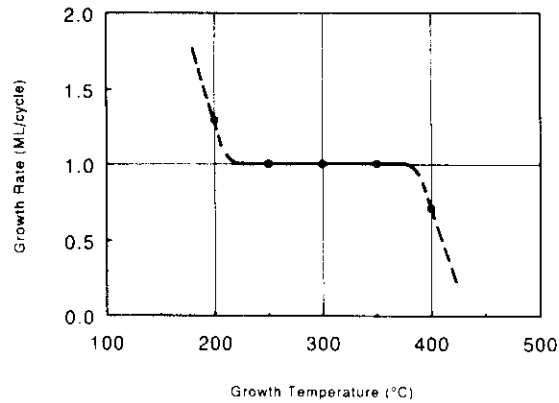


Fig. 22. ALE processing characteristics of ZnSe. Zn + Se [29].

In comparison with MBE-grown ZnSe layers, it can be concluded that the concentration of impurities and point defects in ALE films is substantially reduced, according to a PL spectrum which contained dominant excitonic emission lines [32].

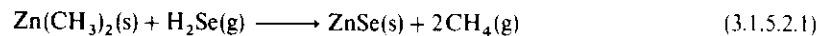
ALE of ZnSe in an MBE-type evaporation system has been reported by Cornelissen et al. [33] as a part of ZnSe/ZnS<sub>x</sub>Se<sub>1-x</sub> superlattice growth. Based on thickness measurements, the saturation level was found to be less than one monolayer per cycle.

By replacing elemental selenium with diethylselenium (DESe) a 1 ML/cycle growth rate has been achieved between 225 and 250 °C [34]. Hydrogen, used as carrier gas for DESe, might have a role in releasing the ethyl groups from the DESe molecules on the Zn surface.

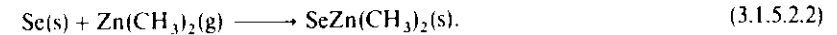
**3.1.5.2. ZnSe/DMZn (dimethylzinc) + H<sub>2</sub>Se.** ZnSe has also been produced from a reaction of DMZn and H<sub>2</sub>Se reactants [35]. However, both reactants were thermally cracked at 950 and 850 °C, respectively, resulting in at least 80% cracking efficiency of the reactants. Depending on the pre-treatment of the GaAs substrate, 0.67 or 0.82 ML/cycle growth was observed. Typical growth temperatures were between 200 and 230 °C.

The basic reaction was explained by an additional reaction of elemental source materials. When hydrogen gas was introduced during ALE growth, a full monolayer growth of ZnSe was observed between 180 and 200 °C. The observed less-than-monolayer growth without hydrogen was explained by surface reconstructions of both the Zn stabilized surface and the Se stabilized surface. In the case of H<sub>2</sub>, the lack of reconstruction was explained by H<sub>2</sub> termination of the surfaces.

One can also consider formation of a H<sub>2</sub>Se gas which could react with a non-cracked DMZn surface according to the equations:



and



**3.1.5.3. ZnSe/DEZn (diethylzinc) + H<sub>2</sub>Se.** ZnSe layers on GaAs from DEZn and H<sub>2</sub>Se have been made in a low-pressure MOVPE reactor. One ML saturation occurs between 350 and 400 °C. The resulting material layer is single crystal ZnSe with high purity and good crystallinity [36].

Yoshikawa et al. [37] compare the ALE of ZnSe in MBE-like and CVD-like modes by comparing the material produced when a cracker has been used or has not been used for the DMZn and H<sub>2</sub>Se reactants. The crystalline material produced in MBE-like ALE refers to the reaction through elemental reactants and was found to be better than the material produced through exchange reactions between DMZn and H<sub>2</sub>Se. The better crystallinity was explained by a higher surface mobility of the elements on the growth surfaces compared to the surface mobilities of the compound reactants. In the cracked mode for elemental reactants the 1 ML/cycle growth window is 200–280 °C. There may also be another stable growth rate of about 0.8 ML/cycle between 300–350 °C, see fig. 23.

Monolayer epitaxy of ZnSe on GaAs substrates by alternative adsorption of diethylzinc and hydrogen selenide has also been reported by Shibata and Katsui [38]. One ML saturation was observed at 350–400 °C.

**3.1.5.4. ZnSe/ZnCl<sub>2</sub> + H<sub>2</sub>Se.** A ZnSe process using zinc chloride (ZnCl<sub>2</sub>) and hydrogen selenide (H<sub>2</sub>Se) as the reactants shows 1 ML/cycle growth between 400–480 °C [39]. The growth has been carried out in a rotating-substrate CVD reactor using H<sub>2</sub>Se and in situ generated ZnCl<sub>2</sub> as the reactants, the purge gas was H<sub>2</sub> (fig. 24). The smoothness of the films improved with increasing temperature.

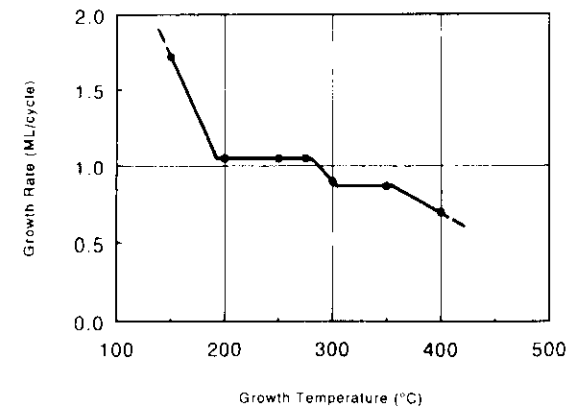


Fig. 23. ALE processing characteristics of ZnSe/DMZn + H<sub>2</sub>Se [37].

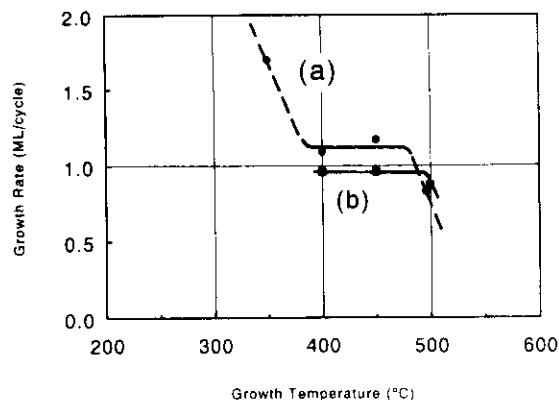


Fig. 24. ALE processing characteristics of ZnSe on (100)GaAs using  $ZnCl_2$  and  $H_2S$  as the reactants [39]. (a) Total flow rate 600 (SCCM), reaction sequences 0.7 s, purge sequences 2 s, (b) total flow rate 1200 (SCCM), reaction sequences 3 s, purge sequences 6 s.

### 3.1.6. Zinc telluride (ZnTe)

**3.1.6.1. ZnTe/Zn + Te.** ALE growth of ZnTe has been carried out in an MBE-type vacuum reactor on an amorphous substrate at temperatures between 320–400 °C. The films show polycrystalline structure with preferred (111) orientation [40]. The substrate used was soda glass. On a (001) GaAs substrate ALE growth of ZnTe has been observed within a temperature range of 200–400 °C [28]. A growth rate of 0.5 ML/cycle has been observed when small doses of Zn and Te were used [41].

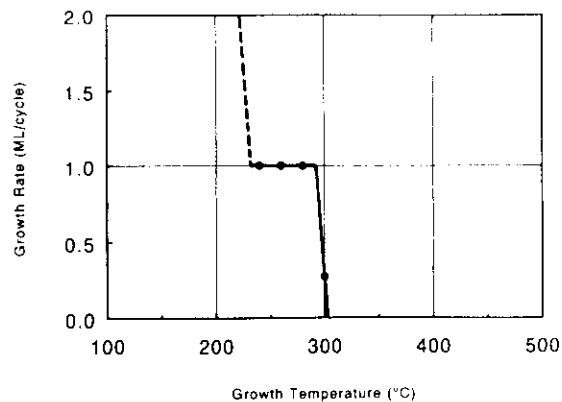


Fig. 25. ALE processing characteristics of the ZnTe - Zn + Te reaction [29].

Dosho et al. [29] have observed 1 ML/cycle growth between 240 and 280 °C, see fig. 25. The best surface morphology was obtained at a growth temperature of 240 °C. The growth rate was 1 ML/cycle; however, due to the low re-evaporation rate of Te at that temperature certain control of the Te beam was necessary. The influence of Zn and Te beam intensities on the growth rate at 250 °C has been studied by Takemura et al. [42]. Saturated growth of 0.5 ML/cycle was observed for Zn overdoses of 7 to 50 times an ML and for Te overdoses of 2 to 15 times an ML.

### 3.1.7. Other sulphides

**3.1.7.1. CaS, SrS, BaS/M(thd)<sub>2</sub> + H<sub>2</sub>S.** Tammenmaa et al. [43] have reported alkaline earth sulfide (CaS, SrS, BaS) thin films prepared on glass substrates using metal thd (thd is 2, 2, 6, 6-tetramethyl-3,5-heptanedionate) and  $H_2S$ . Observed growth rates were 0.3–0.4 ML/cycle. According to X-ray diffraction patterns and PL spectra the films were polycrystalline and chemically pure. All films were slightly oriented, but each towards different directions: CaS along (220), SrS along (111) and BaS along (200) [43].

Strontium sulfide has been grown using  $Sr(thd)_2$  and  $H_2S$  as the reactants at temperatures in the range 260–400 °C. The rate of the growth increases from 0.3 to 0.6 ML/cycle with increasing temperature. Above 450 °C another mode of growth appears. The high-temperature mode of the growth is probably related to thermal decomposition of the  $Sr(thd)_2$  reactant [44].

### 3.1.8. I/III-VI chalcopyrites

There are very few works on ALE of I/III-VI chalcopyrites such as  $Cu(Al, Ga, In)(S, Se)_2$  in spite of their potential in light-emitting devices as well as in solar-cell devices. Otoma et al. [45] have prepared  $CuGaS_2$  using cyclopentadienyltriethylphosphinecopper (CP-Cu-TEP), TEGa and  $H_2S$  as the reactants. Substrate temperatures used were 550 and 600 °C. CP-Cu-TEP and TEGa were supplied simultaneously and  $H_2S$  separated by  $H_2$  purges. A one monolayer per cycle growth was observed within certain feeding rates of the metallic components. Major improvements in the thickness uniformity of the resulting film were observed when compared to films grown in conventional MOCVD mode.

### 3.1.9. II-VI superlattices

Konagai and co-workers [46–48] observed drastic improvement in the interface abruptness of ZnSe/ZnTe superlattice structures (SLS) when the growth modes of the ZnSe and SeTe materials were switched from conventional MBE to the ALE mode. The PL intensity was much higher in the ALE grown SLSs. Strong emission at room temperature was observed in  $(ZnSe)_1(ZnTe)_1$  structures. The ZnSe and ZnTe layers were grown at 400 °C using diethylzinc, diethylselenide and diethyltelluride as the reactants. While pre-cracking was used for all reactants the surface reactions may be primarily elemental reactions.

For ZnSe/ZnTe strained-layer (SL) surfaces the RHEED patterns show surface reconstruction ( $2 \times 1$ ) for the Zn-covered surface and ( $1 \times 2$ ) for the Se- and Te-covered

surface [49]. The substrate was (1 0 0) GaAs and the substrate temperatures were 350 °C for ZnS/ZnTe SLs and 280 °C for ZnSe/ZnTe SLs.

Growth of CdS/ZnS superlattices (SLs) at temperatures of 185 and 190 °C on (1 0 0) GaAs surfaces has been demonstrated by Ohta et al. [50]. The growth was performed in an MBE-type system using the elements as the reactants. The SL growth progressed with a surface reconstruction change from  $c(2 \times 2)$  Zn to  $(2 \times 1)$  S for ZnS and from  $(1 \times 1)$  Cd or  $c(2 \times 2)$  Cd to  $(2 \times 1)$  S for CdS. The SL structures were confirmed by the satellite peaks observed in X-ray diffraction spectra. The SL structure exhibited flat and smooth surfaces. The photoluminescence spectrum of the  $(\text{CdS})_8/(\text{ZnS})_{20}$  (55 SL) shows a sharp peak at 440 nm and suggests that the light emission originated from the quantum level in the SL.

$\text{ZnS}/(\text{ZnSe})_n/\text{ZnS}$  single quantum well structures combining MBE of ZnS and ALE of ZnSe have been demonstrated by Yao et al. [51]. The thickness of the ZnSe layer was 1 to 20 molecular layers.

### 3.2. III-V materials

#### 3.2.1. Aluminium arsenide (AlAs)

**3.2.1.1. AlAs/TMAI, MMAI (tri/monomethylaluminium) + AsH<sub>3</sub>.** AlAs has been made in a vertical MOCVD reactor using H<sub>2</sub> carrier gas at 70 Torr pressure. Reactants were monomethylaluminium (MMAI) and arsine (AsH<sub>3</sub>) [52]. MMAI was produced from trimethylaluminium (TMAI) by cracking at 400 °C temperature. One ML saturation was observed. By using TMAI or DMAIH (dimethylaluminiumhydride) also 2 ML/cycle growth has been observed [53, 54]. A high-speed hydrogen flow may play an important role in the surface reaction mechanism.

AlAs has been made by enhancing the decomposition of TMAI with a pre-cracker [55]. In a vertical MOCVD reactor the pressure was 70 Torr, carrier gas for both AsH<sub>3</sub> and TMAI was H<sub>2</sub>. With the pre-cracker the saturation temperature window was extended to 20 °C from practically zero, to a range of 460–480 °C. In this case only TMAI was pre-cracked, not AsH<sub>3</sub>. Mass spectrometry suggests that Al atoms as well as MMAI and DMAI are formed in the cracking tube. Al atoms are, however, adsorbed on the wall of the cracking tube.

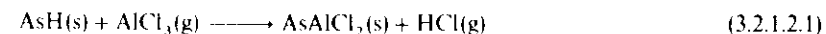
By using a mixture of dimethylaluminiumhydride (30%) and trimethylaluminium (70%) as the Al reactant both 1 and 2 ML/cycle growth rates have been demonstrated, depending on the dosing and the growth temperature [54]. The saturation temperature range for 1 ML/cycle growth mode was 425–525 °C and for 2 ML/cycle growth mode 400–500 °C.

In the case of AlAs, using aluminium alkyls as the reactants for aluminium, the laser enhanced growth mechanism is explained by a site selective desorption model where the laser irradiation enhances the difference between the desorption rate of aluminium alkyl on the Al-terminated surface and the As-terminated surface [56]. Aluminium alkyl adsorbed on the Al-terminated surface is easily desorbed from the surface by the laser irradiation compared to when adsorbed on the As-terminated surface. It is

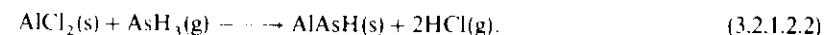
suggested that Al atoms are selectively deposited on the As-terminated surface and that the difference in the desorption rate of aluminium alkyl on each surface provides the ALE growth. A possible role of As-H surface species on the selective adsorption has not been studied.

The energy gap of AlAs is larger than the photon energy of the Ar laser, which means that photon-activated carriers are not generated at the surface. Laser irradiation on adsorbed TMAI is important in achieving a saturation controlled growth of AlAs. In the TMAI + AsH<sub>3</sub> system the TMAI molecules decompose not only on the As-terminated surface but also on the Al-terminated surface. The site selectivity of the decomposition and desorption of TMAI is not enhanced by irradiation. Saturated growth has not been achieved.

**3.2.1.2. AlAs/AlCl<sub>3</sub> + AsH<sub>3</sub>.** AlAs has been grown in an atmospheric-pressure multi-tube CVD reactor with a moving substrate using AsH<sub>3</sub> and AlCl<sub>3</sub> as the reactants and H<sub>2</sub> as the carrier gas [57]. One monolayer per cycle growth was observed at 550 °C. At 600 °C the growth rate was from 1 to 2 ML/cycle in different positions on the substrate. Above 600 °C the growth turned into etching of the AlAs material. A possible reaction path, in analogy to Al<sub>2</sub>O<sub>3</sub> growth is,



and



#### 3.2.2. Gallium arsenide (GaAs)

**3.2.2.1. GaAs/Ga + As<sub>4</sub>.** The ALE of GaAs from elemental reactants suffers from the low vapour pressure of Ga. By controlling the amount of Ga ALE-type growth can be obtained. In the growth of GaAs on silicon by sequential supply of the elemental reactants, it has been shown that a great reduction in defect density associated generally with a three-dimensional growth mechanism has been obtained by a two-dimensional nucleation mode [58–60].

**3.2.2.2. GaAs/TMGa (trimethylgallium) + AsH<sub>3</sub> (arsine).** The most intensively studied ALE process is the growth of gallium arsenide using trimethylgallium (TMGa) and arsine (AsH<sub>3</sub>) as the reactants. Observed saturation characteristics of the TMGa show big differences depending on the experimental conditions. In an ultra-high-vacuum system no saturation [62] or a narrow temperature range of saturation has been detected without photon excitation [63, 64], see figs. 26a and 26b. The temperature range of saturation can be enhanced by laser irradiation [62], see fig. 26c. When a high-speed flow and hydrogen transport in a CVD-type system is used, a wide saturation range has been found without photon excitation [65–68], see figs. 26d and 26e.

Nishizawa [61] has shown remarkable differences in the surface reaction mechanisms on different crystal surfaces. While saturation of the TMGa reaction could be observed on (1 0 0) and (1 1 1)B surfaces, no reaction occurred on a (1 1 1)A surface [61].

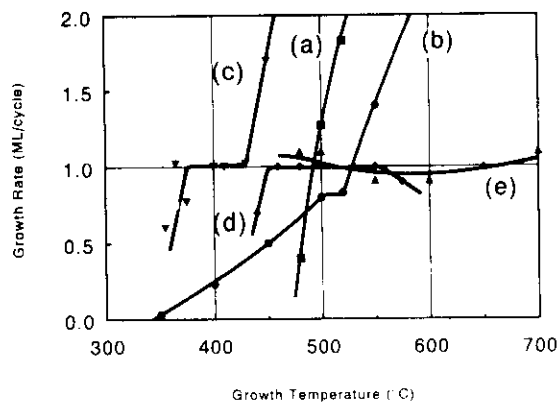


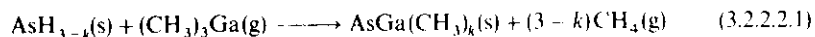
Fig. 26. ALE processing characteristics of the GaAs/TMGa + AsH<sub>3</sub> process in different experimental conditions. (a) No laser irradiation, ultra-high vacuum [62], (b) no laser irradiation, ultra-high vacuum [63], (c) laser irradiation (160 W/cm<sup>2</sup>), ultra-high vacuum [62], (d) high-speed hydrogen transport, CVD system [65], (e) high-speed hydrogen transport, rotating-disk CVD system [68].

According to a site-blocking model [61, 69–71] first proposed by Nishizawa the adsorption sites on an As surface are blocked by a monolayer of GaCH<sub>3</sub> groups which prevents further adsorption of TMGa through a partial decomposition of the reactant.

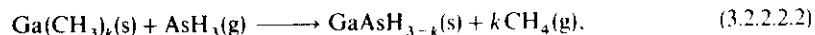
The study of the growth mechanism has been concentrated mainly on the saturation of the TMGa. As-surface saturates over a wide range of temperature and arsine dose, but there are few experimental observations on the chemical nature of the resulting As surface structure under different conditions. From a chemical point of view (see eqs. (1.5.1) and (1.5.2)) one could assume that As-H structures on an adsorbed As surface could play an important role in selective decomposition or surface exchange reaction of the next TMGa exposure by enhancing CH<sub>4</sub> release at the surface. The site-blocking model is not far from a site-selective model [72] which emphasises the role of surface-catalyzed decomposition in the saturation.

Kobayashi et al. [73] applied a surface photoabsorption (SPA) in situ analysis in the study of the saturation of the TMGa reaction on an As surface. A conclusion was that the saturation is primarily due to the formation of GaCH<sub>3</sub> surface, which prevents the adsorption of further TMGa. It was further found that a prolonged H<sub>2</sub> purging sequence after the TMGa sequence results in the release of the CH<sub>3</sub> from the Ga surface, which turns the surface into metallic Ga.

Using the formalism developed in section 1.5 and by ignoring spontaneous thermal decomposition or pre-cracking of the reactants, we can express the reaction paths of the GaAs ALE process using TMGa and arsine as



and



where  $k = 0, 1, 2, 3$ .

Both the site-selective and the site-blocking model refer most closely to  $k = 1$  in the equations above. There is no direct evidence for the role of As-H structures in the removal of methyl groups from the TMGa on an As surface, as suggested by eq. (3.2.2.2.1) when  $k = 1$ . Most in situ studies of the TMGa adsorption are based on analysis which is not sensitive to hydrogen. Also, many of the surface analysis methods are too slow to be directly applicable in ALE growth dynamics.

Annapragada et al. [74], based on information from Fourier-transform infrared spectroscopy (FTIR), suggest that As-H species play an essential role in the removal of hydrocarbon species from the growth surface. Thermal decomposition of As-H structures on a Ga surface is not known in detail. Selectivity in AsH<sub>3</sub> decomposition on different GaAs crystalline surfaces at temperatures from 450 to 650°C has been reported [61]. A continuous hydrogen flux, used as a dilutant of arsine and as a purge gas after the arsine exposure, may also have a role in stabilizing As-H surface structures under certain experimental conditions.

Some enhancement of the TMGa and AsH<sub>3</sub> surface exchange reactions can be obtained by photons [63, 75–77]. Laser-assisted ALE for Ga using TMGa and arsine as the reactants has been done in a vertical MOCVD reactor operated at atmospheric pressure [67]. The carrier gas used was hydrogen; purge times used were 8–20 s. Argon ion lasers with power densities up to 500 W/cm<sup>2</sup> were used either during TMGa or arsine exposition.

Figure 27 [67] shows the dependence of growth rate as a function of laser power density. Similar results were obtained when the laser excitation occurred during the TMGa or the AsH<sub>3</sub> exposure.

In the TMGa + AsH<sub>3</sub> reaction the role of the CH<sub>3</sub> group on the Ga surface and, on the other hand, the role of H<sub>2</sub> in the thermal decomposition of TMGa has been confirmed by changing the carrier gas for TMGa from H<sub>2</sub> to N<sub>2</sub> [78, 79]. The ALE temperature window of the process was increased from the 490–500°C range to 490–520°C, see fig. 28. The carrier gas used for As was still hydrogen.

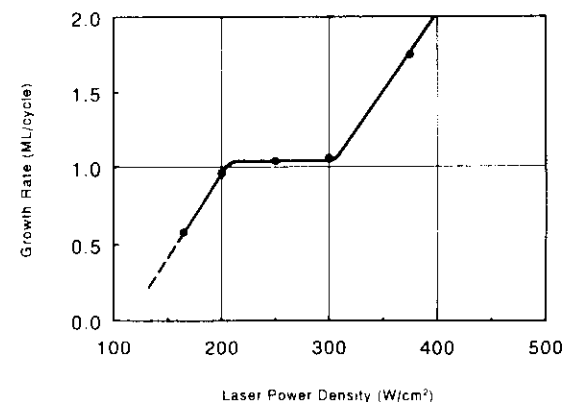


Fig. 27. The effect of laser power density on the growth rate of GaAs in the TMGa + AsH<sub>3</sub> reaction [67].

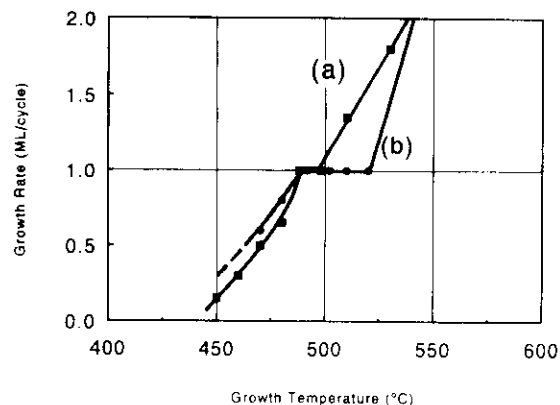
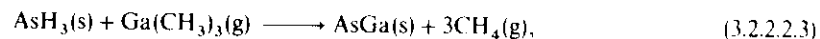


Fig. 28. Effect of TMGa carrier gas on the ALE processing window of the GaAs/TMGa + AsH<sub>3</sub> process [78]. (a) TMGa carrier gas H<sub>2</sub>, (b) TMGa carrier gas N<sub>2</sub>.

By using in situ X-ray photoelectron spectroscopy, Kodama et al. [80] have shown that, when fast injection of TMGa is used, the saturated layer resulting from the TMGa reaction is metallic gallium. This means a complete selective decomposition of the TMGa molecule on an As or AsH surface. It is further suggested that the fast injection of TMGa on the substrate minimizes the thermal decomposition of TMGa, which might dominate over the selective decomposition necessary for monolayer saturation. One can also consider that fast injection of AsH<sub>3</sub> in an H<sub>2</sub> stream may establish an AsH<sub>3</sub> surface which could effectively result in CH<sub>4</sub> gas formation and a full conversion of TMGa into metallic Ga.

As H species play an essential role in promoting the selective decomposition of TMGa [74]. If arsine is assumed to adsorb on a Ga surface as AsH<sub>3</sub> molecules, the reactions could be expressed using  $k = 0$  in eqs. (3.2.2.2.1) and (3.2.2.2.2):

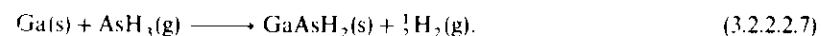
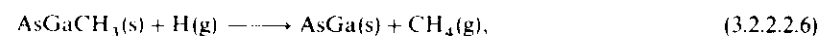
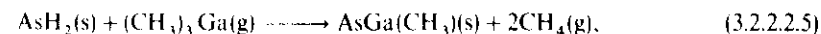


Due to the poor thermal stability of AsH<sub>3</sub> [81] one can assume that an AsH<sub>3</sub> surface can be maintained only in favourable conditions such as a strong H<sub>2</sub> stream and a short purge time before TMGa exposure.

De Keijser and van Opdorp [82] have confirmed the importance of hydrogen in the TMGa/AsH<sub>3</sub> reaction by injecting atomic hydrogen generated by microwave plasma after an AsH<sub>3</sub> or TMGa pulse. They could establish the self-limiting mechanism between 400–500°C. The role of atomic hydrogen was assumed to have to deal with enhancing the selective decomposition of TMGa by As H surface species. When the atomic hydrogen is introduced after the AsH<sub>3</sub>, a complete exchange of TMGa on the AsH<sub>3</sub> surface, as in eqs. (3.2.2.2.3) and (3.2.2.2.4), can be assumed.

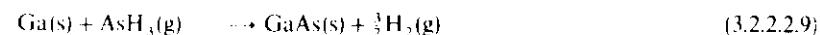
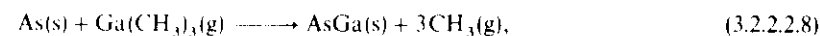
When the atomic hydrogen flux is introduced after the TMGa, one can assume that the partial decomposition of TMGa occurs immediately on the As H surface and is

then completed by further decomposition activated by the atomic hydrogen according to the equations



In the experimental test setup used there was a background pressure of H<sub>2</sub> which might also influence the reaction pathway by enhancing the thermal decomposition of TMGa.

If decomposition of arsine is assumed, generation of both hydrogen and methyl radicals must be assumed:



or



Depending on the experimental setup, cracking of arsine may also occur as thermal decomposition before the reaction with the Ga surface (3.2.2.2.10) and (3.2.2.2.11). At typical reaction temperatures also elemental As is volatile enough to result in a monolayer saturation. For the reaction (3.2.2.2.11) surface dissociation of As<sub>2</sub> molecules must be assumed.

Memmert and Yu [83] showed that the hydrocarbons from TMGa may desorb as CH<sub>3</sub> radicals, which means that the hydrogen incorporation on the As surface is not crucial for the decomposition of TMGa. Yu et al. [84] have developed a dynamic model to explain the saturation of TMGa desorption. Their conclusion was that the site-blocking mechanism alone does not explain the saturation of TMGa. The experimental procedure used to back up the model was based on mere TMGa exposure on an As-rich surface of GaAs, thus excluding any effects of As H species as a part of the reaction mechanism.

A thorough study of TMGa saturation has also been presented by Maa and Dapkus [85]. Their experimental setup consists of a sample preparation chamber and an analysis chamber with X-ray photoelectron spectroscopy (XPS) and reflection high-energy electron diffraction (RHEED) capabilities. For the study of reaction kinetics, reflectance difference spectroscopy (RDS) was applied in the preparation chamber. The gallium reactant used was TMGa, the reactants for arsenic were elemental As<sub>4</sub>, tertiarybutylarsine (TBAs) and monoethylarsine (MEAs).

In this test setup the Ga surfaces, formed at a temperature above 440°C by TMGa exposure, showed a (4 × 6) REED pattern which is characteristic of Ga surfaces. The formation speed of the Ga surface increased rapidly when the reaction temperature was increased from 430 to 500°C. The change of the formation speed was explained by the slow desorption of the CH<sub>3</sub> radicals from the Ga atoms on the surface. In these



experiments, the surface exposed to the TMGa flux was a hydrogen-free As surface of a GaAs crystal.

In [86] Dapkus et al. have summarized some of the key elements of the TMGa + AsH<sub>3</sub> process. It is stated that the dynamical conditions of the process play a very important role in the growth characteristics. For TMGa it is essential to suppress the undesirable thermal decomposition of the precursor which might occur in the gas phase or on any surface of the growing material. The decomposition is enhanced by the presence of hydrogen. One approach to suppressing the decomposition of TMGa is to use nitrogen instead of hydrogen as the carrier gas for the TMGa. Another important issue is the nature of the As stabilized surface after AsH<sub>3</sub> exposure. As-H species on the As surface may not only result in a more favourable surface configuration than a pure arsenic surface but also enhance the desirable decomposition (or exchange reaction) of TMGa on the AsH<sub>x</sub> surface which results in the selectivity of the one monolayer per cycle saturation.

The purge sequence after AsH<sub>3</sub> exposure also may play an important role in maintaining the dynamic As-H balance on the As surface. Maximum occupation of hydrogen is favourable for the selectivity of the TMGa decomposition. Availability of extra hydrogen gas during the TMGa exposure may result in undesirable cracking of the TMGa. At the typical growth temperatures there is a certain rate of thermal decomposition of TMGa which involves a dynamical feature in the saturation mechanism.

Typical c(2 × 8)/(2 × 4) surface reconstruction of As has an As coverage of 0.75 ML which cannot support full 1 ML/cycle growth. Banse and Creighton [87] suggest that a super As-rich surface could be obtained with high AsH<sub>3</sub> dosing to break the surface reconstruction. As-H structures could also explain the 1 ML cycle rather than 0.75 ML/cycle saturation.

The fact that the saturation growth rate of the GaAs/TMGa + AsH<sub>3</sub> reaction is 1 ML/cycle supports the role of As-H and Ga-CH<sub>3</sub> ligand interactions as an essential part of the reaction mechanism under most experimental conditions. This is not only to enhance the selectivity of the process, but also to inhibit the build-up of surface reconstructions typical of both clean Ga and As surfaces. Nishizawa et al. [64] have reported results on 0.8 ML/cycle saturation which might be an indication of a reaction pathway incorporating build-up of surface reconstruction of the Ga or the As surface.

There is also evidence for the slow formation of a saturated Ga surface without any exchange between TMGa and As-H structures. Complete decomposition of TMGa occurs at a certain rate on a hydrogen-free As surface, still maintaining a monolayer saturation feature at a Ga surface reconstruction density [88]. RHEED studies of TMGa adsorption on a (2 × 4) As stabilized GaAs surface shows that a (4 × 1) or (4 × 2) Ga stabilized surface construction results. The surface temperature in the experiment was typically 440–530 °C. In the experimental setup used, the As surface was re-established by using elemental arsenic, which eliminated the formation of As-H structures. Exposure times of TMGa were in excess of 30 min. This type of test setup shows an essentially wider saturation temperature range, 370–530 °C, than fast sequencing of the reactants. To explain the saturation under these conditions one cannot exclude the possibility of continuous slow thermal decomposition of TMGa on both

As and Ga surfaces followed by slow thermal desorption of extra Ga from the reconstructed Ga surface.

Chiu and Cunningham [89] have shown, by using RHEED, that a limiting mechanism which inhibits the continual adsorption of TMGa on a surface saturated with Ga alkyl is found to exist for a short period of time depending on the growth temperature. The dynamical evolution of the surface reconstruction indicates that the saturation coverage of the Ga alkyls instead of Ga atoms is responsible for the limiting mechanism. One ML saturation can be achieved at 55 °C for a finite period of time. The surface reconstruction pattern indicates that adsorption of Ga alkyls during this time period is responsible for the limiting mechanism. When the methyl radicals desorb completely, adsorption and pyrolysis of TMGa is not inhibited.

The (2 × 4) As dimerized surface will change to a (1 × 1) pattern during the initial 4 s deposition time of TMGa. This indicates that a layer of disordered Ga alkyls destroys the surface reconstruction and only the underlying bulk-like structure is observed. In about 1 s after the deposition a clear (4 × 8) pattern appears. Then, 8 s later this pattern converts to a (4 × 6) pattern characteristic of a Ga stabilized surface at this temperature. At low substrate temperature the time required to complete this evolution becomes progressively longer.

The importance of the reaction dynamics can also be seen in the dependence of the saturation on the dosing parameters used. In a low-pressure MOCVD reactor the growth rate per cycle has been observed to be a function of the TMGa pulse length. Also, a dependence of the saturation density on the partial pressure of the reactant has been observed, see fig. 29 [90]. In the experimental test setup used, the arsine and TMGa pulses are injected in a constant H<sub>2</sub> flow of 1 m/s at a temperature of 500 °C. While there is a clear saturation as a function of TMGa partial pressure, the level of saturation is strongly dependent on the length of the TMGa supply. The result

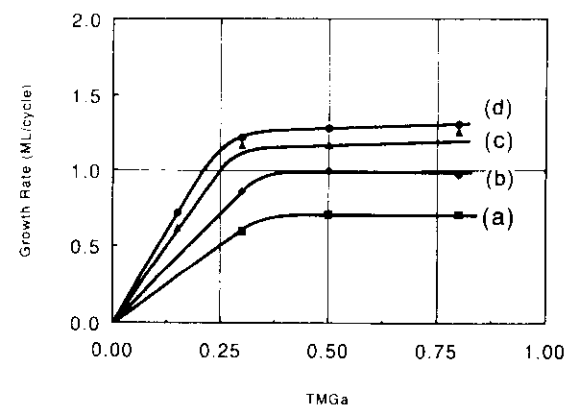


Fig. 29. Effect of the partial pressure of TMGa and the length of the reaction sequence on the saturation [90]. Total pressure is 1500 Pa, partial pressure of AsH<sub>3</sub> is 9.4 Pa, flow speed is 100 cm/s and the temperature is 500 °C. Sequence times for TMGa are (a) 1 s, (b) 2 s, (c) 3 s and (d) 4 s.

emphasizes the importance of surface kinetics in the ALE process of GaAs/TMGa + AsH<sub>3</sub>.

The TMGa + AsH<sub>3</sub> ALE reaction has a very wide saturation region in a rotating-disk reactor [68], (fig. 26e). The rotating disk employs very fast pulsing and effective purging with hydrogen. One monolayer per cycle growth can be observed over a wide temperature range, 450–700°C. In order to minimize the carbon content of the resulting GaAs material, it was essential to minimize the exposure to the TMGa flux especially at high growth temperatures. It was also observed that the carbon content, ranging from 10<sup>15</sup> to 10<sup>20</sup>, in the resulting GaAs material was strongly dependent on the exposure time with increasing exposure of the TMGa and with decreasing temperature of the substrate.

GaAs material produced in a high flow speed rotating-disk reactor with fast pulsing shows excellent electrical characteristics. The background carrier concentration is 10<sup>14</sup>–10<sup>15</sup> cm<sup>-3</sup> and a mobility of about 30 000 cm<sup>2</sup>/Vs for 2 mm thick films at 77 K has been obtained. The 4K photoluminescence indicated high-purity GaAs. The material quality improved with increasing V–III ratio and growth temperature [91]. Essential for the low carrier concentration are optimized TMGa and efficient arsine exposures.

**3.2.2.3. GaAs/TEGa (triethylgallium) + AsH<sub>3</sub> (arsine).** The TEGa + AsH<sub>3</sub> system does not show saturation without laser irradiation [64, 92–94]. Laser irradiation results in an ALE window for the process between 350 and 430°C depending on the power density used [93, 95]. Nishizawa et al. [96] have demonstrated a wide ALE window by UV-excitation with a Hg-lamp, see fig. 30.

Aoyagi et al. [93] explain the TEGa reaction as a surface-selective photochemical decomposition of TEGa on the As surface, which means that, under laser irradiation, the gallium alkyl decomposes more effectively on an As surface than on a Ga surface.

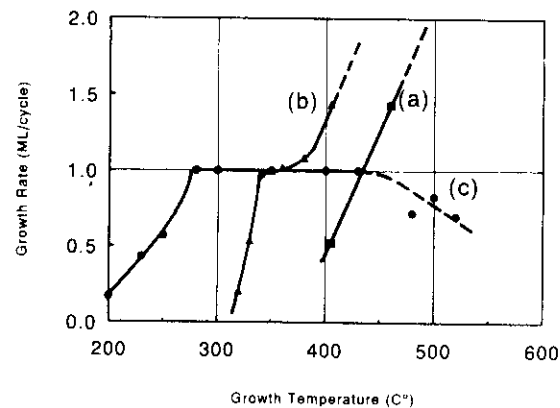


Fig. 30. ALE processing characteristics of GaAs/TEGa + AsH<sub>3</sub> reaction with different photon excitations. (a) No photon excitation [93], (b) laser excitation [93], (c) UV-excitation by Hg-lamp [96].

The mechanism is also called laser-induced site-selective decomposition [94]. The site selectivity is explained by a two step process: (1) photon absorption by chemisorbed gallium alkyl molecules due to the broadening of the optical absorption band and (2) transfer of carriers, generated at the substrate by the laser irradiation, to the chemisorbed molecules.

In the processing characteristics shown in fig. 30 all the observed saturation densities are 1 ML/cycle, which shows that surface reconstructions have been avoided.

Nishizawa et al. [63] report that, in the TEGa + AsH<sub>3</sub> system, electrical properties of the GaAs material depend strongly on the substrate orientation. On (1 0 0) and (1 1 1)A faces the epitaxial layers are p-type, on (1 1 1)B faces the layers are n-type and on a (1 0 0) face the layers exhibit both n- and p-type conduction with changing growth conditions. In the TMGa + AsH<sub>3</sub> system, carrier concentration is in the range of 10<sup>18</sup>–10<sup>20</sup> cm<sup>-3</sup>. In the TEGa + AsH<sub>3</sub> system it improved by as much as three orders of magnitude. With increasing irradiation wavelength the carrier concentration of the layers grown on a (1 0 0) plane in both the TMGa + AsH<sub>3</sub> and the TEGa + AsH<sub>3</sub> system decreases. Especially, with irradiation with a XeCl (308 nm) laser the epitaxial layers show high resistivity. For the (1 1 1)B plane in the TEGa + AsH<sub>3</sub> system, with irradiation the layers become strongly p-type.

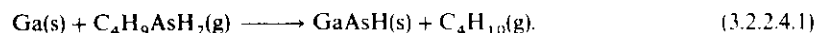
Nishizawa et al. [95, 63] report on the doping characteristics of GaAs with Cd, Zn, Si, Se and Te dopants. The observed carrier concentrations of GaAs films were in the range from 1.8 × 10<sup>16</sup> to 1.9 × 10<sup>19</sup> cm<sup>-3</sup> for p-type and from 1.3 × 10<sup>17</sup> to 2.2 × 10<sup>19</sup> cm<sup>-3</sup> for n-type material, respectively. The GaAs growth was carried out using AsH<sub>3</sub> and TEGa as the reactants. It was also observed that the carrier concentration depended strongly on the order of the injection of the impurity gas components with respect to the main gas sequences in the growth.

**3.2.2.4. GaAs/TMGa (trimethylgallium) + TBAs (tertiarybutylarsine).** Tsen et al. [97] report GaAs growth using TMGa and tertiarybutylarsine (TBAs) as the reactants in ALE and laser-assisted ALE in GaAs. The processes were carried out in a conventional atmospheric-pressure MOCVD system. The carrier gas used was H<sub>2</sub>. One ML/cycle saturation was obtained at 480°C without laser irradiation and at 380°C with argon laser irradiation. When compared with the ALE material obtained in similar conditions using AsH<sub>3</sub> instead of TBAs, one can observe about ten times higher PL efficiency and a lower carbon content in the films. Broad-area laser diodes have been successfully demonstrated from structures grown using TBAs.

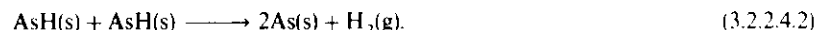
Maa and Dapkus [98] have studied the mechanism of TMGa + TBAs reaction using reflectance difference spectroscopy. Their experiments were performed in an ultra-high-vacuum system consisting of two chambers. The analysis chamber is equipped with X-ray photoelectron spectroscopy (XPS) and reflection high-energy electron diffraction (RHEED). The other reaction chamber provides exposure to TMGa and TBAs in UHV [88].

Under these conditions no carbon can be detected on either TMGa saturated or TBAs saturated surfaces. As compared to AsH<sub>3</sub>, TBAs reacts more effectively on a Ga surface. The most probable surface adsorbate giving rise to the reaction is AsH<sub>x</sub> (x = 1 or 2) [99].

The As-H surface may result from the reaction



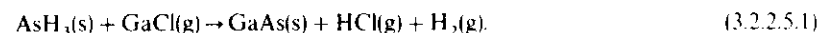
In the case of  $\text{C}_4\text{H}_9$ -radical desorption, an  $\text{AsH}_2$  surface is established. It is further proposed that a possible interaction between pairs of As-H forms arsenic atom on the surface by releasing hydrogen as



The removal of H-ligands from an arsenic surface is observed when the substrate is heated to 500°C, as confirmed by RHEED study [99]. Similar surface behaviour has been observed when monoethyl arsenic, MEAs, is used instead of TBAs. The rate limiting step is the reaction which yields adsorbed  $\text{AsH}_x$  species. Interaction between  $\text{AsH}_x$  pairs on the surface forms arsenic dimers on the surface [100].

**3.2.2.5. GaAs/GaCl + AsH<sub>3</sub>.** Adsorption of gallium chloride (GaCl) on GaAs (100), (111)a and (111)b surfaces is studied by temperature-programmed desorption, TPD [101, 102]. A GaCl molecular beam is produced by letting  $\text{Cl}_2$  gas flow over a Ga source at 650–800°C. For all GaAs surface reconstructions studied, GaCl desorption is observed, while no decomposition or reaction giving  $\text{AsCl}_x$  is observed. This study indicates that in ALE of GaAs using GaCl and As one must assume exchange reaction on the surface between GaCl and  $\text{H}_2$ . The self-limiting mechanism is explained by the shorter residence time of GaCl on the gallium stabilized surface than that on the As stabilized surface.

Another explanation for the saturation GaCl/ $\text{AsH}_3$  process could be an exchange reaction between GaCl gas and an  $\text{AsH}_3$  surface structure completed with or preceded by desorption of  $\text{H}_2$ :



With reference to the TMGa and  $\text{AsH}_3$  discussion one can also consider a full exchange reaction between DEGaCl gas and  $\text{AsH}_3$  on a surface with  $k = 0-3$ , as described by eqs. (3.2.2.2.1) and (3.2.2.2.2).

**3.2.2.6. GaAs/DEGaCl (diethylgalliumchloride) + AsH<sub>3</sub>.** In an ALE process for GaAs using DEGaCl and  $\text{AsH}_3$  a wide saturation temperature range was observed [103]. The growth was carried out in a horizontal low-pressure MOCVD system. The total pressure in the reactor was 100 Torr and the total flow rate of  $\text{H}_2$  was 9000 sccm. The substrate was (100) GaAs. The carrier gas was  $\text{H}_2$ . According to the model proposed, DEGaCl decomposes into GaCl and a Langmuir monolayer adsorption of GaCl on surface As atoms takes place.

The DEGaCl reaction has also been demonstrated with elemental As as the other reactant [104]. The As source was kept at 400°C and the As vapour was transferred with the aid of hydrogen transfer gas. The process resulted in a lower carbon content than with the DEGaCl +  $\text{AsH}_3$  process. The difference may be a different reaction pathway or the different construction of the reactor, especially the hot-wall design, which might promote a pre-decomposition of the DEGaCl into hydrocarbons and GaCl. Possible

formation of  $\text{AsH}_3$  in the As source has not been reported. However, under these conditions, an As-H surface structure on the substrate can probably be produced. The observed temperature range for saturation shows similar behaviour as in the DE-GaCl +  $\text{AsH}_3$  process. At the high end of the temperature range the saturation is slightly below 1 ML.

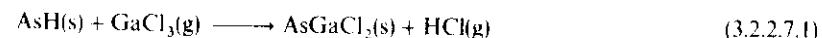
A Hall measurement shows conversion of DEGaCl ALE GaAs from p-type to n-type with increasing growth temperature. In the GaAs material processed at 600°C, a 77 K electron mobility of 22400  $\text{cm}^2/\text{Vs}$  with an electron concentration of  $1.1 \times 10^{15} \text{ cm}^{-3}$  has been obtained. A PL spectrum indicated that the carbon content of the material decreased as the growth temperature was increased [103].  $n^{++}$ -GaAs with an electron concentration of  $1.1 \times 10^{19} \text{ cm}^{-3}$  has been obtained by  $\text{Si}_2\text{H}_6$  plane doping at 450°C [103, 105].

Usui [106] describes a delta-doped FET based on GaAs which was made using the DEGaCl +  $\text{As}_4$  process. The reactant for selenium doping was  $\text{H}_2\text{Se}$ . The gate length was 1  $\mu\text{m}$  and the measured extrinsic transconductance was 190 mS/mm.

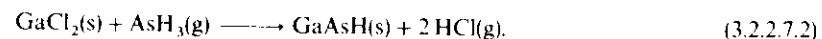
Dependence of the laser enhancement on the photon energy has been demonstrated by comparing the effect of irradiation at 1.6  $\mu\text{m}$  and at the YAG laser wavelength (514.5 nm) [107]. While the YAG laser irradiation results in a sharp saturation as a function of laser power density, no saturation can be observed with the 1.6  $\mu\text{m}$  irradiation.

The adsorption of DEGaCl and TMGa vapours on clean As-terminated GaAs and InAs surfaces prepared by conventional MBE has been studied by Ishii et al. [108]. It was shown that, at temperatures of 300–320°C, a monolayer of Ga was observed on GaAs and InAs surfaces after exposure to TMGa and DEGaCl vapours, respectively. No production of GaCl was observed in either case. The experiment suggests that a complete decomposition of TMGa and DEGaCl occurs on an As surface but not on a Ga surface or on an In surface.

**3.2.2.7. GaAs/GaCl<sub>3</sub> + AsH<sub>3</sub>.** The widest temperature window for 1 ML/cycle ALE growth for GaAs has been reported by Jin et al. [109] using  $\text{GaCl}_3$  and  $\text{AsH}_3$  as the reactants (fig. 31).  $\text{AsH}_3$ , in this case, is supplied without thermal cracking, which suggests an exchange reaction



and



At temperatures above 500°C the growth rate is found to decrease, probably due to desorption of surface ligands necessary for the growth reactions.

**3.2.3. Indium arsenide (InAs)**

**3.2.3.1. InAs/TMIn (trimethylindium) + AsH<sub>3</sub>.** ALE growth of InAs has been done by using TMIn and  $\text{AsH}_3$  as the reactants in an atmospheric-pressure MOCVD reactor at 340°C. The saturation level is affected by the total TMIn exposure. The dose-dependent saturation is explained by steric-hindrance effects of the initial adsorbate [110].

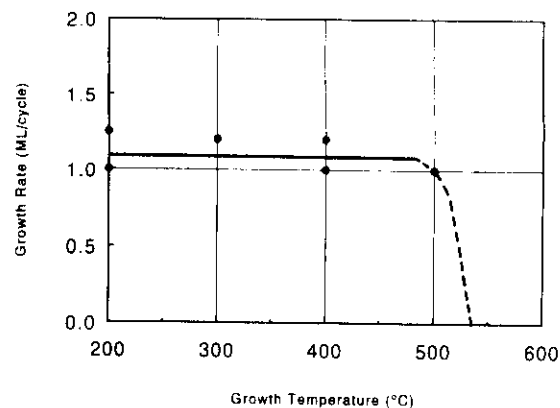


Fig. 31. ALE processing characteristics for the GaAs/GaCl<sub>3</sub> + AsH<sub>3</sub> reaction. The reactor used was a multi-tube vertical atmospheric-pressure CVD reactor with rotating substrate holder. The carrier gas and purge gas was H<sub>2</sub> [109].

### 3.2.4. Indium phosphide (InP)

3.2.4.1. InP/TMIn (trimethylindium) + PH<sub>3</sub> (phosphine). ALE growth of InP has been done on GaAs and InP substrates in the temperature range 320–360°C in a low-pressure MOCVD system with a fast switch-gas manifold. The carrier gas used was argon [111]. The growth temperature was varied from 300–380°C and the working pressure was maintained at 76 Torr. The total flow rate was 7 slm, giving a gas flow speed of about 100 cm/s. The typical number of growth cycles was 300. The thickness of the layers (roughly 9000 Å) was determined by selectively removing InP layers grown on a GaAs substrate using HCl and/or by removing the silicon mask on an InP substrate using HF. The growth characteristics are shown in fig. 32.

The saturation characteristics at 340°C were also studied as a function of TMIn injection time, TMIn flow rate and PH<sub>3</sub> injection time and PH<sub>3</sub> flow rate. The 1 ML/cycle saturation was observed over a wide range of all these parameters. All the surfaces obtained were mirror-like for growth rates up to 1 ML/cycle. For growth rates over 1 ML/cycle or in the case of insufficient supply of PH<sub>3</sub> a hazy surface was observed. The growth was also performed at 300 Torr pressure, with similar results. The temperature range for 1 ML/cycle saturation is wider than the temperature window reported for InP grown in an H<sub>2</sub> atmosphere [97]. This might be due to reduced decomposition of TMIn in the argon flux.

In the ALE of InP by Kobayashi and Kobayashi [112] a long H<sub>2</sub> sequence is needed after the TMIn exposure. By using surface photoadsorption (SPA) analysis they showed that in order to get a 1 ML/cycle growth, a purge with H<sub>2</sub> was needed to complete the decomposition of the TMIn surface. They explain that either PH<sub>3</sub> pyrolysis did not occur or occurred very slowly at a CH<sub>3</sub>-terminated indium surface, while it occurred more effectively on an In-metal surface. Also, this might indicate that

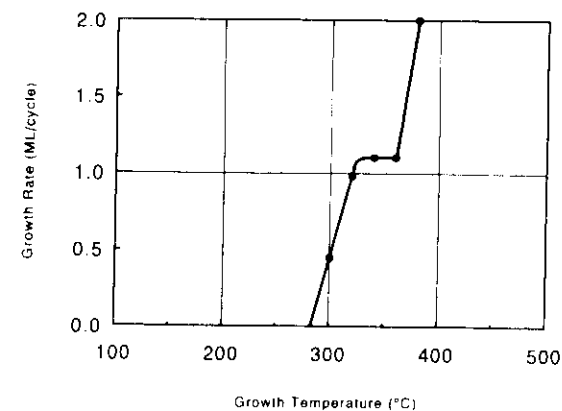


Fig. 32. ALE growth characteristics of the InP/TMIn + PH<sub>3</sub> process [111].

PH<sub>3</sub> has been thermally decomposed before entering the surface and that elemental P is not capable of bonding to a CH<sub>3</sub>-terminated surface but adsorbs on an In-metal surface.

InP has also been grown in a modified MOCVD system at 10 mTorr pressure using TMIn and PH<sub>3</sub> as reactants. One ML/cycle saturation was observed at 340°C [113].

### 3.2.5. III-V superalloys and superlattices

AlGaAs has been processed in a rotating-disk reactor [4]. The substrate rotates between streams of organometallic group-V and group-III hydride reactants. The TMGa and TMAI are supplied simultaneously from one column. The Ga/Al content is controlled by the molar ratio of TMGa and TMAI. Self-limiting growth was observed in the temperature range 550–700°C. The ALE-grown films of AlGaAs have superior photoluminescence properties when compared to the MOCVD-grown films. As-grown ALE films are p-type with carrier concentrations in the 10<sup>17</sup>–10<sup>19</sup> cm<sup>-3</sup> range, depending on the growth conditions [114, 105].

AlGaAs/GaAs structures have been applied to the fabrication of pnp heterojunction bipolar transistors with carbon-doped collector and emitter. AlGaAs/GaAs pnp HBTs have been demonstrated with carbon as the p-type dopant [116].

GaAs/AlAs quantum structures have been reported by Inoue et al. [52], using pre-cracked TMAI and TMGa + AsH<sub>3</sub> diluted with H<sub>2</sub>. The TMAI + AsH<sub>3</sub> reaction does not show saturation without pre-cracking of the TMAI. When this is done, an ALE temperature window can be observed between 460–480°C. This matches the temperature window of the TMGa + AsH<sub>3</sub> process. The growth equipment was a vertical MOCVD system and the operating pressure was 70 Torr. Based on mass spectroscopic observations, the cracking was concluded to result in monomethyl aluminium. Resonant tunneling structures were demonstrated with ALE-grown AlAs

barriers. Negative resistance is observed in the  $I$ - $V$  characteristics of a  $120\ \mu\text{m}^2$  resonant tunneling structure at liquid-nitrogen temperature.

GaAs/InAs structures have been prepared in a vertical atmospheric-pressure MOCVD system using TMGa and AsH<sub>3</sub> as the reactants. The processing temperature for GaAs was 350–450°C [117] and for InAs 300°C. The reactants for InAs were DMIn and AsH<sub>3</sub>. The application here was superlattice structures of GaAs and InAs.

AlAs/InAs-layer superlattices have been grown on (100), (311) and (211) GaAs substrates at 350°C using elemental molecular beams in MBE-type equipment. Due to the low vapour pressures of Al and In, saturation may only occur during the As<sub>4</sub> pulse [59]. Pulsing of the elements enhances surface mobility and the nucleation mode [118].

Extremely high beryllium doping of gallium indium arsenide by low-temperature atomic layer epitaxy has been done by Ohtsuka et al. [119]. The growth temperature was 350°C and the reactants used were TMIn, TEGa and AsH<sub>3</sub>.

Short-period (GaAs)<sub>*n*</sub>(GaP)<sub>*n*</sub> for  $n = 1$ –5 superlattices have been grown by Kodama et al. [120] using a pulsed-jet epitaxy mode of ALE. Zone-folding effects on the longitudinal acoustic (LA) phonons were observed. The Raman peak observed for the (GaAs)<sub>*n*</sub>(GaP)<sub>*n*</sub> monolayer superlattice was also assigned to the scattering from zone-folded LA phonons. The result indicates that the growth of the material has occurred in full atomic planes without significant interdiffusion or roughness at the GaAs/GaP interface.

Al<sub>0.3</sub>Ga<sub>0.7</sub>As/GaAs double heterostructures have been made by combining laser-assisted ALE (LALE) and conventional MOCVD. Quantum-well lasers with an active region grown by LALE are demonstrated [121].

GaInP has been made by using in situ formed GaCl and PH<sub>3</sub> pre-decomposed into P<sub>4</sub> and in situ produced InCl as the reactants [122]. The growth temperature was 450°C and the reactor pressure 1 atm. The reactor used was a three-tube moving-substrate system.

GaInP has also been grown in a vertical-flow rotating-disk reactor using TMGa, TEIn and PH<sub>3</sub> as reactants. The growth was carried out at 480–550°C. For TMGa the exposure time was 0.3 s and for PH<sub>3</sub> 15 s. While the substrate was under PH<sub>3</sub> flow, the TMGa flux was shut off and the TEIn one turned on. The sample was then rotated under TEIn for 0.3 s and back to PH<sub>3</sub> for another 15 s to deposit InP. It turned out that the critical parameter for self-regulation proved to be the lead time after the III element (Ga, In) deposition. This indicates a definite time-dependent mechanism when the exposure time of PH<sub>3</sub> is not sufficient [123].

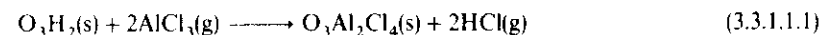
### 3.2.6. GaAs/Si interface

The use of ALE for an interface layer for Si on GaAs has been demonstrated by Hajafuji et al. [124]. Experiments with 100-cycle ALE-grown buffer layers indicated that the final GaAs layer of 1.5 μm was both the more uniform among the different substrates in the reactor and also better in quality than similar layers made on MOCVD-grown buffer layers. The growth of the buffer layers was done at 450°C. Similar results have been reported with ALE buffer layers grown at 500°C from TMGa and AsH<sub>3</sub> [125].

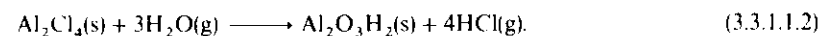
### 3.3. Oxides, nitrides

#### 3.3.1. Aluminium oxide (Al<sub>2</sub>O<sub>3</sub>)

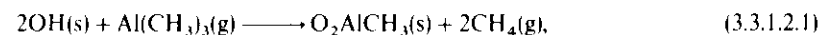
3.3.1.1. Al<sub>2</sub>O<sub>3</sub>/AlCl<sub>3</sub> + H<sub>2</sub>O. Based on a mass spectrometric study of the Al<sub>2</sub>O<sub>3</sub>/AlCl<sub>3</sub> + H<sub>2</sub>O reaction, there is HCl production both after the H<sub>2</sub>O and the AlCl<sub>3</sub> sequence [126]. A possible reaction path is



and



3.3.1.2. Al<sub>2</sub>O<sub>3</sub>/TMAI(trimethylaluminium) + H<sub>2</sub>O. Al<sub>2</sub>O<sub>3</sub> growth has been performed at substrate temperatures between 100 and 500°C by using TMAI and H<sub>2</sub>O as the reactants. The growth was carried out in a vacuum chamber where the TMAI and H<sub>2</sub>O pulses of 0–5 s were fed through pulse valves. The chamber was evacuated for 5 s between the reactant exposures. The growth rate was about 1 ML/cycle, based on a thickness measurement. The substrate used was p-type Si(100) [127, 128]. The proposed reaction pathway can be expressed by the equations



3.3.1.3. Al<sub>2</sub>O<sub>3</sub>/AlCl<sub>3</sub> + O<sub>2</sub>. Al<sub>2</sub>O<sub>3</sub> has been made on single crystal sapphire (1102) and (0001) substrates using a AlCl<sub>3</sub> and the He + 15% O<sub>2</sub> gas mixture as the reactants [129]. Pulse times for AlCl<sub>3</sub> were 30 s and for He + 15% O<sub>2</sub> 60 s and the temperature was 660°C. For Nb(100) substrates the growth temperature used was 450°C. On both substrates the growth rate was 0.09 nm/cycle. Saturation density is explained by a geometrical limitation of AlCl<sub>3</sub>-molecule adsorption.

3.3.1.4. Al<sub>2</sub>O<sub>3</sub>/TMAI(trimethylaluminium) + H<sub>2</sub>O<sub>2</sub>. High-quality Al<sub>2</sub>O<sub>3</sub> films for optical and mechanical coatings have been made using TMAI and H<sub>2</sub>O<sub>2</sub> as the reactants [130]. At the reaction temperature of 150°C a growth rate of 1.13 Å/cycle was observed. Room-temperature reaction was also demonstrated.

3.3.1.5. Al<sub>2</sub>O<sub>3</sub>/AlCl<sub>3</sub>, Al(OR)<sub>3</sub>(aliphatic alcohols) + H<sub>2</sub>O, O<sub>2</sub>. Al<sub>2</sub>O<sub>3</sub> on a glass substrate has been grown using “water-free” oxidants, such as aliphatic alcohols together with aluminium chloride as the reactant for aluminium [131]. Growth rates from 0.4 to 0.7 Å/cycle were observed between 300 and 500°C. Aluminium ethoxide together with water vapour gave a growth rate of 1.2 Å/cycle.

#### 3.3.2. Tantalum pentoxide (Ta<sub>2</sub>O<sub>5</sub>)

3.3.2.1. Ta<sub>2</sub>O<sub>5</sub>/TaCl<sub>5</sub> + H<sub>2</sub>O. Ta<sub>2</sub>O<sub>5</sub> thin films have been grown in a vacuum system using tantalum chloride and water vapour as the reactants. The in situ Auger spectra

indicate that chlorine stays on the surface after the  $\text{TaCl}_5$  pulse and completely disappears after the  $\text{H}_2\text{O}$  pulse [132].

### 3.3.3. Titanium dioxide ( $\text{TiO}_2$ )

3.3.3.1.  $\text{TiO}_2/\text{TiCl}_4 + \text{H}_2\text{O}$ . The initiation of  $\text{TiO}_2$  growth on a silica substrate and OH-group interaction have been studied using large-area porous substrates [133–136]. This also indicates an extension of the applications of ALE to the manufacture of heterogeneous catalysts in a surface-controlled mode.

When applying ALE to catalysts on porous supports, a single reaction cycle may be enough to obtain the necessary surface structures. The chemistry of the starting surface, typically silica or alumina, is therefore critical for the process. As an example, the interaction with the support surface and the reaction temperature of  $\text{TiCl}_4$  at the formation of  $\text{TiO}_2$  on silica is reviewed.

The knowledge of the amount, type and character of the bonding sites of silica is important. Silica consists of two types of bonding site: OH-groups and siloxane bridges. OH-groups are divided into isolated or "free" and H-bonded OH-groups.

Isolated OH-groups are further divided into single and paired OH-groups and the H-bonded ones into strongly and weakly H-bonded OH-groups. The strongly H-bonded OH-groups are present on the silica surface and thus involved in the reactions, whereas the weakly H-bonded OH-groups (so-called inaccessible or bulk OH-groups) are unreactive. The amount of these different reactive sites depends on the heat-treatment temperature of the silica and the type of silica used. A simplified picture of the surface species is shown in fig. 33.

The interaction between  $\text{TiCl}_4$  and the OH-groups of silica is highly dependent on the reaction temperature. Lower reaction temperatures ( $< 280^\circ\text{C}$ ) favour the formation of amorphous titanium species, whereas an increase of the reaction temperature up to  $320^\circ\text{C}$  initiates agglomeration into  $\text{TiO}_2$  with anatase and rutile crystal structure, as shown in fig. 34. The pre-heating temperature of silica has an effect on the amount and in some cases also on the character of the different titanium species. Despite the agglomeration, the reactions are surface controlled with a precise saturation density.

At lower temperatures ( $< 280^\circ\text{C}$ )  $\text{TiCl}_4$  reacts both mono-functionally and bi-functionally with the OH-groups of silica and HCl is evolved. The formed amorphous titanium species is quantitatively etched with dilute sulphuric acid without the decomposition of silica. The amount of doubly bonded titanium species depends on the pre-heating temperature of silica and the reaction temperature used. The pre-heating temperature of the silica determines the internuclear distance between neighbouring OH-groups and the reaction temperature determines the minimum energy needed for  $\text{TiCl}_4$  to be capable of reacting bi-functionally.

To obtain the highest possible surface coverage of covalently bonded amorphous titanium species,  $\text{TiCl}_4$  is reacted at  $175^\circ\text{C}$  with silica pre-heated at  $200^\circ\text{C}$ . In this case a bi-functional reaction takes place with strongly H-bonded OH-groups still present on the silica. A singly bonded titanium species is formed with isolated OH-groups. The strongly H-bonded OH-groups are the first ones to be removed on raising the pre-heating temperature of the silica. When the strongly H-bonded OH-groups are

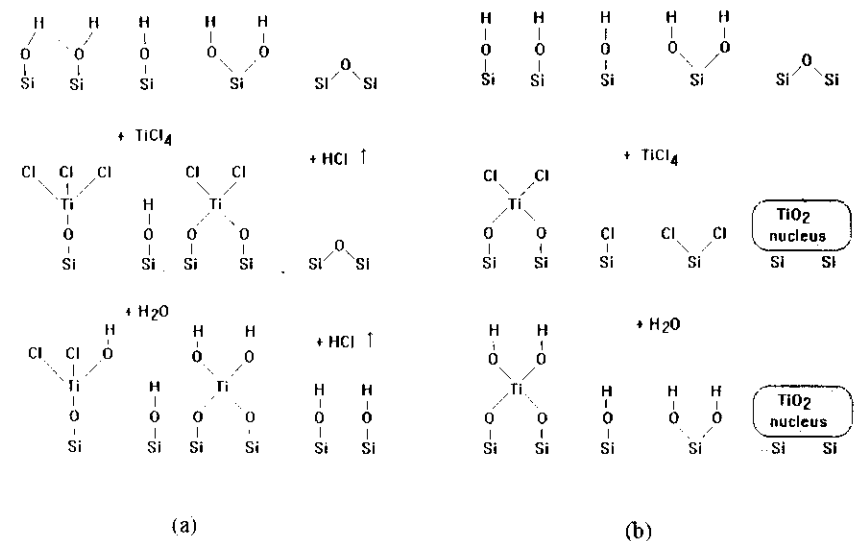


Fig. 33. Bonding sites of silica and titanium surface species (a) at reaction temperatures of 175 and  $250^\circ\text{C}$  and (b) at  $350^\circ\text{C}$  and higher, after exposures to  $\text{TiCl}_4$  and subsequent  $\text{H}_2\text{O}$  sequences [134].

removed from the surface, the amount of titanium species decreases and the amount of doubly bonded titanium species is controlled by the distance between the remaining OH-groups and by the reaction temperature. Upon water treatment, anatase-like  $\text{Ti-OH}$  groups are generated.

Etching with sulphuric acid reveals the amount of amorphous titanium species present on the silica surface. After  $\text{TiCl}_4$  reaction, carried out at  $300^\circ\text{C}$ , the character of the titanium species is changed, as reflected by the decreasing amount of etched titanium species. When the reaction temperature is raised to  $320^\circ\text{C}$  and above, agglomeration into  $\text{TiO}_2$  with anatase and rutile crystal structure takes place. Reaction temperatures below  $450^\circ\text{C}$  lead to anatase crystalline structure and at  $450^\circ\text{C}$  the rutile crystalline structure appears as well. A reaction temperature of  $550^\circ\text{C}$  leads exclusively to the rutile crystalline structure.

The amount of amorphous titanium species is a function of reaction temperature at a constant pre-heating temperature of the silica and also a function of pre-heating temperature at a constant reaction temperature. Therefore both the reaction temperature and the pre-heating temperature of the silica have an effect on the amount of the different titanium species to be bonded to silica. Furthermore, the higher pre-heating temperatures of the silica at a constant reaction temperature favour the formation of rutile. It must be emphasized that  $\text{TiO}_2$  is formed during the main reaction, not upon water treatment. Water treatment of these Ti/silica samples generates  $\text{Ti-OH}$  groups due to amorphous titanium species, and most of the OH-groups of silica re-appear.

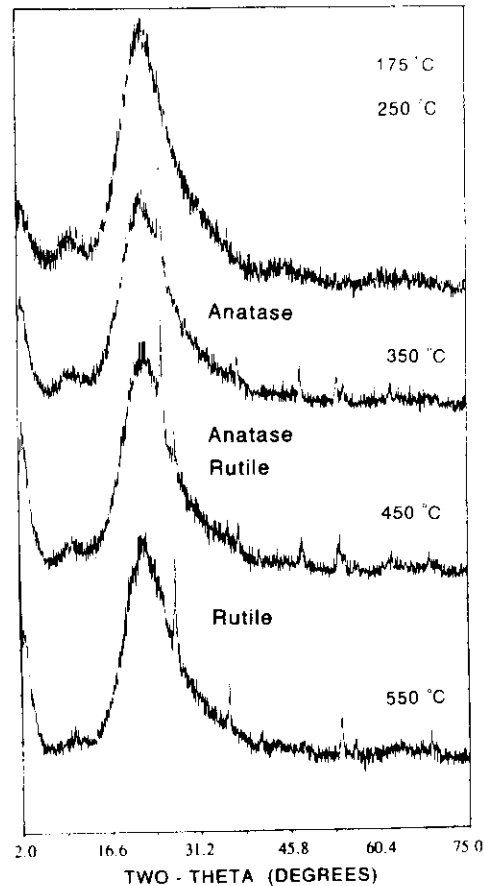


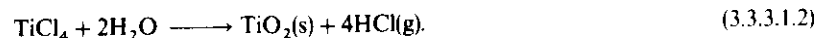
Fig. 34. XRD-spectra of a silica surface after  $\text{TiCl}_4$  exposures at 175–550 °C. The pre-treatment temperature of the silica surface is 560 °C [136].

This is because, with an increasing reaction temperature, an increasing amount of OH-groups are exchanged for chloride by  $\text{TiCl}_4$  except for those binding to amorphous titanium species.

In continuous ALE growth on a planar surface, it has been observed that at 400 °C the  $\text{TiO}_2/\text{TiCl}_4 + \text{H}_2\text{O}$  reaction produces HCl only after  $\text{H}_2\text{O}$  exposure, as confirmed by mass spectrometry. This suggests the reactions



and



The latter reaction in its complete form is valid only if all the chloride is removed during the  $\text{H}_2\text{O}$  exposure. The above reaction scheme is also consistent with the results from growth on porous silica surfaces at high temperatures, where most of the OH-groups of silica were occupied by chloride and no Ti–OH groups due to crystalline  $\text{TiO}_2$  were observed.

Polycrystalline  $\text{TiO}_2$  can be grown over a wide range of temperatures, from 150 to 600 °C [137]. The rate of the growth is about 0.3 ML/cycle.

### 3.3.4. Nitrides

So far, the use of ALE in the growth of nitrides has been rare. Hiltunen et al. [44] published the first ALE-nitride work in 1988. Polycrystalline metal-nitrides of titanium, niobium, tantalum and molybdenum were grown on soda-glass substrates at 500 °C using chlorides and ammonia as reactants. In all cases the growth rate was low, i.e. 0.2–0.3 Å/cycle, which is much less than 1 ML/cycle. Chlorine was found to be present as an impurity in the TiN films, but not in other films. Later, the work concentrated on III–V thin films of AlN, GaN and  $\text{Al}_x\text{Ga}_{1-x}\text{N}$ , which have many potential applications in microelectronic and sensor technology [137].

**3.3.4.1. Indium nitride (InN).** InN from indium chloride ( $\text{InCl}_3$ ) and ammonia ( $\text{NH}_3$ ) [139] has been grown at 420 to 520 °C in an atmospheric-pressure hot-wall reactor.

**3.3.4.2. Gallium nitride (GaN)/TMGa, TEGa +  $\text{NH}_3$ .** Khan et al. [140, 141] started their work with the growth of GaN, but they extended their studies to include  $\text{Al}_x\text{Ga}_{1-x}\text{N}$  prepared from triethylgallium (TEGa), triethylaluminium (TEAl) and ammonia ( $\text{NH}_3$ ) on sapphire substrates, typically at 800–1000 °C. The optical and electrical quality of the films was equal or better than the quality of conventional low-pressure MOCVD films. The studies showed that single crystal epitaxy was possible at temperatures as low as 450 °C, whereas with conventional techniques a temperature of at least 700 °C was required. ALE films were smoother when compared to conventional films. GaN single crystal films were highly insulating [142].

**3.3.4.3. Aluminium nitride (AlN).** Mayer et al. [138] outlined the conditions under which atomic layer growth of AlN from trimethylaluminium (TMAI) and ammonia ( $\text{NH}_3$ ) should be possible. They restricted the temperature of growth to the range from 550 to 650 K. At temperatures higher than 650 K adsorption of TMAI was no longer self-limiting. At temperatures lower than 550 K the elimination of  $\text{CH}_3$  was incomplete and reaction with  $\text{NH}_3$  slow. Actual growth experiments on Si(100) substrates at 600 K, studied by XPS and LEED, showed significant carbon contamination of the films. Also, no indication of crystalline film formation was observed. Mayer et al. mentioned, however, that they did not attempt to optimize the growth, nor to extend it past three full cycles.

**3.3.4.4. Niobium nitride (NbN).** Niobium nitride made by Hiltunen et al. [44] shows superconductivity below 10 K. The films were (111)-oriented  $\delta$ -NbN films.

### 3.4. Group-IV semiconductors

#### 3.4.1. Germanium (Ge)

3.4.1.1. *Ge/GeH<sub>4</sub> (germane) + thermal cycling.* Atomic layer epitaxy of Ge on silicon has been demonstrated using flash heating for chemical vapour deposition [143]. The reactant used for Ge was GeH<sub>4</sub>, which was decomposed on the surface by heating it with an Xe flash lamp. Silicon (111) and (100) surfaces were subjected to continuous interaction with GeH<sub>4</sub> vapour, which resulted in a monolayer coverage of GeH<sub>4</sub> surface. When a 1 ms Xe lamp shot of 20 J/cm<sup>2</sup> was applied, decomposition of the surface Ge hydrides occurred. The formation speed of a new monolayer of GeH<sub>4</sub> was from 20 to 60 s depending on the partial pressure of GeH<sub>4</sub>. Saturated growth at one monolayer per shot was observed at temperatures between 260 and 270°C. (See fig. 35.)

3.4.1.2. *Ge/DEGeH<sub>2</sub> (diethylgermane) + thermal cycling.* Monolayer growth of single crystal germanium films is obtained without carbon contamination [144] by thermal cycling of Ge(C<sub>2</sub>H<sub>5</sub>)<sub>2</sub>H<sub>2</sub> (diethylgermane), which is adsorbed at 320°C. At heating by an argon laser, the desorbing surface species is the ethyl radical. Layer-by-layer growth has also been observed by DEGe adsorption at 220°C and desorption at 510°C [145].

#### 3.4.2. Silicon (Si)

3.4.2.1. *Si/Si<sub>2</sub>H<sub>6</sub> (or Si<sub>3</sub>H<sub>8</sub>) (di- or trisilane) + thermal cycling.* Monolayer growth of silicon has been obtained by combining self-limiting adsorption of Si<sub>2</sub>H<sub>6</sub> on Si(100)(2 × 1) and ArF-laser irradiation. After exposing an Si(100)(2 × 1) clean surface to an Si<sub>2</sub>H<sub>6</sub> dose of 2 × 10<sup>17</sup> cm<sup>-2</sup>, a uniform dihydride surface is formed. This adsorption process is found to be essentially self-limiting at room temperature.

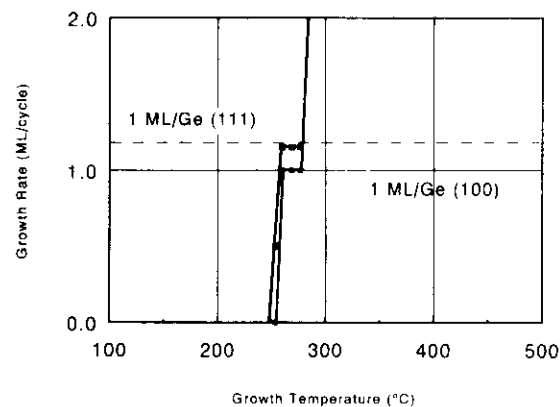


Fig. 35. ALE of Ge and Si on Ge(111) and Ge(100) surfaces [143].

In order to release hydrogen, the Si-H surface is heated to at least 450°C. Hydrogen can also be released by pulsed KrF-laser irradiation which keeps the average surface temperature almost constant. A growth rate of 0.4 ML/cycle has been demonstrated [146, 147, 113].

Single crystal silicon has also been made by thermal cycling using Si<sub>3</sub>H<sub>8</sub> as the reactant [148]. Si<sub>3</sub>H<sub>8</sub> is first adsorbed on a (111) surface at a substrate temperature below 380°C. Hydrogen staying on the surface is subsequently desorbed at a temperature above 520°C. The experiment has been carried out in an MBE system. The observed growth rate was 0.8 ML per cycle.

3.4.2.2. *Si/DESiH<sub>2</sub> + thermal cycling.* Study of diethylsilane decomposition on silicon surfaces suggests that DESiH<sub>2</sub> is a potential reactant candidate for ALE on silicon while adsorbing DESiH<sub>2</sub> at 640°C. DESiH<sub>2</sub> adsorbs associatively (CH<sub>2</sub>=CH<sub>2</sub>) via β-hydride elimination and deposits silicon and hydrogen on the silicon surface. If this is followed by a thermal annealing to 800 K to desorb H<sub>2</sub>, saturated ALE growth of 0.13 ML/cycle can be performed [149].

3.4.2.3. *Si/SiH<sub>2</sub>Cl<sub>2</sub> (chlorosilane) + thermal cycling.* The chemisorption of SiH<sub>2</sub>Cl<sub>2</sub> on a silicon surface has been proposed as an alternative for ALE on silicon. In the chemisorption, a SiCl surface is formed which probably could be reduced with atomic hydrogen at 600°C. Atomic hydrogen is probably needed to remove the chlorine [150].

Adsorption of SiH<sub>2</sub>Cl<sub>2</sub> on the Ge(100) surface is found to be self-limiting below 350°C, according to X-ray photoelectron spectroscopy and thermal desorption measurements [151].

#### 3.4.3. Silicon carbide (SiC)

ALE of silicon carbide has been demonstrated by Fuyuki et al. [152] by using disilane (Si<sub>2</sub>H<sub>6</sub>) and acetylene (C<sub>2</sub>H<sub>2</sub>) as the reactants. In situ RHEED analysis of the surface structure after Si<sub>2</sub>H<sub>6</sub> exposure shows a (3 × 2) pattern and a (1 × 1) pattern after C<sub>2</sub>H<sub>2</sub> exposure. The rate of the growth was determined by the Si-atom density in the (3 × 2) reconstructed monolayer, which means <sup>1</sup>/<sub>6</sub> monolayers per cycle. The growth was carried out in gas-source MBE equipment at about 10<sup>-5</sup> Torr. The substrate was cubic SiC crystal and the temperatures used were 1000 and 1050°C.

## 4. Summary

Atomic layer epitaxy is a surface-controlled method of producing atomic surface layers, epitaxial layers and thin films. In spite of the principal simplicity of the process, the surface chemistry of ALE is not very well understood. The surface chemistry is strictly individual for each material to be processed and for each combination of reactants used for the process. In ALE, chemical reactions are divided into well-defined sub-reactions. This helps, by penetrating deeper into the reaction mechanisms and reaction pathways in ALE, to serve as a link between theoretical and experimental chemistry.



Application-oriented work with ALE is directed to areas like:

- Epitaxy of III–V and II–VI single crystals: optoelectronic devices, etc.
- Superlattices of III–V and II–VI single crystals: semiconductor lasers, quantum devices.
- Layer-by-layer controlled epitaxy of covalent materials: conformational growth, advanced semiconductor devices.
- Interfaces, thin dielectric layers, controlled superalloys: advanced semiconductor devices.
- Large-area thin-film applications: EL devices, thin-film solar cells.
- Tailored molecular surfaces: heterogeneous catalysts.

ALE has already shown its productive capability in the electroluminescent flat-panel display technology [3]. The cost efficiency of the process is based on the inherent self-control, which makes handling of large batches in a small volume possible. ALE also makes it possible to produce different types of materials in one process. For electroluminescent thin-film structures the whole stack of dielectric semiconducting-dielectric thin films can be made in one process by using ALE. While ALE was originally developed to meet the qualitative requirements of the materials [2], it has turned out that the inherent self-control of ALE is also a key to productive and cost-effective processing.

### Acknowledgements

The author thanks Dr. Eeva Lakomaa, Dr. Marina Lindblad, Dr. Suvi Haukka, Ms. Arla Kytökivi, Mr. Jaakko Hyvärinen and Ms. Heli Vaara for their assistance in collecting data and preparing the manuscript.

### References

- [1] T. Suntola, *Mater. Sci. Rep.* 4(7) (1989) 261.
- [2] T. Suntola and J. Antson, Patent US 4058430 (1977).
- [3] T. Suntola, J. Antson, A. Pakkala and S. Lindfors, *SID 80 Digest* (1980) 108.
- [4] T. Suntola and M. Simpson, *Atomic Layer Epitaxy* (Blackie & Son, Glasgow, London, 1990) ch. 4.
- [5] J. Hyvärinen, M. Sonninen and R. Törnqvist, *J. Cryst. Growth* 86 (1–4) (1988) 695.
- [6] P.C. Colter, S.A. Hussien, A. Dip, M.U. Erdogan and S.M. Bedair, *MRS Symp. Proc.* 222 (1991) 157.
- [7] T. Suntola, A. Pakkala and S. Lindfors, Patent US 4389973 (1980).
- [8] T. Suntola, A. Pakkala and S. Lindfors, Patent US 4413022 (1980).
- [9] A. Rautiainen, Y. Koskinen, J. Skarp and S. Lindfors, *MRS Symp. Proc.* 222 (1991) 263.
- [10] W. Faschinger and H. Sitter, *J. Cryst. Growth* 99 (1990) 566.
- [11] W. Faschinger, P. Juza and H. Sitter, *J. Cryst. Growth* 115 (1991) 692.
- [12] M. Pessa, O. Jylhä, P. Huttunen and M.A. Herman, *J. Vac. Sci. Technol.* A2(2) (1984) 418.
- [13] M. Pessa, P. Huttunen and M.A. Herman, *J. Appl. Phys.* 54(10) (1983) 6047.
- [14] M. Pessa, O. Jylhä and M.A. Herman, *J. Cryst. Growth* 67 (1984) 255.
- [15] A. Kytökivi, Y. Koskinen, A. Rautiainen and J. Skarp, *MRS Symp. Proc.* 222 (1991) 269.
- [16] M. Sopanen and T. Tuomi, *Acta Polytech. Scand. Chem. Technol. Metall. Ser.* 195 (1990) 179.
- [17] M. Lindblad and T.A. Pakkanen, *J. Comput. Chem.* 9 (1988) 581.
- [18] T.A. Pakkanen, V. Nevalainen, M. Lindblad and P. Makkonen, *Surf. Sci.* 188 (1987) 456.
- [19] V.-P. Tanninen, T. Tuomi, M.C. Typpi, R.O. Törnqvist, T. Suntola, J. Antson, A. Pakkala and S. Lindfors, *Proc. of the 8th Int. Vacuum Congress*, Sept. 22–26, 1980, Cannes, Vol. I, *Thin Films* (1980) p. 401.
- [20] V.-P. Tanninen, M. Oikkonen and T.O. Tuomi, *Phys. Status Solidi* (a) 67 (1981) 573.
- [21] V.-P. Tanninen, *Acta Polytech. Scand. Appl. Phys. Ser.* 137 (1983) 33.
- [22] W. Busse, H.-E. Gumlich, R.O. Törnqvist and V.-P. Tanninen, *Phys. Status Solidi* (a) 76 (1983) 553.
- [23] M. Oikkonen, *J. Appl. Phys.* 62(4) (1987) 1385.
- [24] A. Hunter and A.H. Kitai, *J. Cryst. Growth* 91 (1988) 111.
- [25] Y. Wu, T. Toyoda, Y. Kawakami, S. Fujita and S. Fujita, *Jpn. J. Appl. Phys.* 29(5) (1990) L727.
- [26] S. Yamaga and A. Yoshikawa, *J. Cryst. Growth* 117 (1992) 152.
- [27] T. Yao, Z.Q. K. Zhu, K. Uesugi, S. Kamiyama and M. Fujimoto, *J. Vac. Sci. Technol.* A8(2) (1990).
- [28] T. Yao and T. Takeda, *Appl. Phys. Lett.* 48(2) (1986) 160.
- [29] S. Dosho, Y. Takemura, M. Konagai and K. Takahashi, *J. Appl. Phys.* 66(6) (1989) 2597.
- [30] Z. Zhu, M. Hagino, K. Uesugi, S. Kamiyama, M. Fujimoto and T. Yao, *J. Cryst. Growth* 99 (1990) 441.
- [31] Z. Zhu, M. Hagino, K. Uesugi, S. Kamiyama, M. Fujimoto and T. Yao, *Jpn. J. Appl. Phys.* 28(9) (1989) 1659.
- [32] T. Yao and T. Takeda, *Appl. Phys. Lett.* 48(23) (1986) 1615.
- [33] H.J. Cornelissen, D.A. Cammack and R.J. Dalby, *NATO Advanced Res. workshop on Growth and Optical Properties of Wide Band Gap II–VI's Low Dimensional Semiconductors*, Regensburg, FRG, 2–5 Aug. 1988 *NATO ASI Ser. B200* (1988) p. 257.
- [34] R. Kimura, M. Konagai and K. Takahashi, *J. Cryst. Growth* 116 (1992) 283.
- [35] Y. Kawakami, T. Toyoda, Y. Wu, S. Fujita and S. Fujita, *J. Cryst. Growth* 107 (1991) 1072.
- [36] N. Shibata and A. Katsui, *J. Cryst. Growth* 101 (1990) 91.
- [37] A. Yoshikawa, T. Okamoto, H. Yasuda, S. Yamaga and H. Kasai, *J. Cryst. Growth* 101 (1990) 86.
- [38] N. Shibata and A. Katsui, *IV Int. Conf. on II–VI-compounds*, Sep. 17–22 (1989) Berlin, FRG, Mo-P-10.
- [39] C.D. Lee, B.H. Lim, C. Lim, H.L. Park, C.H. Chung and S.K. Chang, *J. Cryst. Growth* 117 (1992) 148.
- [40] M. Ahonen, M. Pessa and T. Suntola, *Thin Solid Films* 65 (1980) 301.
- [41] Y. Takemura, M. Konagai, H. Nakanishi and K. Takahashi, *J. Cryst. Growth* 117 (1992) 144.
- [42] Y. Takemura, H. Nakanishi, M. Konagai and K. Takahashi, *Jpn. J. Appl. Phys.* 30(2B) (1991) L246.
- [43] M. Tammenmaa, H. Antson, M. Asplund, L. Hiltunen, M. Leskelä and L. Niinistö, *J. Cryst. Growth* 84 (1987) 151.
- [44] L. Hiltunen, M. Leskelä, M. Mäkelä, L. Niinistö, E. Nykänen and P. Soininen, *Thin Solid Films* 166 (1988) 149.
- [45] H. Otoma, T. Honda, K. Hara, J. Yoshino and H. Kukimoto, *J. Cryst. Growth* 115 (1991) 807.
- [46] M. Konagai, S. Dosho, Y. Takemura, N. Teraguchi, R. Kimura and K. Takahashi, *NATO Advanced Research Workshop on Growth and Optical Properties of Wide Gap II–VI's Low Dimensional Semiconductors*, Regensburg, Germany, 2–5 Aug. (1988).
- [47] S. Dosho, Y. Takemura, M. Konagai and K. Takahashi, *J. Cryst. Growth* 95 (1989) 580.
- [48] Y. Takemura, H. Nakanishi, M. Konagai, K. Takahashi, Y. Nakamura and N. Otsuka, *J. Cryst. Growth* 111 (1991) 802.
- [49] T. Takeda, T. Kurosu, M. Iida and T. Yao, *Surf. Sci.* 174 (1986) 548.
- [50] S. Ohta, S. Kobayashi, F. Kaneko and K. Kashiro, *J. Cryst. Growth* 106 (1990) 166.
- [51] T. Yao, M. Fujimoto, S.K. Chang and H. Tanino, *J. Cryst. Growth* 111 (1991) 823.
- [52] N. Inoue, H. Yokoyama, M. Shinohara and T. Murashita, *Surf. Sci.* 267 (1992) 34.
- [53] M. Ozeki, K. Mochizuki, N. Ohtsuka and K. Kodama, *J. Vac. Sci. Technol.* B5(4) (1987) 1184.
- [54] M. Ishizaki, N. Kano, J. Yoshino and H. Kukimoto, *Jpn. J. Appl. Phys.* 30(3B) (1991) L435.
- [55] H. Yokoyama, M. Shinohara and N. Inoue, *Appl. Phys. Lett.* 60(3) (1992) 377.
- [56] T. Meguro, S. Iwai, Y. Ayoagi, K. Ozaki, Y. Yamamoto, T. Suzuki, Y. Okano and A. Hirata, *J. Cryst. Growth* 99 (1990) 540.
- [57] H. Yamaguchi, R. Kobayashi, Y. Jin and F. Hasegawa, *Jpn. J. Appl. Phys.* 38(1) (1989) L4.
- [58] A. Vila, A. Cornet, J.R. Morante, Y. Gonzalez, L. Gonzalez and F. Briones, *Mater. Lett.* 11(5–7) (1991) 155.

- [59] P. Castrillo, G. Armelles, P.S. Dominguez, J. Melendez and F. Briones, *Surf. Sci.* 267(1-3) (1992) 413.
- [60] M. Vazquez, J.P. Silveira, L. Gonzalez, M. Perez, G. Armelles, J.L. De Miguel and F. Briones, *J. Cryst. Growth* 102(4) (1990) 891.
- [61] J. Nishizawa, *J. Cryst. Growth* 115(1-4) (1991) 12.
- [62] A. Doi, Y. Aoyagi and S. Namba, *Appl. Phys. Lett.* 49 (13) (1986) 785.
- [63] J. Nishizawa, T. Kurabayashi, H. Abe and N. Sakurai, *J. Vac. Sci. Technol.* A5 (1987) 1572.
- [64] J. Nishizawa, T. Kurabayashi, H. Abe and N. Sakurai, *J. Electrochem. Soc.* 134(4) (1987) 945.
- [65] M. Ozeki, N. Mochizuki, N. Ohtsuka and K. Kodama, *Appl. Phys. Lett.* 53(16) (1988) 1509.
- [66] M.A. Tischler and S.M. Bedair, *Appl. Phys. Lett.* 48(24) (1986) 1681.
- [67] N.H. Karam, H. Liu, I. Yoshida and S.M. Bedair, *Appl. Phys. Lett.* 52(14) (1988) 1144.
- [68] K.G. Reid, H.M. Urdianyk and S.M. Bedair, *Appl. Phys. Lett.* 59(19) (1991) 2397.
- [69] J. Nishizawa and T. Kubayashi, *J. Cryst. Growth* 93 (1988) 98.
- [70] A. Watanabe, T. Kamijoh, M. Hata, T. Isu and Y. Katayama, *Vacuum* 41(4-6) (1990) 965.
- [71] J.R. Creighton, *Surf. Sci.* 234 (1990) 287.
- [72] Y. Sakuma, M. Ozeki, N. Ohtsuka and K. Kodama, *J. Appl. Phys.* 68(11) (1990) 5660.
- [73] N. Kobayashi, Y. Yamauchi and Y. Horikoshi, *J. Cryst. Growth* 115(1-4) (1991) 353.
- [74] A.V. Annappagada, S. Salim and K.F. Jensen, *MRS Symp. Proc.* 222 (1991) 81.
- [75] Y. Aoyagi, S. Iwai and T. Meguro, *Denki Kagaku Oyobi Kogyo Butsuri Kagaku* 59(12) (1991) 1037.
- [76] H. Ishikawa, Y. Kawakyu, M. Sasaki and M. Mashita, *Jpn. J. Appl. Phys.* 28(12) (1989) L2327.
- [77] Y. Kawakyu, H. Ishikawa, M. Sasaki and M. Mashita, *Jpn. J. Appl. Phys.* 28(8) (1989) L1439.
- [78] H. Yokoyama, M. Shinohara and N. Inoue, *Appl. Phys. Lett.* 59(17) (1991) 2148.
- [79] H. Yokoyama, M. Shinohara and N. Inoue, *J. Cryst. Growth* 115(1-4) (1991) 89.
- [80] K. Kodama, M. Ozeki, K. Mochizuki and N. Ohtsuka, *Appl. Phys. Lett.* 13 (1989).
- [81] P.E. Gee and R.F. Hicks, *MRS Symp. Proc.* 222 (1991) 47.
- [82] M. de Keijser and C. van Opdorp, *Appl. Phys. Lett.* 58(11) (1991) 1187.
- [83] U. Memmert and M.L. Yu, *Appl. Phys. Lett.* 567 (1990) 1883.
- [84] M. Yu, N. Buchan, R. Souda and T. Kuech, *MRS Symp. Proc.* 222 (1991) 3.
- [85] B.Y. Maa and P.D. Dapkus, *MRS Symp. Proc.* 222 (1991) 25.
- [86] P.D. Dapkus, B.Y. Maa, W. Chen, W.G. Jeong and S.P. Den Baars, *J. Cryst. Growth* 107(1-4) (1991) 73.
- [87] B.A. Banse and J.R. Creighton, *Appl. Phys. Lett.* 60(7) (1992) 856.
- [88] B.Y. Maa and P.D. Dapkus, *J. Electron. Mater.* 19(4) (1990).
- [89] T.H. Chiu and J.E. Cunningham, *J. Cryst. Growth* 105(1-4) (1990) 155.
- [90] J. Wissler, P. Czuprin, D. Grundmann, P. Balk, M. Waschbusch, R. Luckeath and W. Richter, *J. Cryst. Growth* 107(1-4) (1991) 111.
- [91] J.R. Gong, P.C. Colter, D. Jung, S.A. Hussien, C.A. Parker, A. Dip and F. Hyuga, *J. Cryst. Growth* 107(1-4) (1991) 83.
- [92] Y. Aoyagi, A. Doi, S. Iwai and S. Namba, *J. Vac. Sci. Technol.* B5 (1987) 1460.
- [93] Y. Aoyagi, T. Meguro, S. Iwai and A. Doi, *Mater. Sci. Eng.* B10 (1991) 121.
- [94] T. Meguro, T. Suzuki, K. Ozaki, Y. Okano, A. Hirata, Y. Yamamoto, S. Iwai, Y. Aoyagi and S. Namba, *J. Cryst. Growth* 93 (1988) 190.
- [95] J. Nishizawa, H. Abe, T. Kurabayashi and N. Sakurai, *J. Vac. Sci. Technol.* A4 (1986) 706.
- [96] J. Nishizawa, H. Abe and T. Kurabayashi, *J. Electrochem. Soc.* 136 (1989) 478.
- [97] W. Tsen, J. Tsen, L. Anthony and P. Liu, *Appl. Phys. Lett.* 55 (1989) 987.
- [98] B.Y. Maa and P.D. Dapkus, *Appl. Phys. Lett.* 58(20) (1991) 2261.
- [99] B.Y. Maa and P.D. Dapkus, *J. Electron. Mater.* 20(8) (1991).
- [100] B.Y. Maa and P.D. Dapkus, *Appl. Phys. Lett.* 58(16) (1991) 1762.
- [101] C. Sasaoka, Y. Kato and A. Usui, *Jpn. J. Appl. Phys.* 30 (10A) (1991) L1756.
- [102] C. Sasaoka, Y. Kato and A. Usui, *J. Cryst. Growth* 1995 (1991) 94.
- [103] K. Mori, M. Yoshida and A. Usui, *Inst. Phys. Conf. Ser.* 91(3) (1988) 187.
- [104] C. Sasaoka, M. Yoshida and A. Usui, *Jpn. J. Appl. Phys.* 27 (1988) L490.
- [105] K. Mori, M. Yoshida, A. Usui and H. Terao, *Appl. Phys. Lett.* 52(1) (1988) 27.
- [106] A. Usui, 19th Conf. on Solid State Devices and Materials, Tokyo (1987) p. 471.
- [107] S. Iwai, T. Meguro, Y. Aoyagi and S. Namba, *MRS Symp. Proc.* 129 (1989) 171.
- [108] H. Ishii, H. Ohno, K. Matsuzaki and H. Hasegawa, *J. Cryst. Growth* 95 (1989) 132.

- [109] Y. Jim, R. Kobayashi, K. Fujii and F. Hasegawa, *Jpn. J. Appl. Phys.* 29(8) (1990) L1350.
- [110] W.G. Jeong, F.P. Menu and P.D. Dapkus, *Appl. Phys. Lett.* 55(3) (1989) 244.
- [111] D. Bertone, *J. Electron. Mater.* 21(3) (1992) 265.
- [112] Y. Kobayashi and N. Kobayashi, *Jpn. J. Appl. Phys.* 31 (1992) L71.
- [113] W.K. Chen, J.C. Chen, L. Anthony and P.L. Liu, *Appl. Phys. Lett.* 55(10) (1989) 987.
- [114] J.R. Gong, D. Jung, N.A. El-Masry and S.M. Bedair, *Appl. Phys. Lett.* 57(4) (1990) 400.
- [115] S.M. Bedair, K.G. Reid, S.A. Hussien, P.C. Colter, A. Dip, H.M. Urdianyk and V. Erdogan, *Inst. Phys. Conf. Ser.* 112 (1990) 143.
- [116] T. Henderson, B. Bayraktaroglu, S. Hussien, A. Dip, P. Colter and S.M. Bedair, *Electron. Lett.* 27(9) (1991) 692.
- [117] H. Ohno, S. Ohtsuka, A. Ohuchi, T. Matsubara and H. Hasegawa, *J. Cryst. Growth* 93 (1988) 342.
- [118] F. Briones and A. Ruiz, *J. Cryst. Growth* 111 (1991) 194.
- [119] N. Ohtsuka, K. Kodama, M. Ozeki and Y. Sakuma, *J. Cryst. Growth* 115(1-4) (1991) 460.
- [120] K. Kodama, M. Ozeki, Y. Sakuma and N. Ohtsuka, *J. Appl. Phys.* 69(9) (1991) 6713.
- [121] Q. Chen, J.S. Osinski and P.D. Dapkus, *Appl. Phys. Lett.* 57(14) (1990) 1437.
- [122] A. Usui and H. Sunakawa, Extended abstract of 20th 1988 Int. Conf. on Solid State Devices and Materials, Aug. 24-26, 1988, Kejo Plaza Hotel, Tokyo, Japan.
- [123] B.T. McDermott, N.A. El-Masry, B.L. Jiang, F. Hyuga and S.M. Bedair, *J. Cryst. Growth* 107 (1991) 96.
- [124] N. Hajafuji, M. Miyashita, H. Kumabe and T. Murotani, *J. Cryst. Growth* 106 (1990) 421.
- [125] K. Fujita, H. Kanao and Y. Shiba, *Jpn. J. Appl. Phys.* 30(4) (1991) 633.
- [126] M. Soinenen, Lohja Corp, private communication (1987).
- [127] G.S. Higashi and C.G. Fleming, *Appl. Phys. Lett.* 55(19) (1989) 1963.
- [128] S.M. George, O. Sneh, A.C. Dillon, M.L. Wise, A.W. Ott and L.A. Okada, 3rd Int. Symp. on Atomic Layer Epitaxy and Related Surface Processes (A1E-3) Abstracts, Sendai, Japan, 25-27 May (1994) p. 38.
- [129] G. Oya and Y. Sawada, *J. Cryst. Growth* 99(1-4, pt. 1) (1990) 572.
- [130] J.F. Fan, K. Sugioka and K. Toyoda, *MRS Symp. Proc.* 222 (1991) 327.
- [131] L. Hiltunen, H. Kattelus, M. Leskela, M. Mäkelä, L. Numistö, E. Nykänen, P. Soinenen and M. Tüitta, *Mater. Chem. Phys.* 28(4) (1991) 379.
- [132] M. Pessa, R. Mäkelä and T. Suntola, *Appl. Phys. Lett.* 38(3) (1981) 131.
- [133] E.-I. Lakomaa, S. Haukka and T. Suntola, *Appl. Surf. Sci.* 60/61 (1992) 742.
- [134] S. Haukka, E.-I. Lakomaa and T. Suntola, *Thin Solid Films* 225 (1993) 280.
- [135] S. Haukka, E.-I. Lakomaa and A. Root, *J. Phys. Chem.* 97 (1993) 5085.
- [136] S. Haukka, E.-I. Lakomaa, O. Jylhä, J. Vilhunen and S. Hornytzkyj, *Langmuir* 9 (1993) 3497.
- [137] M. Ritala, M. Leskela, E. Nykänen, P. Soinenen and L. Numistö, *Thin Solid Films* 225 (1993) 288.
- [138] T.M. Mayer, J.W. Rogers Jr and J.A. Michalske, *Chem. Mater.* 3(4) (1991) 641.
- [139] K. Higuchi, A. Unno and T. Shirashi, *MRS Symp. Proc.* 222 (1991) 169.
- [140] M.A. Khan, J.N. Kuznia, R.A. Skogman, D.T. Olson, M. MacMillan and W.J. Choyke, *Appl. Phys. Lett.* 61(21) (1992) 2539.
- [141] M.A. Khan, R.A. Skogman, J.M. van Hove, D.T. Olson and J.N. Kuznia, *Appl. Phys. Lett.* 60(11) (1992) 1366.
- [142] M.A. Khan, 2nd Int. Symp. on A1E, Raleigh, June 2-5, 1992.
- [143] M. Sakuraba, J. Murota, N. Mikoshiba and S. Ono, *J. Cryst. Growth* 115(1-4) (1991) 79.
- [144] Y. Takahashi, Y. Sese and T. Urisu, *Jpn. J. Appl. Phys.* 28(11) (1989) 2387.
- [145] Y. Takahashi, H. Ishii and K. Fujinaga, *J. Electrochem. Soc.* 136(6) (1989).
- [146] Y. Suda, D. Lubben, T. Motooka and J.E. Greene, Extended Abstracts of the 21st Conference on Solid State Devices and Materials Tokyo, Japan: Bus. Center for Acad. Soc. Japan (1989) p. 57.
- [147] Y. Suda, D. Lubben, T. Motooka and J.E. Greene, *J. Vac. Sci. Technol.* B7 (5) (1989) 1171.
- [148] S. Imai, S. Tagaki, O. Sugiura and M. Matsumura, *Jpn. J. Appl. Phys.* 30 (12B) (1991) 3646.
- [149] A.C. Dillon, M.B. Robinson, M.Y. Han and S.M. George, *J. Electrochem. Soc.* 139(2) (1992) 537.
- [150] J.A. Yarmoff, D.K. Shuh, T.D. Durbin, C.W. Lo, D.A. Lapiono-Smith, F.R. McFeely and F.J. Himpsel, *J. Vac. Sci. Technol.* A10 (4) (1992) 2303.
- [151] Y. Takahashi and T. Urisu, *Jpn. J. Appl. Phys.* 30 (2A) (1991) 1209.
- [152] T. Fuyuki, M. Nakayama, T. Yoshinobu, H. Shiomi and H. Matsunami, *Appl. Phys. Lett.* 58(11) (1991) 1187.

### Surface Chemistry of Materials Deposition at Atomic Layer Level

Tuomo Suntola  
Microchemistry Ltd  
P.O. Box 45  
FIN-02151 Espoo  
Finland

#### Abstract

Structures in modern semiconductor devices are getting smaller and smaller coming close to atomic dimensions. Demand for materials processing at an atomic layer level can be approached from extreme process control or from delicate utilization of surface chemistry. The opportunity in the surface chemistry approach is to create conditions for monoatomic layer buildup through saturated surface reactions. Material layer processing through sequentially performed saturated surface reactions is generally referred to as Atomic Layer Epitaxy (ALE). ALE has been successfully applied in commercial manufacturing of thin film electroluminescent displays. Also, extensive scientific work has been done for applying atomic layer controlled growth of epitaxial layers and superlattice structures of III-V and II-VI semiconductors. Surface controlled build-up of molecular structures has recently been applied to porous supports for heterogeneous catalysts. For further progress in atomic layer level controlled materials processing well understood surface chemistry is of major importance.

#### Introduction

Modern process control in physical vapor deposition systems such as vacuum evaporation or Molecular Beam Epitaxy (MBE) makes it possible to approach the accuracy of individual atomic layers in materials deposition. Another approach to controlled material deposition at atomic layer level is to let the surface chemistry take over the external process control. This is the case in Atomic Layer Epitaxy (ALE) technology [1,2] where the saturation of sequentially applied surface reactions is utilized as digitalized control of the deposition procedure. For a good result one must assume a fair knowledge of the chemical reactions taking place in each reaction sequence. Sequencing and saturation of the reactions in ALE process gives also new possibilities for better understanding of chemical interactions on surfaces.

Material deposition in atomic layers has importance in very different applications. In single crystal epitaxy atomic layer control is needed for superlattice structures and abrupt interface layers. In semiconductor devices the dimensional demands are approaching atomic layers both in interfaces and dielectric layers. Material deposition in atomic layers can also be utilized for extreme conformality on non-planar structures and for achieving highly uniform layer thicknesses in thin films on large-area substrates. A recent extension of atomic layer controlled surface processing is the manufacturing of heterogeneous catalysts by applying Atomic Layer Epitaxy techniques for producing tailored molecular surfaces on porous materials [3].

#### Saturated surface reactions

In order to deposit a monoatomic or monomolecular layer on a surface through a surface reaction between a gas phase precursor and a solid surface one must assume strictly controlled dosing of the precursor uniformly delivered onto the surface or saturation of the reaction. Saturation of a surface reaction into a monolayer formation takes place when all available bonding sites on a surface are filled and the surface species formed in the reaction do not create new bonding sites for the precursor used. Surface after a saturated reaction is chemically different from the surface before the reaction. For the next saturated reaction the surface shall be exposed to a different precursor or shall be treated somehow in order to recreate the necessary bonding sites.

Filling density of surface species obtained in a surface reaction is dependent on the density of bonding sites available on the surface and the size of the surface species formed. Both of these factors, on the other hand, may be functions of the reaction temperature used. This is the case when the bonding sites or the resulting surface species are not of single

type but posses different bonding options or a diversity of structural forms.

Figure 1 shows the effect of reaction temperature to the density of tungsten atoms on alumina and silica surfaces. The precursor used for tungsten is tungsten oxychloride (WOCl<sub>4</sub>) which is assumed to react with the OH-groups on the oxide surfaces. Density of the OH-groups on the original surface is pre-regulated by heat treatment. On alumina there is a diversity of tungsten bonding options which can be seen as a strong dependence between tungsten monolayer density and the reaction temperature. Based on the observed chlorine/tungsten ratio it can be concluded that at higher temperatures direct chlorination of the surface occurs in parallel with a decreased density of tungsten atoms [3,4].

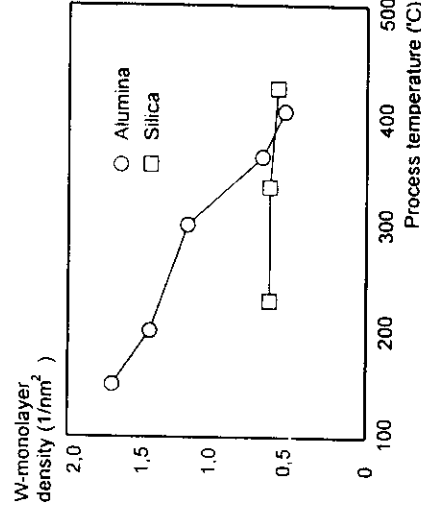
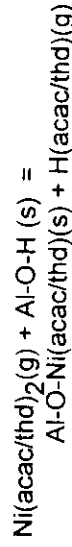


Figure 1. Effect of reaction temperature on the saturation density of tungsten on alumina and on silica.

On silica, on the other hand, the effect of reaction temperature is small which indicates dominantly single bond type and a discrete surface reaction. On both alumina and silica surfaces the saturation densities of tungsten are proportional to the O-H group density on the surface.

The effect of precursor size is illustrated in Figure 2. Nickel monolayer obtained with nickel acetylacetonate, Ni(acac)<sub>2</sub>, with a ligand area of 0,47 nm<sup>2</sup> has a saturation density of about 2,5 Ni-atoms/nm<sup>2</sup> whereas with nickel dipivaloylimethane, Ni(thd)<sub>2</sub>, as precursor the resulting saturation density is about one Ni-atom/nm<sup>2</sup>. Excellent match was found between the observed saturation density and the calculated maximum density of the assumed surface species based on estimated ligand areas. The form of surface species was concluded from the measured IR-spectrum and the C/Ni ratio determined. The surface reactions for saturated Ni(acac) and Ni(thd) surfaces can be described as



For completing the Al-O-Ni(acac/thd) surface structure formation into buildup of nickel oxide a reaction with water vapor is needed. H<sub>2</sub>O releases the acac- or thd-ligands by forming H(acac) or H(thd) gas molecules and new Ni-O-H surface structures for the next Ni(acac/thd) exposure:



After the first reaction cycle including the reactions with Ni-precursor and water vapor there are still Al-O-H structures available on the original alumina surface. In next reaction sequences between Ni-precursor and the surface the build-up of new Ni-surface species occurs both on the Al-O-H and the Ni-O-H sites. In a few cycles the original surface is fully covered and only Ni-O-H sites are available.

For a detailed analysis of the surface reactions not only the density of the surface sites but also knowledge of the type and character of the bonding sites is important. In the case of silica both OH-groups and siloxane bridges may act as bonding sites for metal precursors. OH-groups may appear in form of isolated single/paired groups or in form of weakly/strongly H-bonded OH-groups. The shares and quantities of the different OH-groups depend on the pre-treatment of the silica surface. In the reaction cycle of TiCl<sub>4</sub> and H<sub>2</sub>O on silica surface the resulting type and density of Ti-species is not only dependent on the type and density of the available bonding sites but is also strongly dependent on the reaction temperature used. At temperatures below 250 °C the resulting TiO<sub>2</sub> appears mainly in amorphous form whereas at temperatures above 300 °C TiO<sub>2</sub> agglomerates into anatase and rutile crystallites from the very first reaction cycles. Despite [5-8] agglomeration the reactions saturate and result

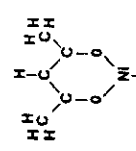
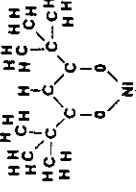
precursor	Ni (C <sub>9</sub> H <sub>7</sub> O <sub>2</sub> ) <sub>2</sub> acac	Ni (C <sub>11</sub> H <sub>19</sub> O <sub>2</sub> ) <sub>2</sub> thd
surface structure		
calculated filling area	A = 0,47 nm <sup>2</sup>	A = 0,87 nm <sup>2</sup>
calculated max density	2,1 Ni / nm <sup>2</sup>	1,1 Ni / nm <sup>2</sup>
observed saturation density	2,5 Ni / nm <sup>2</sup>	0,92 Ni / nm <sup>2</sup>

Figure 2. The effect of precursor size on the saturation density obtained.

in a digitally controlled thickness in the  $\text{TiO}_2$  layer with increased number of reaction cycles. Figure 3 summarises main surface structures in the  $\text{TiCl}_4$  and  $\text{H}_2\text{O}$  reaction sequences on silica surface at different temperature ranges.  $\text{TiO}_2$  buildup at high temperatures shows strong agglomeration. Mobility of any surface species formed increases with an increasing temperature resulting in higher probability of nucleation.

The complexity of surface structures and the multitude of mechanisms in the buildup of such structures gives an indication of the difficulty in defining the terms "monoatomic layer"

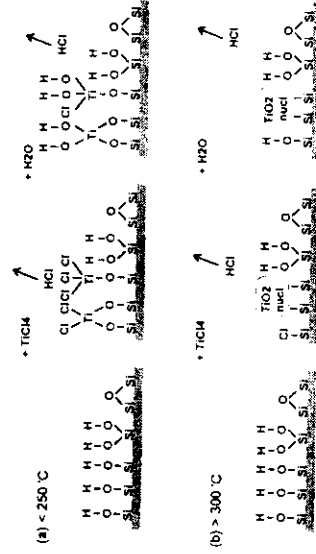


Figure 3. Surface structures on silica in  $\text{TiCl}_4$  and  $\text{H}_2\text{O}$  reaction sequences at reaction temperatures (a)  $< 250^\circ\text{C}$  and (b)  $> 300^\circ\text{C}$ .

or "monolayer". For crystalline materials an ideal "full monolayer" could be defined as a layer of atoms identical to layers of corresponding atoms inside the lattice in the direction parallel to the surface studied. In general terms a monoatomic layer could be defined as a surface configuration formed by add-atoms directly bonded to the underlying surface. Maximum density of atoms in a monoatomic layer is a close-pack configuration provided that there are chemical bonding possibilities for such packing density. Stoichiometrically ideal density of a monoatomic layer is referred to as the density of atoms in crystalline planes parallel to the surface studied. Energetically ideal density of a monoatomic layer is obtained in surface configuration with minimum free energy. Practically achievable density of a monoatomic layer refers to bonding sites available on the surface processed, to the precursor used and the type of surface species formed in the surface reaction at the processing temperature used. Advantages like precise control, conformality, stoichiometric balance and high density achieved by utilizing saturated reactions are almost independent of the saturation density obtained. For the layer by layer growth of single crystal materials a full monolayer per cycle mode may be advantageous. For the speed of growth it is always advantageous to have a high saturation density.

Experiments referred to in the examples of monoatomic layer formation in saturated surface reactions on alumina and silica surfaces have been made as a part of ALE-catalyst development in Microchemistry Ltd [9]. The supports used in the experiments are porous powders of alumina and silica with surface areas of 200 to 500  $\text{m}^2/\text{g}$ . The large surface area makes it possible to use standard chemical analysis for determining the surface species. Surface densities of the species have been obtained by dividing the determined number of atoms by the measured surface area of the support used. The reaction sequences have been performed in a modified ALE research reactor F-120 by Microchemistry Ltd. The reactor is able to handle 10 grams of powder support placed in a cavity with sinter bottom. The precursors are fed through the powder bed with the aid of an inert gas stream from the top to the bottom [10]. Observing the densities of the surface species near the top of the bed and near the bottom of the bed gives a direct indication of the perfection of the saturation, Figure 4.

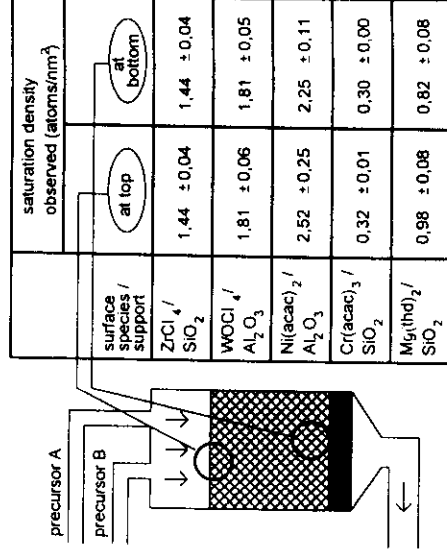


Figure 4. Saturation density of different metals on alumina and silica substrates. Samples taken at top and at bottom of the support bed indicate the uniformity of saturation.

Differences between repeated runs for each metal are small enough to fall into the accuracy of the determination indicated in the table of Figure 4. SEM-EDS microanalysis made inside the powder particles shows same uniformity in the monolayer densities as observed from particle to particle [11].

Results obtained with porous materials are complementary to the results with planar surfaces.  $\text{TiO}_2$  can be grown through atomic layer control in an ALE process at a growth rate of 0.3 molecular layers (ML) per reaction cycle [12]. It has been shown in the ALE process of  $\text{TiO}_2$  thin films by mass spectroscopy that at reaction temperatures above  $300^\circ\text{C}$  the sequenced  $\text{TiCl}_4 + \text{H}_2\text{O}$  reaction produces HCl only after  $\text{H}_2\text{O}$  exposure. In the  $\text{TiCl}_4$  reaction, most probably, some dissociation of  $\text{TiCl}_4$  occurs resulting in chlorination of Ti surface atoms.

### Full monolayer saturation

In the literature on Atomic Layer Epitaxy of III-V and II-VI single crystals there is a lot of discussion on "full monolayer per cycle" growth [2]. Full monolayer per cycle has been seen as a perfect mode of Atomic Layer Epitaxy. As stated in the discussion above the chemistry of surface reactions is far more complicated than simply laying atomic layers on top of each other. This is also true in the case of additive reactions with minimal chemistry involved. Surface always creates a discontinuity of the bulk which means that either there are dangling bonds on the surface or the unsaturated bonds are terminated by surface reconstructions or chemical groups such as OH-groups on many oxides.

Ligands originating from precursors in ALE reaction sequences may act as chemical terminations to surface atoms and prevent undesired surface reconstructions. One of the most widely studied ALE processes is the process for gallium arsenide using trimethyl or triethylgallium (TMG or TEG) and arsine as the precursors [13-25]. While both clean Ga and As surfaces show preferred surface reconstructions with less than a full monolayer surface atom density the reported growth rates of ALE for GaAs are mostly a full monolayer per cycle, Figure 5. It can be seen from the curves of Figure 5 that processing dynamics together with complex surface chemical interactions result in big differences in different experimental set-ups.

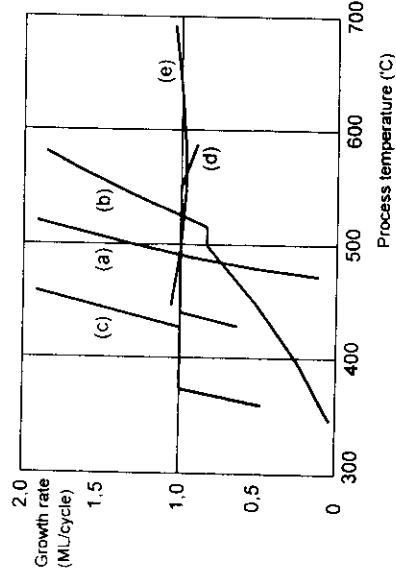
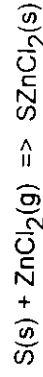


Figure 5. ALE processing characteristics of GaAs. (a) No laser irradiation, ultra-high vacuum [13], (b) no laser irradiation, ultra-high vacuum [15], (c) ultra-high vacuum, laser irradiation involved [13], (d) high speed hydrogen transport applied [16], (e) high-speed hydrogen, rotating disk applied for sequencing [17].

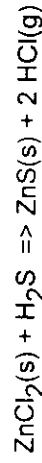
Saturation density consistent with surface atom densities in known typical surface reconstructions of clean Ga or As surfaces has been obtained by Nishizawa et al. [15] shown as curve (b) in Figure 5. The wide processing windows in curves (d) and (e) involve high speed gas flow and pulsing, which reminds of the

importance of the dynamical behaviour of the surface in the reactions [16, 17].

Single crystal ALE of most II-VI compounds have been demonstrated in full monolayer mode [26-31]. At the same time ZnS and CdS typically have a preferred growth rate of 1/3 monolayers/cycle when grown as a polycrystalline thin film using the elements as the precursors. In  $\text{ZnCl}_2 + \text{H}_2\text{S}$  process for ZnS the rate of the growth is also 1/3 monolayers/cycle. By mass spectroscopy it has been shown [32] that HCl is released only after  $\text{H}_2\text{S}$  exposure which suggest reactions:



and



Quantum chemical analysis of the  $\text{ZnCl}_2 + \text{H}_2\text{S}$  reaction also supports the 1/3 monolayers/cycle growth mode as the energetically most favorable mode [33,34]. The two chlorine atoms on the Zn-surface after  $\text{ZnCl}_2$  exposure terminate the discontinuity of the ZnS lattice which in principle could prevent surface reconstructions. The size of the Cl ligand, however, seems to create a steric hindrance for full zinc monolayer formation. In the  $\text{CdCl}_2 + \text{H}_2\text{S}$  process for CdS a full monolayer/cycle growth rate has been observed [35]. On a Cd surface, probably due to the higher ionic radius of the Cd atom compared to Zn as well as higher lattice dimensions of CdS lattice compared to ZnS, the Cl ligand does not create similar steric hindrance or a full metal atom monolayer formation as in the case of ZnS.

### Temperature window for saturation

As a summary to the discussion on monolayer formation and saturation in a surface reaction we can construct a temperature window for saturation, Figure 6. A necessary precondition for saturation always is sufficient dosing. Saturation occurs when available bonding sites are filled with species originating from a reaction between a precursor and a bonding site on the surface. It must be further assumed that the surface species formed do not create new bonding sites for the precursor used in the reaction. Two different saturation densities illustrated as W1 and W2 in Figure 6 may occur for different reasons. If the higher saturation density W1 occurs at a lower temperature than the lower saturation density W2 then most probably a part of bonding sites result in a lower bond strength for the surface species formed. If the lower saturation density occurs at a lower

temperature than the higher saturation density then most probably the difference could be explained as a higher activation energy for a part of the available bonding sites or as reduction of ligand size at a higher temperature. In case atomic layer growth is performed on disordered surface such as amorphous or polycrystalline surfaces a continuously changing saturation density as a function of temperature may be observed as a consequence of multitude of bonding options with different bond strengths and activation energies, dashed line in Figure 6.

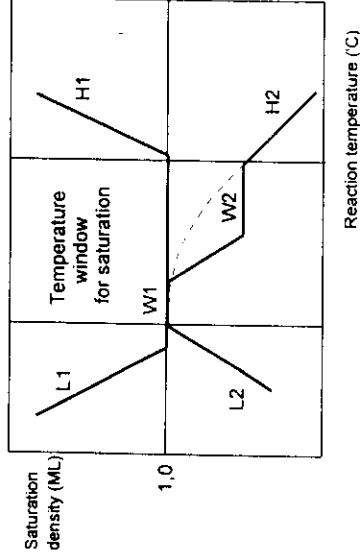


Figure 6. Processing window for saturated monolayers.

In the low temperature region below saturation temperatures excess or deficiency of surface species is observed depending on whether the limiting mechanism is condensation of the precursor on a monolayer or insufficient energy for the surface reaction to occur, L1 and L2 in Figure 6, respectively. In the high temperature region above saturation temperatures excess surface species may be cumulated if the precursor used is decomposed into non-volatile molecules or atoms, H1. For thermally stable precursors the high temperature region shows as a declining surface coverage due to desorption of any surface species, H2.

Temperature range for saturation is specific for any precursor and surface used. Process comprising two or several reaction sequences has a processing window fulfilling the saturation demand of each individual reaction sequence in the process. If the saturation windows of the different reactions needed in a process do not overlap the only way to carry out the process is to change temperature between the reaction sequences or to use extra energy to enhance the saturation window of one or several reaction sequences.

### Atomic Layer Epitaxy

Material deposition based on sequentially saturated surface reactions is

generally referred to as Atomic Layer Epitaxy. Basically, at least two different reaction sequences are required in a growth cycle in order to re-establish the necessary bonding conditions for a digitally proceeding growth process. ALE has been mainly applied to compound materials where each reaction sequence typically adds one saturated atomic layer of a component of the compound deposited. While adding an atomic layer on a surface each reaction sequence activates the surface to the second precursor. Accordingly, it is essential to match the pair of precursors used in such a way that complementary reactions can be applied. It is also important that surface configurations created in each reaction sequence are stable enough to stay available for the next reaction sequence.

The surface condition resulting from a saturated reaction is not a static structure. For any surface species there is a finite surface mobility and desorption probability which might result in time and occupation dependent changes in the surface structures. Change in a surface ligand during a purge sequence in ALE process may have a major effect on the next reaction sequence. Most probably this is the case in the TMG+AsH<sub>3</sub> process for GaAs which is strongly dependent on processing parameters such as the length of the purge sequence and the speed of precursor supply. Chemically, we can see a big difference in the surface reactions of TMG with As surface and AsH<sub>n</sub> (n=1..3) surface. One can expect full methane exchange in Ga(CH<sub>3</sub>)<sub>3</sub> + AsH<sub>3</sub> reaction while Ga(CH<sub>3</sub>)<sub>3</sub> + As reaction suffers from lack of chemical enhancement for any ligand release in Ga chemisorption [13-23].

In ALE processes for compound materials each reaction sequence generally provides an additional, full or partial, atomic layer on the surface grown. In some cases it might, however, be necessary to use an additional reaction sequence just for activating the surface for the next additional reaction. In a process for TiNx using TiCl<sub>4</sub> and NH<sub>3</sub> as the reactants an extra Cl-reduction sequence after the TiCl<sub>4</sub> exposure can be used to control the stoichiometry of the resulting TiNx [36]. In ALE processes for elemental materials such as silicon, germanium or diamond a surface activation sequence is needed unless a pair of precursors for a complete surface ligand exchange are available. For Atomic Layer Epitaxy of silicon reactants like di- or tri-silanes, diethylsilane and chlorosilanes together with thermal cycling has been demonstrated [37-42].

### Material processing by atomic layers

Utilization of cyclically repeated sequences of saturated surface reactions gives

atomic layer level control in material buildup. Instead of being precursor rate or flux controlled, the saturation results in a digital mode control including the possibilities of tailored material structures and a precise thickness control of the material layers formed. Surface control also gives some extra freedom in processing set-up and reactor design. In any conventional rate controlled material deposition method it is important to introduce the precursors uniformly and equally onto any parts of the substrates handled. In surface controlled processing it is enough to take care of sufficient dosing onto any parts of the substrates. Sufficient dosing is strongly dependent on the mechanism of the surface reaction in question. In surface reactions with small or zero activation energy an immediate reaction at a precursor molecule hit on an unoccupied bonding site can be assumed. If no surface mobility through possible precursor states is assumed exponential filling of the surface states will result. Full coverage assumes surface hits in excess to the density of bonding sites in any reaction sequence.

tailored molecular structures, interfaces, superlattices, high quality thin films and coatings in a highly productional way. The layer by layer buildup of material ensures excellent controllability of the deposition process as well as the quality of the resulting material layer. The technology has only partly matured to industrial level major part of its potential is still waiting for utilization. At the same time work with layer-by-layer controlled material deposition creates valuable information on detailed understanding of surface reactions.

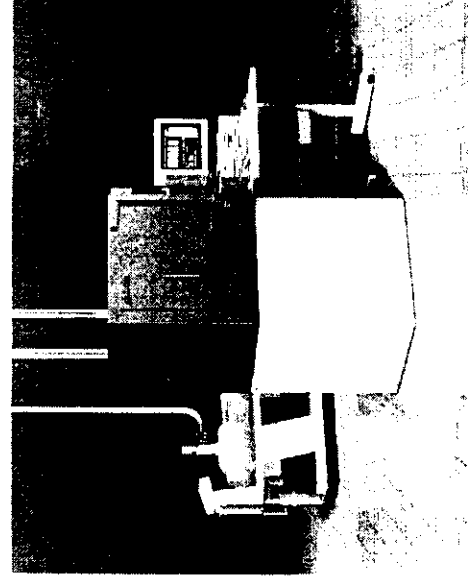


Figure 8. Traveling wave reactor F-850 (Microchemistry Ltd) for high throughput material layer production for insulators and dielectric layers on silicon wafers and for manufacturing of flat panel displays

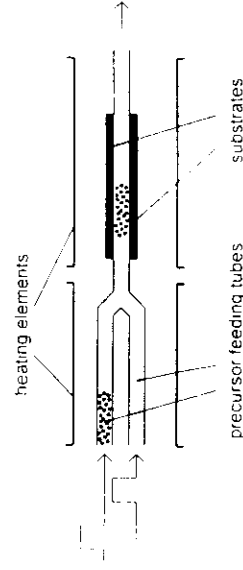


Figure 7. Schematic structure of a traveling wave reactor

For high material utilization efficiency it is advantageous to create conditions for "effective overdosing" by multiple hit arrangement [43,44]. Multiple hit condition is achieved in a "traveling wave" ALE reactor design as schematically presented in Figure 7. The speed of the carrier gas flow is typically in the order of 10 m/s which is about two orders of magnitude below the thermal speed of gas molecules which in turn ensures an effective multiple hitting condition in the flow spacing. The biggest advantage of a traveling wave reactor is its huge throughput in comparison to the size of the reactor. While the spacings between the substrates may be as small as a few millimeters for substrate areas larger than a squarefoot hundreds of squarefeet of active substrate area can be loaded into a cube-like reactor of less than one squaremeter footprint still maintaining a processing speed of about 1-4 s/cycle, Figure 8

#### Summary

Atomic layer controlled material layer deposition is a technology for the production of

#### References

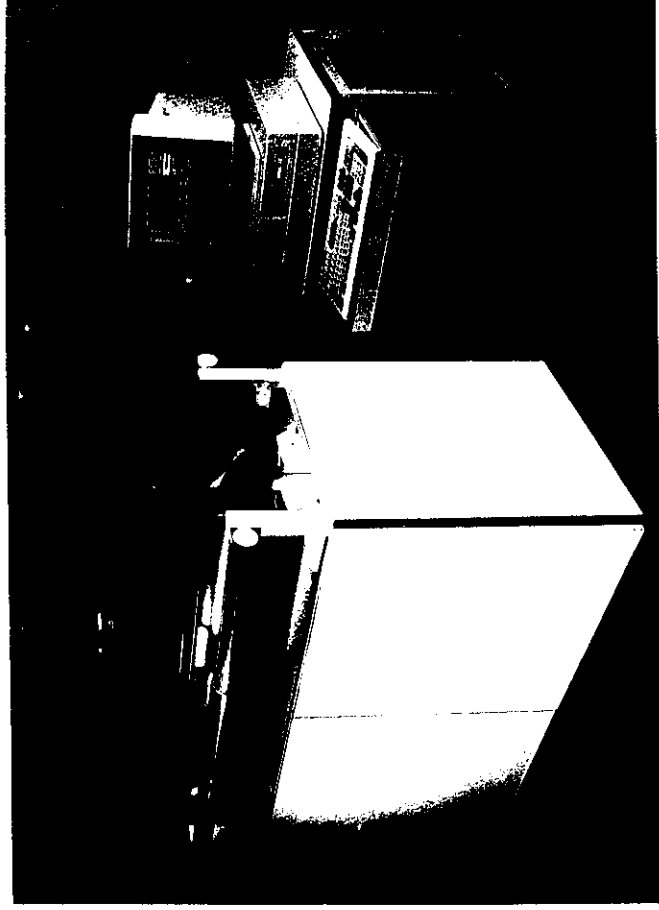
- [1] T Suntola, Atomic Layer Epitaxy. Mat. Sci. Rep. 4 (1989) 261.
- [2] T. Suntola, Atomic Layer Epitaxy, Handbook of Crystal Growth 3, Thin Films and Epitaxy, Part B: Growth Mechanisms and Dynamics, Chapter 14, Elsevier, 1994
- [3] E.-L. Lakomaa. Appl. Surf. Sci. 75 (1994) 185
- [4] E.-L. Lakomaa, S. Haukka and T. Suntola. Appl. Surf. Sci. 60/61 (1992) 742
- [5] A.A. Gomenyuk, I.V. Babich, Yu.V. Plyuto and A.A. Chuico. Russ. J. Phys. Chem. 64 (1990) 891
- [6] S. Haukka, E.-L. Lakomaa and T. Suntola. Thin Solid Films 225 (1992) 280
- [7] S. Haukka, E.-L. Lakomaa and A. Root, J. Phys. Chem. 97 (1993) 5085
- [8] S. Haukka, E.-L. Lakomaa, O. Jylhä, J. Vilhunen and S. Hornyitzkyj. Langmuir 9 (1993) 3497
- [9] S. Haukka, E.-L. Lakomaa and T. Suntola. Appl. Surf. Sci. 82/83 (1994) 548



- [10] S. Haukka, A. Kytökiivi, E.-I. Lakomaa, U. Lehtovirta, M. Lindblad, V. Lujala and T. Suntola, *Studies in Surface Science and Catalysis*, B. Delmon and J.T. Yates (Editors), Vol. 91, Elsevier Science B.V., Amsterdam, 1995, p.957
- [11] M. Lindblad, L.P. Lindfors and T. Suntola, *Catal. Lett.* 27 (1994) 323
- [12] M. Ritala, M. Leskelä, E. Nykänen, P. Soininen and L. Niinistö, *Thin Solid Films* 228 (1993) 32
- [13] J. Nishizawa, *J. Cryst. Growth* 115 (1991) 12
- [14] M.A. Tischler and S.M. Bedair, *Appl. Phys. Lett.* 48 (1986) 1681
- [15] J. Nishizawa, T. Kurabayashi, H. Abe and N. Sakurai, *J. Vac. Sci. Technol.* A 5 (1987) 1572
- [16] M. Ozeki, N. Mochizuki, N. Ohtsuka and K. Kodama, *Appl. Phys. Lett.* 53 (1988) 1509
- [17] K.G. Reid, H.M. Urdianyk and S.M. Bedair, *Appl. Phys. Lett.* 59 (1991) 2397
- [18] A. Watanabe, T. Kamijoh, M. Hata, T. Isu and Y. Katayama, *Vacuum* 41 (1990) 965
- [19] A. Doi, Y. Aoyagi and S. Namba, *Appl. Phys. Lett.* 49 (1986) 785
- [20] B.Y. Maa and P.D. Dapkus, *MRS Symp. Proc.* 222 (1991) 25
- [21] B.A. Banse and J.R. Creighton, *Appl. Phys. Lett.* 60 (1992) 856
- [22] Y. Aoyagi, T. Meguro, S. Iwai and A. Doi, *Mater. Sci. Eng.* B10 (1991) 121
- [23] J. Nishizawa, H. Abe and T. Kurabayashi, *J. Electrochem. Soc.* 136 (1989) 478
- [24] H. Yokoyama, M. Shinohara and N. Inoue, *Appl. Phys. Lett.* 59 (1991) 2148
- [25] A.V. Annapragada, S. Salim and K.F. Jensen, *MRS Symp. Proc.* 222 (1991) 81
- [26] M. Ahonen, M. Pessa, T. Suntola, *Thin Solid Films* 65 (1980) 301
- [27] M. Pessa, O. Jylhä, *Appl. Phys. Lett.* 45 (1984) 646
- [28] W. Faschinger, P. Juza and H. Sitter, *J. Crystal Growth* 115 (1991) 692
- [29] T. Yao, T. Takeda, *Appl. Phys. Lett.* 48 (1986) 160
- [30] S. Doshō, Y. Takemura, M. Konagai and K. Takahashi, *J. Cryst. Growth* 95 (1989) 580
- [31] J.G. Nelson, *J. Vac. Sci. Technol.* A 5(1987) 2140
- [32] J. Hyvärinen, M. Sonninen and R. Törnqvist, *J. Crystal Growth* 86 (1988) 695
- [33] M. Lindblad and T.A. Pakkanen, *J. Comp. Chem.* 9 (1988) 581
- [34] T.A. Pakkanen, V. Nevalainen, M. Lindblad and P. Makkonen, *Surf. Sci.* 188 (1987) 456
- [35] A. Rautiainen, Y. Koskinen, S. Lindfors and J. Skarp, *MRS Symp. Proc.* 222 (1991) 263
- [36] M. Ritala, M. Leskelä, E. Rauhala and P. Haussalo, *J. Electrochem. Soc.*, 142 (1995) 2731
- [37] W.K. Chen, J.C. Chen, L. Anthony and P.L. Liu, *Appl. Phys. Lett.* 55 (1989) 987
- [38] Y. Suda, D. Lubben, T. Motooka and J.E. Greene, *J. Vac. Sci. Technol.* B. 7 (1989) 1171
- [39] S. Imai, S. Tagaki, O. Sugiura and M. Matsumura, *Jpn. J. Appl. Phys.* 30 (1991) 3646
- [40] A.C. Dillon, M.B. Robinson, M.Y. Han and S.M. George, *J. Electrochem. Soc.* 139 (1992) 537
- [41] J.A. Yarmoff, D.K. Shuh, T.D. Durbin, C.W. Lo, D.A. Lapiono-Smith, F.R. McFeely and F.J. Himpfel, *J. Vac. Sci. Technol.* A. 10 (1992) 2303
- [42] Y. Takahashi and T. Urisu, *Jpn. J. Appl. Phys.* 30 (1991) L209
- [43] T. Suntola, *Thin Solid Films* 225 (1993) 96.
- [44] T. Suntola, *Display Manufacturing Technology Conference*, Santa Clara, CA, January 31 - February 2, 1995



## F-120 Reactor for R&D thin film growth by Atomic Layer Epitaxy



*The F-120 reactor is designed for R&D purposes, for high flexibility and for fast processing of multi-layer thin film structures, oxides, nitrides, II-VI and III-V compounds.*

### Atomic Layer Epitaxy

Atomic Layer Epitaxy (ALE) is a digitally controlled layer-by-layer deposition method for the production of thin films with atomic layer accuracy. Each atomic layer formed in the sequential process is the result of a saturating reaction. The thin films formed are virtually free of voids and pinholes and have near perfect step coverage, which is required in sub-micron semiconductor technology and flat panel display manufacturing. The surface control achieved in Atomic Layer Epitaxy results in thin films with bulk density and excellent uniformity on large area substrates. Atomic Layer Epitaxy can be used for producing single or multiple layers of oxides, nitrides, II-VI and III-V compounds.

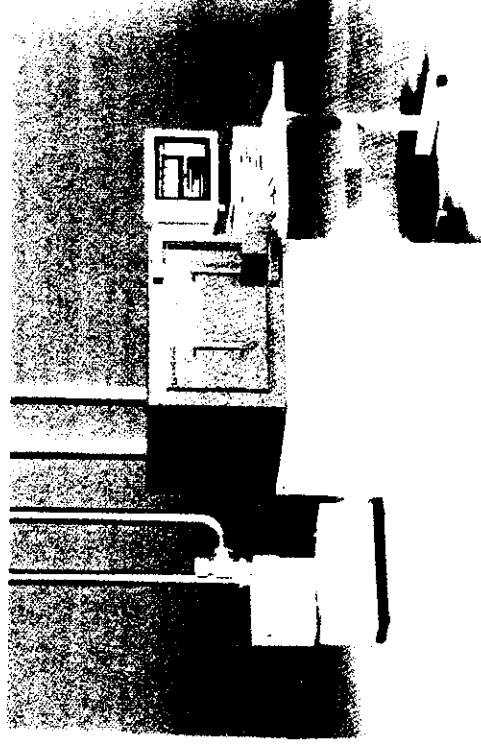
### The F-120 reactor

The F-120 reactor is designed for research purposes, for high flexibility and for easy operation and maintenance. It is equipped with four individually controlled sources for solid precursors inside the reactor body and with a definable number of external sources for gas and liquid precursors. The construction materials of the reactor allow a wide choice of reactants. The reaction zone is formed by a 2 mm space between two 50 x 50 mm<sup>2</sup> substrates.

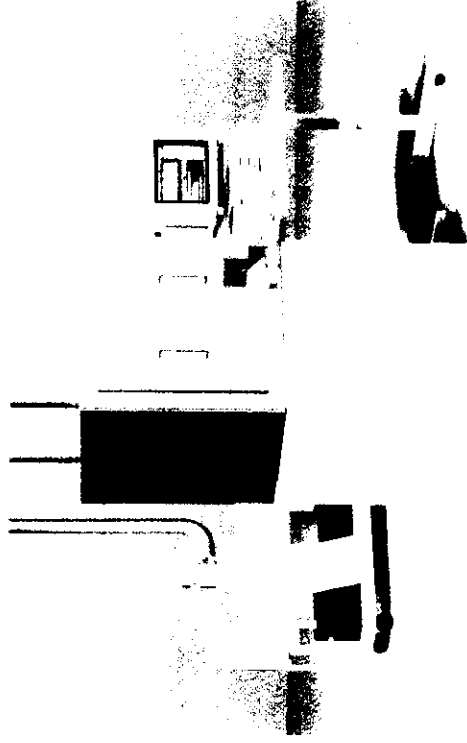
- + **Small Size Research Reactor**
- + **High Flexibility**
- + **Excellent Conformality, Uniformity and Reproducibility**
- + **Fully Automated Processing**
- + **Multi-Layer Structures in Single Pump Down**
- + **Oxides, Nitrides, II-VI and III-V Compounds**



## Thin Film Reactors for sub-micron semiconductor and flat panel manufacturing



*The F-450 reactor is designed for R&D and pilot purposes for full size substrates.*



*The F-850 is a high throughput production reactor for wafers and large plates.*

## Atomic Layer Epitaxy

Atomic Layer Epitaxy (ALE) is a digitally controlled layer-by-layer deposition method for the production of thin films with atomic layer accuracy. Each atomic layer formed in the sequential process is the result of a saturating surface reaction. The thin films formed are virtually free of voids and pinholes and have near-perfect step coverage, which is required in sub-micron semiconductor technology and flat panel display manufacturing. The surface control achieved in Atomic Layer Epitaxy results in thin films with bulk density and excellent uniformity on large area substrates. Atomic Layer Epitaxy can be used for producing single or multiple layers of oxides, nitrides, II-VI and III-V compounds.

- + **Wafers up to 12 inches, plates up to 12 x 16 inches**
- + **High Throughput, up to 10 wafers / min**
- + **Excellent Conformality, Uniformity and Reproducibility**
- + **Fully Automated Processing**
- + **Multi-Layer Structures in Single Pump Down**
- + **Oxides, Nitrides, II-VI and III-V Compounds**

# The F-450 and F-850 reactors

## R&D, pilot and production

The unique design of Microchemistry F-450 and F-850 reactors avails Atomic Layer Epitaxy for cost effective thin film processing of large area substrates in R&D, pilot and production scales. The two reactors complement each other and combine the quick handling of single substrates in the F-450 reactor with the high throughput and production line compatibility of the F-850 reactor.

## Large area substrates

The F-450 and F-850 ALE reactors are designed to effectively use Atomic Layer Epitaxy on semiconductor wafers with up to 12 inch diameter as well as on plates of sizes up to 12 x 16 inches. Development and pilot runs in the F-450 reactor can be directly scaled up into production in the F-850 reactor due to the equal process design and control software used in the two reactors. The surface controlled growth mode results in excellent uniformity and reproducibility of the thin films over large areas. The thickness of the films is determined solely by the number of reaction sequences applied.

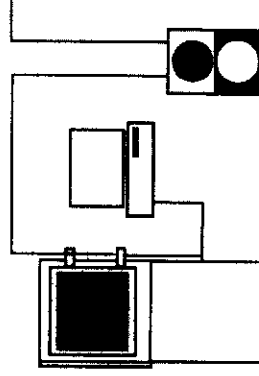
## Cleanliness and easy to maintain

The design of the reactors minimizes the number of moving parts and the maintenance required. Cleanliness is enhanced with a double space - hot wall design which minimizes adsorption of residues in the reaction walls without requiring high vacuum pumping. The unique substrate cassette design minimizes the need for cleaning of any fixed part of the reactor. Inert gas is used for precursor vapor transport as well as for completing the high speed valving functions needed in the sequential Atomic Layer Epitaxy processing. The gas pressure used during processing is 1-5 mbar.

## Modular design

The modular design and the medium pressure operation of the reactors facilitates many installation options. Vacuum pumps and

precursor gas containers can be installed in service areas. The reactors themselves can be placed in a clean room or can be made to open into the clean room.



2 Å per second depending on the surface saturation density of the precursors used.

## High throughput

A 200 pcs batch of 6 inch wafers in the F-850 production reactor and a typical 1 Å/s growth speed results in a net throughput of 4 wafers/min for thin films of 3000 Å thickness. For final throughput some additional time is needed to load and de-load the wafers as well as for temperature stabilization of the wafers before the actual growth process. External preheating and cooling units can be used with both the F-450 and the F-850 reactors. Maximum processing temperature is 500 °C.

## Complete elimination of gas phase reactions

The sequencing eliminates any gas phase reactions between the precursors. This allows and promotes the use of highly reactive precursors which is advantageous for high material utilization efficiency. The complete elimination of gas phase reactions is a key factor in the high structural quality of the thin films formed.

## Tailored structures

As a consequence of the atomic level sequencing the F-450 and F-850 reactors can produce precisely tailored interface layers and superlattice type multilayer structures in one process. This is supported by the unique software enabling easy sequence programming.

## Gas monitoring

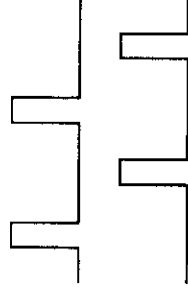
The reactors are supplied with optional exhaust gas monitoring capability for monitoring the reaction chemistry in R&D or for controlling the precursor feeds in the production.

## The precursors

The F-450 and F-850 reactors allow the use of both volatile and non-volatile precursors. Volatile precursors are supplied from separate gas containers. The necessary vapor pressure of non-volatile precursors is generated in thermally isolated source units inside the reactor body. The reactors allow simultaneous use of eight different non-volatile (plus several volatile) precursors in one process.

## The principle of operation

In reactors inert gas transports the precursors one at a time through a cassette of substrates. The inherent surface



control of Atomic Layer Epitaxy makes the substrate surfaces accept one atomic or molecular layer of the precursor in each pass. The dimensions and flow dynamics of the transport channels are optimized for fast sequencing of the precursors and to ensure a complete purging between each precursor in the sequence. Reaction and purge sequences as fast as 1/3 seconds can be obtained. This results in growth speeds up to 0,5 or

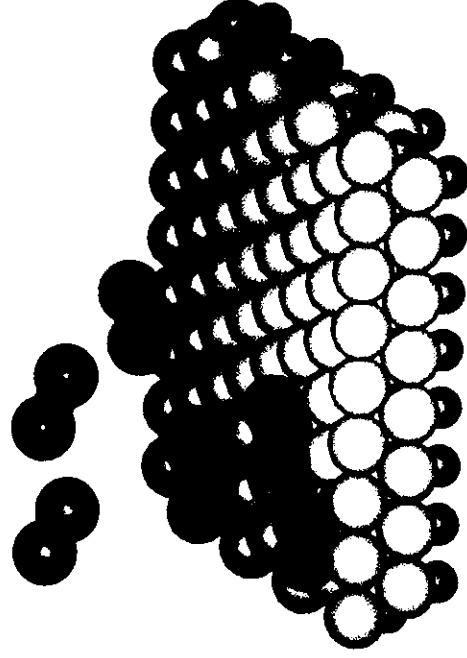
# Specifications

Reactor Type:	F-450	F-850
Use:	R&D and pilot production. Provides easy handling and quick processing of individual full size substrates.	High throughput production. Compatible with loading and unloading robotics.
Reactor:	<p>Temperature range: 100 to 500 °C</p> <p>Substrate size: up to 300 x 400 mm (12" x 16 ")</p> <p>Batch size: 12" x 16" 2 pcs 12" wafers 2 pcs 8" wafers 4 pcs 6" wafers 8 pcs 4" wafers 24 pcs</p>	<p>Temperature range: 100 to 500 °C</p> <p>up to 300 x 400 mm (12" x 16 ")</p> <p>12" x 16" 50 pcs 12" wafers 50 pcs 8" wafers 100 pcs 6" wafers 200 pcs 4" wafers 600 pcs</p>
Sources:	<p>Non-volatile precursors: 7 sources of 100 cc 100 to 500 °C</p> <p>Volatile precursors: As specified by user</p>	<p>7 sources of 100 cc 100 to 500 °C</p> <p>As specified by user</p>
Pumping:	Mechanical pump 60 m <sup>3</sup> /h (2100 ft <sup>3</sup> /h)	Roots and mechanical pump 300 m <sup>3</sup> /h (10600 ft <sup>3</sup> /h)
Operating pressure:	1 - 5 mbar	1 - 5 mbar
Utilities:	<p>Power Europe: 380-400 V, 3 phase 50 Hz (10 kVA)</p> <p>Power US: 200-230 V, 3 phase 60 Hz (10 kVA)</p> <p>Carrier gas: Typ. N<sub>2</sub> 1-5 SLM</p> <p>Cooling: Water</p> <p>Exhausts: For vacuum pump, hood and liquid/gas cabinet(s)</p>	<p>380-400 V, 3 phase 50 Hz (10 kVA)</p> <p>200-230 V, 3 phase 60 Hz (10 kVA)</p> <p>Typ. N<sub>2</sub> 5-15 SLM</p> <p>Water</p> <p>For vacuum pump, hood and liquid/gas cabinet(s)</p>
Dimensions:	<p>Weight max.: 550 kg (1200 lb)</p> <p>WxDXH: Reactor: 0.9 x 1.0 x 1.5 m (3 x 3.3 x 4.9 ft)</p> <p>Pump: 0.3 x 0.8 x 0.4 m (1 x 2.5 x 1.5 ft)</p>	<p>750 kg (1650 lb)</p> <p>Reactor: 1 x 1.2 x 1.8 m (3.3 x 4 x 6 ft)</p> <p>Pump: 0.7 x 1.3 x 1.3 m (2.3 x 4.3 x 4.3 ft)</p>
Special options:	Connection for residual gas analyzer	Yes

All rights to changes reserved

## Chemistry at Atomic Level

---



*Atomic Layer Epitaxy is based on sequential saturated surface reactions resulting in a digitally controlled thin film growth.*

Microchemistry Ltd. is a technology unit specializing in advanced thin film processing and surface chemistry development. It was established in 1987 as a subsidiary of Neste Corporation, the largest industrial enterprise in Finland. Microchemistry Ltd. has its research facilities in Espoo, Finland.

Microchemistry Ltd. possesses unique expertise in Atomic Layer Epitaxy (ALE) technology. ALE is a surface controlled thin film process that can be used to produce microstructures in semiconductor devices and in the production of large area thin film devices such as flat panel displays and thin film solar cells. It is also used for producing controlled molecular surface structures in porous materials such as supports of heterogeneous catalysts. Microchemistry produces ALE reactors for research and production purposes in all application areas of Atomic Layer Epitaxy.

## Equipment, Licences, Services

Microchemistry Ltd. offers standard and custom processing equipment for Atomic Layer Epitaxy, technology licenses, development services and consultation in the areas of its special expertise. Major developments made include solar cell technology for Neste Advanced Power Systems as well as fundamental development of heterogeneous catalysts based on tailored molecular surfaces for Neste Corporation.

Microchemistry Ltd.  
P.O. Box 45  
FIN-02151 ESPOO  
FINLAND

tel. +358-0-450-5719  
fax +358-0-450-5700  
e-mail [ale@microchem.fi](mailto:ale@microchem.fi)

USA and Canada:

Advanced Thin Films  
12623 Cambridge Dr.  
Saratoga, CA 95070

tel. +1-408-725-1344  
fax +1-408-973-0923

---

**MICROCHEMISTRY LTD**

---